PHOTOCATALYTIC HYDROGEN PRODUCTION

LAYLA S. ALMAZROAI

A thesis submitted in candidature for degree of PhD in Physical Chemistry

Supervised by

Professor Michael Bowker

And

Doctor Philip Davies

Cardiff University

2009

ProQuest LLC
789 East Eisenhower Parkway
P.O. Box 1346
Ann Arbor, MI 48106-1346

APPENDIX 1:
Specimen layout for Thesis Summary and Declaration/Statements page to be included in a Thesis

DECLARATION

This work has not previously been accepted in substance for any degree and is not concurrently submitted in candidature for any degree.

Signed ..... (candidate) Date .....8.12.1.2010.....

STATEMENT 1

This thesis is being submitted in partial fulfillment of the requirements for the degree of .....(insert MCh, MD, MPhil, PhD etc, as appropriate)

Signed ..... (candidate) Date .....8.12.1.2010.....

STATEMENT 2

This thesis is the result of my own independent work/investigation, except where otherwise stated. Other sources are acknowledged by explicit references.

Signed ..... (candidate) Date .....8.12.1.2010.....

STATEMENT 3

I hereby give consent for my thesis, if accepted, to be available for photocopying and for inter-library loan, and for the title and summary to be made available to outside organisations.

Signed ..... (candidate) Date .....8.12.1.2010.....

STATEMENT 4: PREVIOUSLY APPROVED BAR ON ACCESS

I hereby give consent for my thesis, if accepted, to be available for photocopying and for inter-library loans **after expiry of a bar on access previously approved by the Graduate Development Committee.**

Signed ..... (candidate) Date .....8.12.1.2010.....

To my husband

Acknowledgments

I would like to express my gratitude to my supervisor and co-supervisor, Professor Michael Bowker and Doctor Phillip Davies. Their expertise, understanding, and patience have helped to guide this work. For that, the author would like to thank them. I appreciate their knowledge and skill in interaction with students in the lab, presentation at conferences and their assistance with the preparation of this thesis

My sincere thanks go out to my sisters, Sabah in particular, and my friends, Abeer, Matheaw, Andrew, liza, polina, and all of my group for their assistance.

Lastly, but most importantly my infinite thanks are given to my husband for his unfailing support throughout my studies.

Abstract

Due to the environmental problems arising from the combustion of fossil fuels and their depletion, the production and use of renewable fuels have grown rapidly in recent years. Hydrogen is among the promising fuels of the future as the only material that can be produced from the burning of hydrogen in air is water. The production of hydrogen by the photocatalytic water splitting method involving a semiconductor is a promising development in the field of energy and the environment, and this technique was employed in this work.

TiO_2 and palladium were the main photoactive support and loaded metal used in this project, respectively. The hydrogen production, whether from water/methanol solution or water alone, was investigated by illumination of the catalyst by UV irradiation produced from an Xe arc lamp. The reactions were performed in liquid or gas phase under an argon atmosphere as an inert gas. The gaseous products were collected and analysed using gas chromatography. The main method used in Pd loading was the impregnation method.

0.5% and 0.1% wt Pd loading were the best in terms of hydrogen production rate in liquid and gas phase reactions respectively. 0.5% Pd/TiO_2 (P25) was used in the remaining experiments to investigate some of the variables, to maximize the rate of H_2 production. Glycerol displayed an activity and produced hydrogen and carbon dioxide, as in the case of methanol but in much higher quantities. Loading of mesoporous TiO_2 by a different weight of Pd, which had a high surface area, gave less hydrogen than Pd/P25 whether in liquid or gas phase reactions.

The efficiency of Pd loaded titania (P25, pure anatase or anatase prepared by CHFS) doped by non-metals such as nitrogen, silver or strontium was low and less than Pd/TiO_2.

Hydrogen produced over Pd/TiO_2, Au/TiO_2 and TiO_2 from water photolysis was also very low. The recombination between hydrogen and oxygen (back reaction) was studied over these catalysts and it was found that it was fastest on Pd/TiO_2 whether in the dark or in the presence of light. For Au/TiO_2, the light enhanced the hydrogen and oxygen reaction.

TABLE OF CONTENTS

CHAPTER ONE

Introduction

1.1 Introduction

The economies of all industrial countries are completely dependent on fossil fuels (coal, oil and natural gas). The combustion of these fuels provides energy, which is needed for heating, transportation, electricity generation and other industries.

Although fossil fuels have played an important role in making western societies what they are today, there are some problems related to the use of these sources of fuels:

a) Air pollution

In the process of converting of fossil fuels to energy, waste gases are released into the atmosphere causing air pollution, which affects the environment, human health, and the quality of life. Among these harmful gases are carbon dioxide; carbon monoxide; nitrogen oxides; sulphur dioxide; and particulates, that is, tiny solid particles, including lead from gasoline additives. Currently, the concentration of CO_2 in the atmosphere is above 360 parts per million (ppm), although before the industrial revolution, the CO_2 concentration had been close to 280 parts per million (ppm). The increasing CO_2 concentration has led to global warming[1].

B) Depletion of fossil fuels

Over the next few decades, the world will face the dilemma of what to do when the remaining reserves of fossil fuels run out. Fossil fuels play a crucial role in developing societies, especially in the transport sector,

which consumes 95% of oil worldwide[2]. Table 1.1 displays the distribution of outstanding reserves of fossil fuels in the reservoirs throughout the world in giga tonnes of oil equivalent. As can be seen in this table, coal exists in huge amounts compared to oil and gas over the world and constitutes 65% of fossil fuel reserves, which means that it will be the fuel of the future and may last for as long as the next 200 years. In contrast, reserves of gas and oil are limited by size and location, which affects the world energy market.

Table 1.1: The estimated distribution of remaining reserves of fossil fuels in 2006[3, 4].

Region	Fossil fuels reserve (giga tonnes of oil equivalent)			
	Oil	Coal	Gas	Sum
North America	8	170	7	185
South America	15	13	6	34
Europe	2	40	5	47
Africa	16	34	13	63
Russia	18	152	52	222
Middle East	101	0	62	167
India	1	62	1	64
China	2	76	2	80
Australia and east Asia	2	60	10	72
Total	165	607	162	934

Because a finite amount of fossil fuels is available, the global production of oil and natural gas will peak around 2010, according to the Association for the Study of Peak Oil (ASPO). For coal, the Energy Watch Group (EWG) claims that the peak of global coal production will occur around 2025. In 1956, Hubber[5] created a mathematical model that predicts the date of maximum oil production output (peak) for an oilfield, multiple oil fields, or an entire region, and this model can be applied to other fossil fuels. According to Hubber's peak theory, when fossil fuel reserves are discovered, the production increases exponentially until it reaches a peak, a singular event in the history of production, then after this peak, production starts declining. This behaviour follows a bell curve, which can be applied for estimating the fuel production by replaced X and y scales by the time and the production scale, respectively (Figure 1.1).

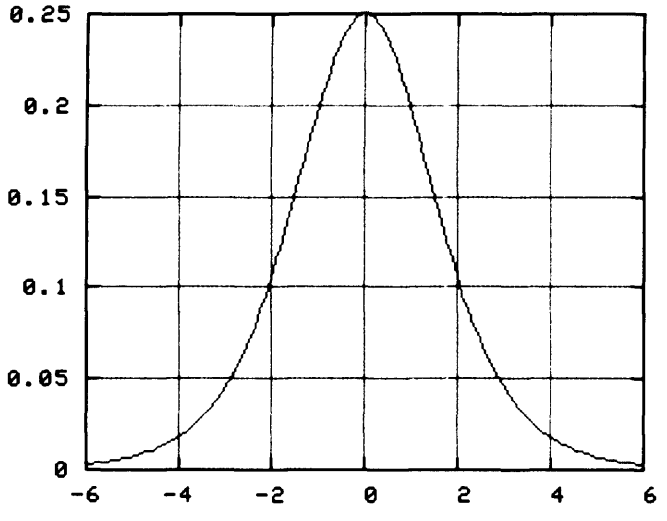

Figure 1.1: Standard Hubber's curve.

Due to the environmental problems arising from the combustion of fossil fuels and their depletion, the production and use of renewable fuels have grown rapidly in recent years. Many studies have focused on the sources of alternative and renewable energy to face the challenge of conventional fuels running out. These studies include the energy from water, wind, the sun, geothermals, and biomass sources. Although these energy sources have been known about in the past, their use was limited owing to various difficulties. The renewable sources are more expensive to use than fossil fuels and they are often located in distant regions, so great effort is required to transport this energy to cities. Moreover, renewable energy fuels are not always available. Renewable fuels are considered as primary energy sources and they are transformed to a secondary energy source, such as electricity and cleaner fuel by energy conversion processes. Among the secondary energy sources is hydrogen, which has the highest specific energy content of all conventional fuels, that is, fossil fuels and nuclear power.

1.2 Hydrogen as future fuel

Hydrogen is considered an energy carrier, not a primary energy source. Despite that, it is the dream fuel of the future. The only material that can be produced from the burning of hydrogen in air is water, a renewable eco-friendly product. Therefore, no pollutants are released that might have a negative effect on global warming, the ozone layer, and climate change.

Hydrogen is a promising option for replacing fossil fuels. Table 1.2 displays the physical and chemical properties of hydrogen compared to those of some of the fossil fuels. The energy of each fuel can be represented by the value of heat produced from the complete combustion of that fuel.

Table 1.2: The energy content of different fuels[6].

Fuel	Density (g/l)	Lower heating value (MJ/Kg)	Carbon Percentage %
Crude Oil	845	42.8	85.0
Natural gas	0.654	50.1	75.0
Conventional Gasoline	737	43.7	85.5
Conventional diesel	856	41.8	87.0
Hydrogen	0.0818	121.0	0

Despite the abundance of a large amount of hydrogen in the universe, nearly all of it exists as a compound, rather than in its pure form. Thus, to use it as fuel, it has to be extracted from its compounds by several methods, as shown in the next section.

The economy of the world depends on what type of energy source is used, and eras are named according to those sources. Two hundred and fifty years ago, the invention of the steam engine gave the name to

that era of modern technology. However, due to the extraction of fossil fuels and their use in all aspects of daily life, the world moved into the petroleum epoch. The considerable amount of research regarding the development of the production and application of hydrogen fuel has prepared the world to receive a new era, that is, the era of hydrogen.

The hydrogen economy, or the hydrogen market, is a term created by John Bockris during his talk in 1970 at General Motors (GM) Technical Center; it covers the generation of hydrogen from renewable and non-renewable energy sources, the storage, the transportation and the application. There is controversy about the feasibility of a hydrogen economy. The proponents of this technology claim that the use of hydrogen fuel has many advantages in terms of economic and energetic considerations:

- It is an environmentally friendly fuel; water is the only by-product from the combustion of hydrogen and there are no greenhouse gases.
- Decentralization of energy generation: because of the inherent nature of some areas for fossil fuels, the economy of developed and developing countries depends on oil importation. Additionally, some of them have reached their oil peak. In contrast, the production of hydrogen will not be limited to those countries, as hydrogen can be produced anywhere as long as water and electricity are available.

- Because of the abundance of hydrogen and because it can be produced from many cheap renewable energy sources, as mentioned previously, it will be considered the 'forever fuel'.

On the other hand, a hydrogen economy faces several obstacles, which are still the subject of controversy among scientists:

- Currently, 48% of the global supply of hydrogen is produced from natural gas, 30% from oil, 18% from coal and only 4% from electricity[7]. Hydrogen production from fossil fuels creates CO_2, that is, greenhouse gases. Furthermore, nitrogen oxides can be formed on account of hydrogen leakage. Consequently, developing technologies that can overcome CO_2 emission and the use of fossil fuels is a major target.
- Currently, the cost of generating and transporting hydrogen is greater than the cost of extracting, processing and transporting gasoline.
- Storage is one of the most important aspects of a hydrogen economy. Hydrogen can be stored as a compressed gas, as a liquid or by dissolving hydrogen gas in a metal. In addition, it can be stored as a solid in different types of chemicals, such as carbon nanotubes, or amine borane complex. The difficulties of hydrogen storage methods are almost all concerned with the storage density, which in turn affects its transportation. "The physical limits for the storage density of compressed and liquid hydrogen have more or less been reached, while there is still potential in the development of solid materials for hydrogen storage, such as

systems involving metal hydrides"[8]. So, the issues arising from the storage and transportation technologies of hydrogen can be overcome by continual research to make these technologies more convenient and economic.

1.3 Hydrogen production methods

To meet energy needs in the transport sector, where nearly all the H_2 would be used, and to power homes, businesses, plants and other industrial fields, the development of the production and storage of hydrogen will be an urgent issue. Hydrogen is produced industrially as a gas or liquid. The extraction of hydrogen from its compounds is achieved by several methods, which still need to be developed and modified to discover the economical feasibility of the commercial production of hydrogen. Figure 1.2 shows that there is a quite steady increase in the amount of global hydrogen produced from different methods.

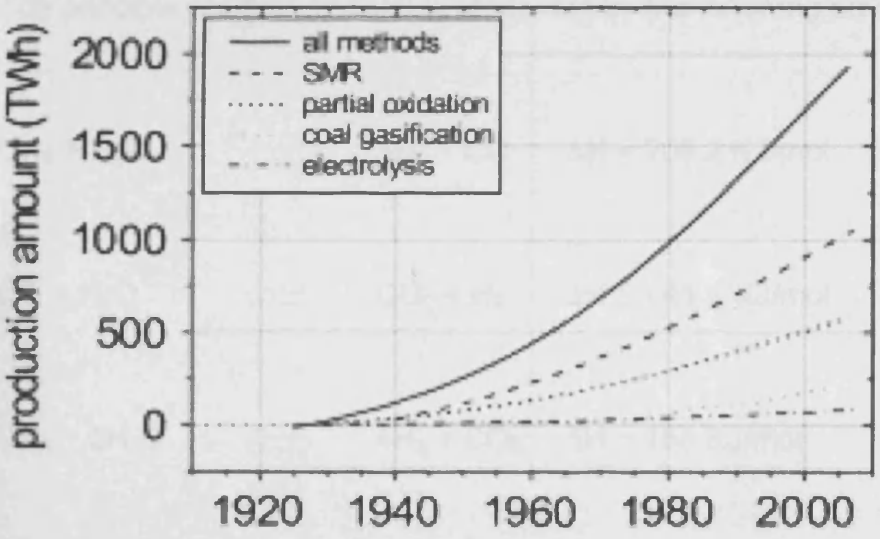

Figure 1.2: The annual global amount of hydrogen produced by different methods[9].

Today, over 90% of hydrogen is produced by steam reformation of natural gas. Due to the release of carbon dioxide from this process, the trend has been shifted to develop and create other methods, thus generating a clean fuel.

There are, however, several ways to produce hydrogen with renewable energy; most of them involve splitting water into its two components of hydrogen and oxygen, as water makes up 70% of the earth's surface. Some of these methods are described below, but not all the methods are appropriate for a hydrogen economy or are environmentally safe.

1.3.1 Steam reforming

Steam Methane Reforming (SMR) was developed in 1930 and became one of the most important processes for hydrogen production. The principle reaction of SMR is presented by the following equations[10]:

$$CH_4 + H_2O \Longleftrightarrow 3H_2 + CO \quad \Delta H = 206.2\ KJ/mol \qquad 1\text{-}1$$

$$CO + H_2O \Longleftrightarrow CO_2 + H_2 \quad \Delta H = -41.2\ KJ/mol \qquad 1\text{-}2$$

$$CH_4 + 2H_2O \Longleftrightarrow 4H_2 + CO_2 \quad \Delta H = 165\ KJ/mol \qquad 1\text{-}3$$

This process is reversible and endothermic, so it is carried out at 700 -900 °C and 15 – 30 × 10^5 Pa with nickel supported on alumina as a

catalyst. Despite the importance of this method, it faces some problems and limitations:

a) hydrogen production is limited to the equilibrium conversion of methane owing to the reversibility of the reaction[11],

b) it has CO_2 production as a by-product, which affects climate change,

c) there is catalyst deactivation due to carbon formation; therefore, there is a limit to the lifetime of the catalyst, and finally,

d) this process relies on the use of a fossil fuel (methane).

1.3.2 Electrolysis

Another method to produce hydrogen is the splitting of water into H_2 and O_2 when an electric current is sent through the water. This process is called electrolysis; it consists of an oxidation process at the anode to produce oxygen, and a reduction process at the cathode to produce hydrogen, as observed in the following equations:

Cathode (Reduction): $2H_2O(l) + 2e^- \longrightarrow H_2(g) + 2OH^-(aq)$ 1-4

Anode (Oxidation): $4OH^-(aq) \longrightarrow O_2(g) + 2H_2O(l) + 4e^-$ 1-5

Overall: $2H_2O(l) \longrightarrow 2H_2(g) + O_2(g)$ 1-6

This process is slow if the above reaction occurs in pure water, so an electrolyte (such as potassium chloride) must be added.

Hydrogen produced by electrolysis accounts for about 4% of production worldwide. Most of it is produced as a by-product of chlorine production. The efficiency of the electrolysis of water is about 50-80% to convert the electrical energy to hydrogen's chemical energy.

1.3.3 Thermochemical production

Splitting water into hydrogen and oxygen in this case can be achieved by using high temperature heat, though not electricity as in electrolysis, since thermal energy is cheaper than electrical energy. This method has great potential in the hydrogen economy. The heat source can be from concentrated solar energy that generates high temperatures reaching 2,000 °C. In addition, nuclear power supplies heat that reaches 1,000 °C.

1.3.4 Reforming of biomass and waste

Hydrogen can be produced from biomass and wastes as new renewable energy sources. The gasification of biomass is efficient, environmentally friendly, and has operational advantages. This process is classified according to the type of gasifying agent: air, steam, steam–oxygen, air–steam, oxygen-enriched air, and so on [12, 13]. There have been extensive studies regarding hydrogen production from waste materials and wastewater from industrial processes. The problems arising from this method are the low hydrogen production rate and yield [14, 15].

1.3.5 Photolysis

Two decades ago, great interest was shown in the photochemical reduction of water to generate hydrogen. Photolysis of water, photodecomposition, involves splitting water into hydrogen and oxygen using the photons. In other words, it is the conversion of photon energy to chemical energy, which is stored as hydrogen fuel. This process is presented in equation 1-7:

$$H_2O\ (l) + hv \longrightarrow H_2\ (g) + \tfrac{1}{2}O_2\ (g) \qquad 1\text{-}7$$

This reaction occurs when the potential difference is equal to or greater than 1.23 eV, the electromotive force, which is also derived from the following equation 1-8[16]:

$$E = \Delta G^{\circ}_{(H2O)} / 2N_A \qquad 1\text{-}8$$

where the standard Gibbs free energy (ΔG°) is 237.2 KJ/mol (2.46 eV) at 25 °C and Avogadro's number (N_A) is 6.022×10^{23}.

The enthalpy change, ΔH, of this reaction is 2.96 eV. This value corresponds to the wavelength of light of λ = 420 nm, which lies in the blue light region of the electromagnetic spectrum. The solar spectrum, figure1.3, consists of the regions from the near infrared to the near ultraviolet while water absorbs light at λ < 200 nm, figure 1.4[17]. Therefore, the water will not split if it is exposed directly to sunlight In

addition to that, according to the Born-Haber cycle[18], breaking the H-OH bond requires a high amount of energy (494.8 kJ/mole) which is greater than the thermodynamic bond energy. So to form hydrogen and oxygen gases, the energy required to remove both hydrogen atoms must be found. This can be achieved by a mediator or chemical species to convert the solar energy to chemical energy. This point leads to the discussion in section 1.4 of what is known as photocatalysis.

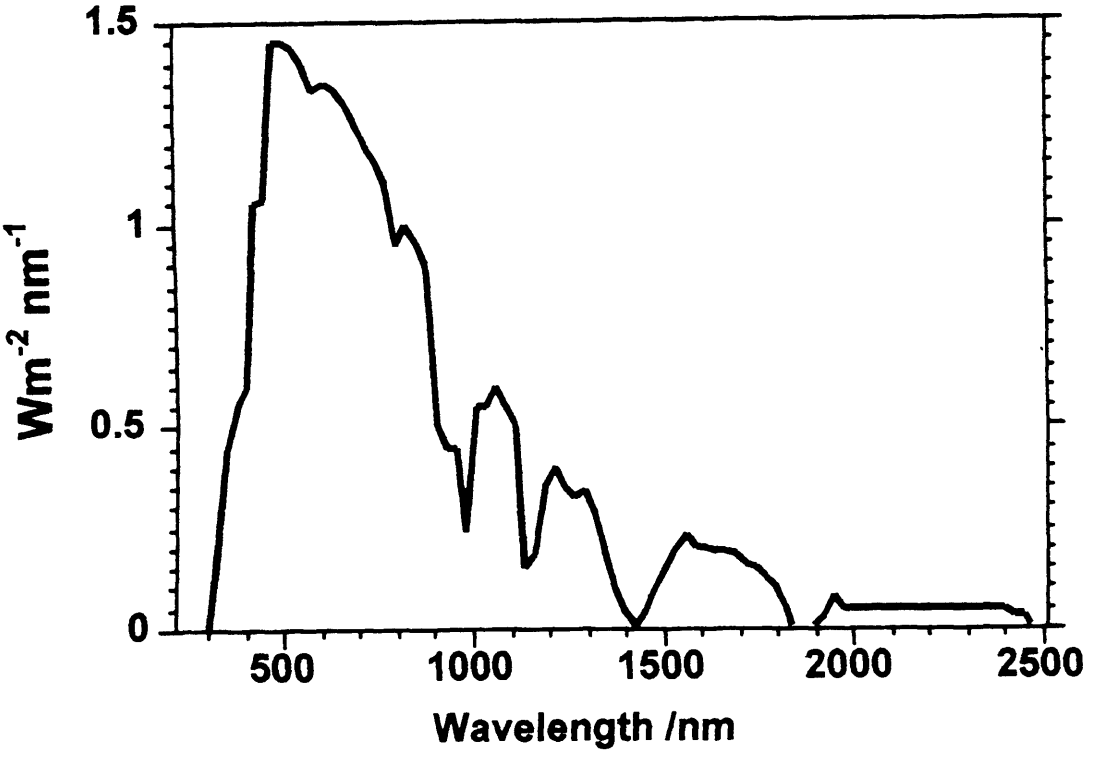

Figure 1.3: The solar emission spectrum.

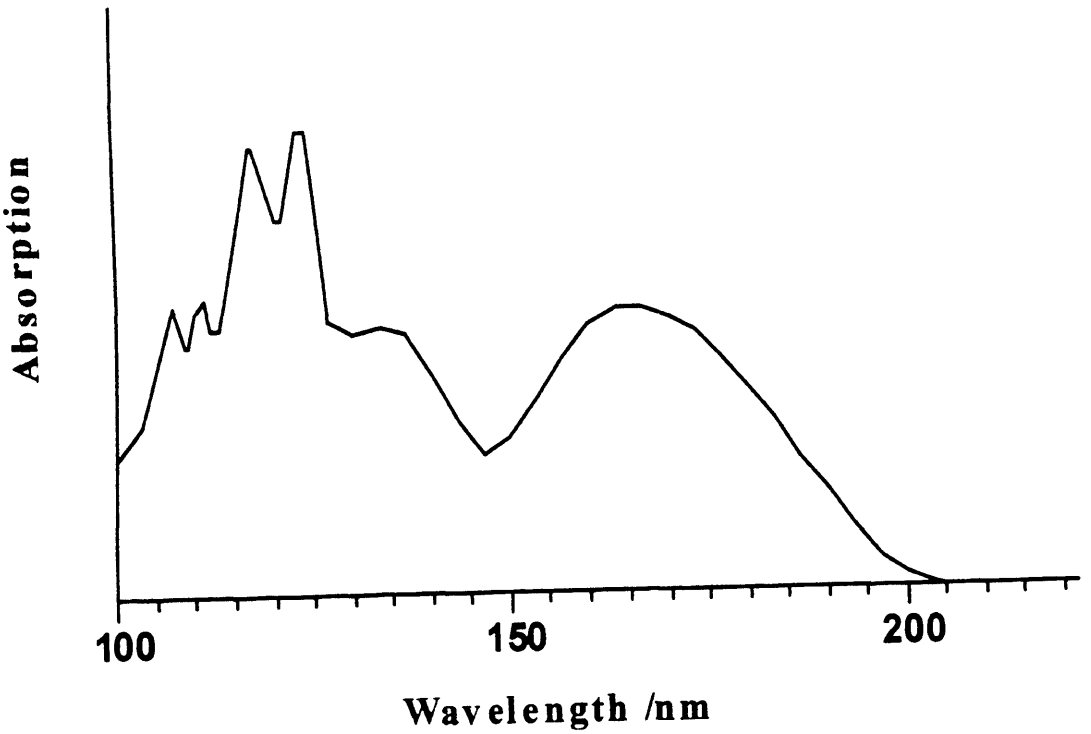

Figure 1.4: The absorption spectrum of water.

1.4 Photocatalysis

A catalyst increases the rate of chemical reactions by reducing of the activation energy; therefore, many people have been searching for a catalyst to increase the rate of water splitting.

"Photocatalysis is the acceleration of a photoreaction by the presence of a catalyst"[19]. Heterogeneous photocatalysis involves two kinds of photoreaction. On the one hand, if the catalyst interacts with a photoexcited adsorbed molecule, the process is called a catalysed photoreaction. On the other hand, if the adsorbate molecule interacts with the photoexcited catalyst, the process is referred to as a sensitized photoreaction. After the innovative work by Fujishima and Honda, which

involved the photoelectrocatalytic water splitting on TiO_2 electrodes[20], there have been a significant number of studies in the field of heterogeneous photocatalysis. Fujishima and Honda's work is a simulation of what occurs in nature, since during the photosynthesis process that takes place in plants, CO_2 and water, readily available materials, are converted to O_2 and carbohydrates using solar energy. Therefore, photosynthesis has been taken as a model for artificial photosynthesis in the generation of hydrogen as a clean fuel from solar energy.

The significance of photocatalysis stems from the possibility that it can achieve an enormous number of reactions, which can play a significant role in economical and commercial development. Because of the promising features of the photocatalytic processes, they are applied in the following technologies as a replacement for traditional methods:

a) Synthesis of organic compounds

Some reactions, such as oxidation and oxidative cleavage, reduction, isomerization, substitution, and polymerization, can be accomplished using TiO_2 in an oxidatively inert solvent[21, 22].

b) Synthesis of inorganic compounds

Photocatalysis has attained significant importance in the synthesis of coordinatively unsaturated species, transition metal compounds with a changed oxidation state, free ligands and ligand redox products [23].

c) Air purification

Air pollution is among the threats to humans and other living organisms, as it causes climate change, global warming, and ozone depletion. This problem has grown in recent years owing to the industrial revolution and the population explosion. Because of the limitations of the conventional methods used in air cleaning, photocatalytic detoxification technology is of great interest[24].

d) Water purification

The developed and developing countries in particular face a major environmental problem, that is, water pollution, even though it is considered a global issue. Photocatalytic degradation is an alternative method in the treatment of wastewater. This technology has proved its success and effectiveness for the removal of persistent organic and inorganic impurities[25-28].

e) Solar energy conversion

Solar energy is versatile since it can be converted to electricity, heat and fuel. Hydrogen as fuel can be generated from sunlight and water, both are renewable sources. This method, which is known as solar water splitting, has gained great importance due to it providing clean, renewable fuel [29-32]. In recent years, studies have focused on developing methods to obtain the maximum efficiency of solar conversion and quantum yield, and, therefore, to meet the energy requirements of large-scale manufacturing and practical uses. Several methods have been used to

generate hydrogen fuel from solar water splitting; these have varying restrictions, such as direct or indirect photothermal, photosynthetic, photoelectrochemical limitations. Table 1.3 summarises the limitations and potential of these processes.

Table 1.3: Solar water splitting processes[33].

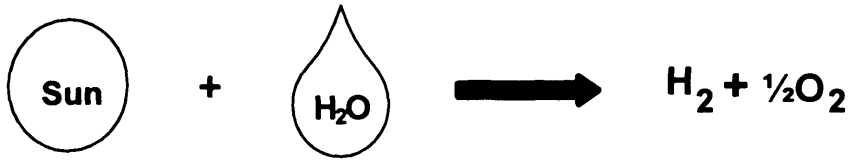

Process	Limitations, potential
Photosynthetic, biological & photochemical	Demonstrated efficiencies very low, Generally < 1% solar energy conversion
Photothermal, single step(direct)	Gas recombination limitations, high temperature material limitations, generally < 1% solar energy conversion
Photothermal, multistep	Lower temp than single step, although stepwise reaction inefficiencies lead to losses, generally < 10% solar conversion
Photoelectrochemical	10-20% solar conversion
Photothermal, electrochemical	potential for > 20% solar conversion, requires solar concentration

The production of hydrogen by the photocatalytic water splitting method involving a semiconductor is a promising development in the field of the energy and the environment. Figure 1.5 presents a simple model for a solar hydrogen system.

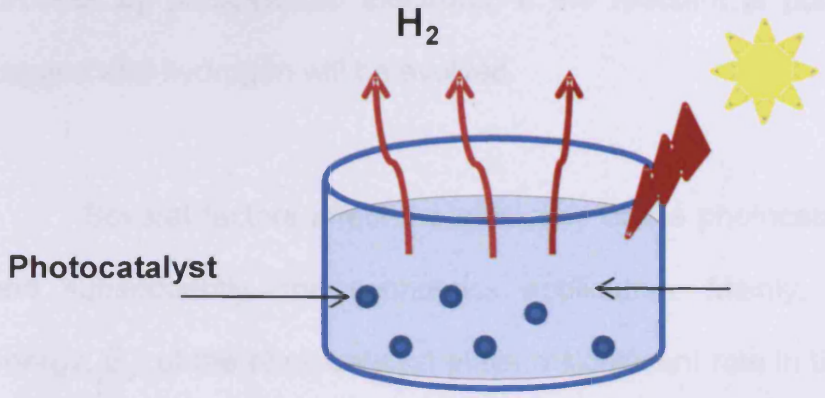

Figure 1.5: Production of solar hydrogen by photocatalytic water splitting.

Because water itself does not absorb radiation within the solar spectrum, many materials have been investigated that can harvest sunlight; these are known as photocatalysts. Such materials convert the photon energy to chemical or electrical energy by forming electron/hole pairs. When the photocatalyst is exposed to light, an electron absorbs the photon, becomes excited, and moves from a lower energy level to a higher one, forming a hole. The photoexcitation takes place when the energy of the photon is equal to, or greater than, the difference in the

energies of those levels, E_g, which will be described in more detail in section 1.5.1. The carrier charge species (electron/hole pairs) are employed for reductive and oxidative processes. Thus, photocatalysis involves two processes that occur simultaneously. The first is water being oxidized by photogenerated holes and the second is the reduction process by photoexcited electrons. If the reactant is pure water, both oxygen and hydrogen will be evolved.

Several factors affect the efficiency of the photocatalytic reaction, and subsequently, the economics application. Mainly, the threshold energy, E_g, of the photocatalyst plays a significant role in these reactions and in particular, the production of solar hydrogen through water splitting. Another factor that plays a major role in the activity of photocatalysis is the rate of recombination of photogenerated carriers. Many successful attempts have been made to separate the photoexcited electron-hole and thus reduce the recombination rate. The conversion of light energy is still low, as is the quantum yield of the photoreactions. This is the most important factor that restricts the practical use of photocatalytic reactions[34].

1.5 Photocatalyst

Enormous numbers of photochemical, chemical and electrochemical processes occur on the surface of photocatalysts. The

efficiency and rates of these reactions depend on several factors, some of which are related to the type of photocatalyst.

Semiconductors have been studied intensively and used widely in all the applications of photocatalysis. This will be discussed in detail in the next section, since this project uses mainly semiconductors as photocatalysts.

1.5.1 Semiconductors

The electronic and physico-chemical properties of semiconductors play an essential role in the photocatalytic mechanism. According to band theory, the valence electrons occupy a number of levels, which are grouped together as bands. The highest occupied band called the valence band (VB) is fully occupied in a semiconductor. The next band called the conduction band (CB) is empty and exists only if some electrons are excited to this band, whereby its energy level becomes higher than that of the VB. These bands are separated by a forbidden region, which can contain no electron states; it extends from the top of the VB to the bottom of CB, and is known as the band gap. The size of this region affects the properties of semiconductors. This kind of photocatalyst is strongly affected by temperature, as is its conductivity. Increasing the temperature leads to increase the energy of the electrons. The conductivity depends on the number of electrons that have been promoted across the band gap. Thus, the conductivity increases in proportion to the increase in the temperature.

Illuminating of the semiconductor catalyses many interesting reactions, including uphill chemical reactions, like hydrogen production from water. When the energy of a photon is equal to or greater than the band gap, the semiconductor absorbs it and an electron in the VB is excited to the CB leaving a positive hole (h^+) in the VB. Figure 1.6 represents this process. In the case of applying an electric field, the electrons in the VB will occupy the generated holes, hence, current flows. Therefore, the direction of electrons in the CB is contrary to that of the holes. The band gap of semiconductors is in the range of 0.3-3.5 eV; in some definitions, the upper limit is at 4 eV. Materials with band gaps larger than this are closed as insulators.

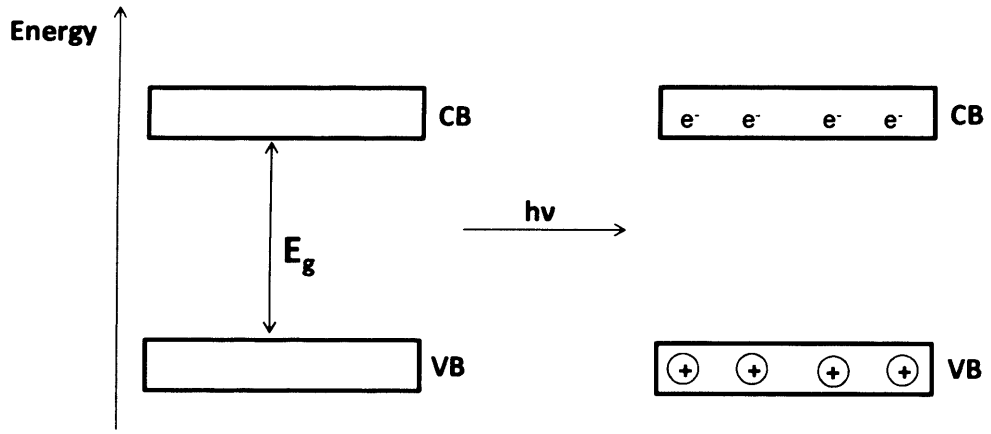

Figure 1.6: Photoexcitation of semiconductor.

Photogenerated charge carriers (e^- in CB and h^+ in VB) undergo different competitive pathways, as shown in Figure 1.7, which can be summarised as follows:

a) Transferring the free electron to the surface and reducing the adsorbed acceptor (reduction).
b) Transferring the positive hole to the surface and oxidising the adsorbed donor (oxidation).
c) Recombining the trapped electron and hole either at the bulk of the semiconductor or at or near the surface, thus producing light emission.

Anion vacancies can act as electron 'traps'. For the holes, oxygen vacancies or other defect sites may be suitable traps to separate the photogenerated charge carriers. Such trapped electrons and holes are employed in chemical reactions or photocorrosion. The latter is undesirable since it is an irreversible separation and leads to loss of the photocatalyst. The recombination of electron and hole reduces the efficiency of the photochemical reaction. Given the difficulty of measuring the actual amount of absorbed light in heterogeneous system as the light is scattered by semiconductor, the efficiency is estimated as a quantum yield, which is defined as the number of events occurring per photon absorbed.

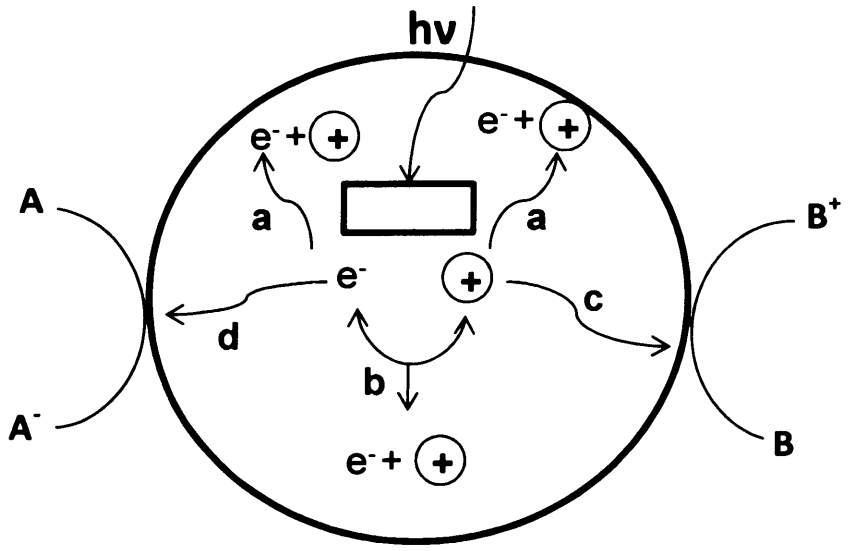

Figure 1.7: Schematic photoexcitation and deexcitation in semiconductors. a) recombination at the surface, b) recombination in the bulk, c) oxidation and d) reduction.)

Besides the need for the separation of charge carriers, there is another constraint that limits the use of most semiconductors as photocatalysts. The transfer of photogenerated electrons and holes to the adsorbed molecules on the surface is ruled by the band edge positions of the semiconductor and the redox potentials of the adsorbates. Table 1.4 represents the band edge positions, the energy of the band gap and the equivalent wavelength of some semiconductors.

Table 1.4: Energies of the conduction band, the valence band, the band gap and the wavelengths of some common semiconductors in water at pH = 1[35].

Semiconductors	E_{VB} (V vs. SCE)	E_{CB} (V vs. SCE)	E_g (V)	λ(Eg) (nm)
GaAs	0.8	- 0.6	1.4	890
InP	1.2	- 1.0	1.3	950
GaP	1.4	- 0.9	2.3	540
CdSe	1.4	- 0.3	1.7	730
CdTe	1.4	0.0	1.4	890
CdS	2.2	- 0.2	2.4	520
ZnO	2.9	- 0.1	3.0	390
$SrTiO_2$	3.0	- 0.2	3.2	390
SnO_2	3.8	- 0.3	3.5	350
TiO_2	3.0	0.0	3.0	410

There is a high tendency for the photogenerated electron-hole pair to recombine and increase the energy of the band gap of semiconductors so they are able to absorb visible light, which is discussed in Chapter 4; this is overcome by modifying their surface. Improving the photocatalytic activity by modification has become a rule of great importance in the scientific community in recent years.

Doping metal on oxide semiconductors is one of the successful solutions to suppress charge recombination and enhance the photocatalytic reaction. Metal plays an apparent role in changing the electronic properties of semiconductors, as the Schottky barrier produced at the interface of metal-semiconductors can trap the photogenerated electrons efficiently and, therefore, inhibit recombination. The effect on the efficiency of photocatalytic processes of adding metal to semiconductor depends on the preparation method and the formed physicochemical properties of the metal doped semiconductor. Thermal impregnation and photodeposition are good examples for preparing such photocatalysts. The latter is more effective than others. Numerous studies have been conducted to demonstrate the value of this kind of modification[36-38].

The presence of dissolved metal ions with semiconductors in photocatalytic systems also has a beneficial effect on the oxidation of many organic compounds, such as phenol[39, 40], and aliphatic hydrocarbons[41, 42]. If the standard reduction potential of a metallic couple is more positive than the CB of a semiconductor, the metal ion will be photoreduced (Figure 1.8). That means that the photoinduced electrons are trapped and, hence, the undesired recombination is inhibited during the illumination.

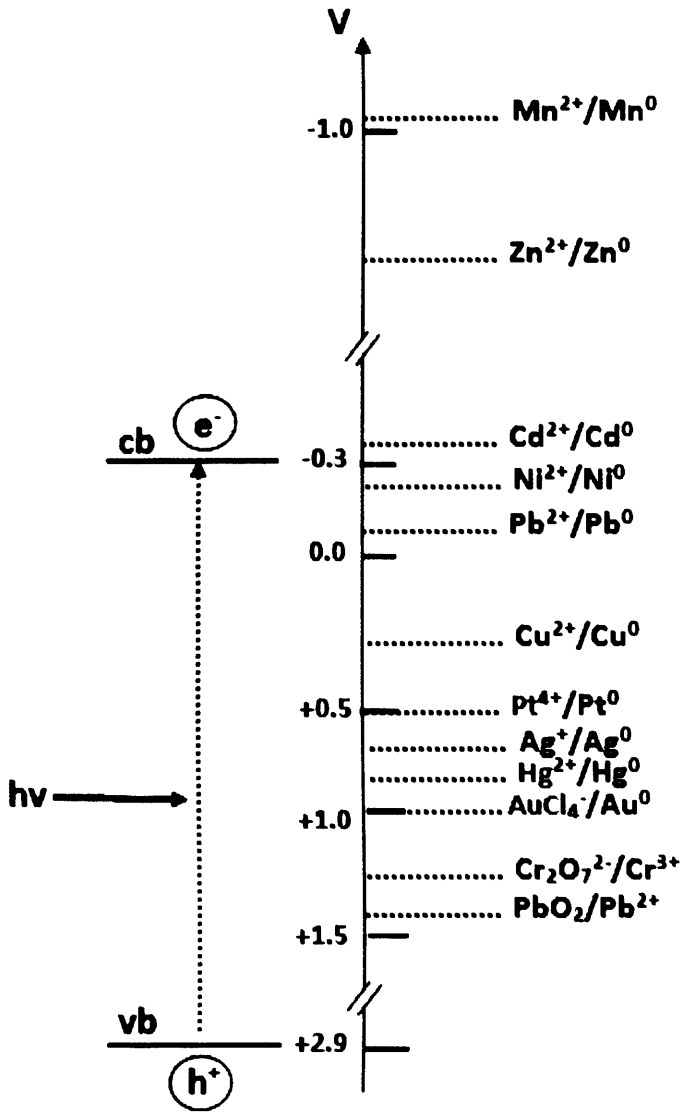

Figure 1.8: The standard redox potentials of various metallic couples against the band edge positions of TiO_2(P25) at pH = 0[43].

Coupling two kinds of semiconductors that have different energy band gaps is an alternative and promising approach in the development of efficient photocatalysts for water splitting. Compositing two different semiconductors can separate the photogenerated electrons and holes on different semiconductor surfaces. Thus, the reduction and oxidation can

occur with great efficiency. When CdS (Eg = 2.42 eV) is coupled with TiO_2 (Eg = 3.2 eV), the electron is excited from the VB of Cd, leaving behind a hole, and the electron migrates to the CB of TiO_2. This behaviour takes place according to the geometric interaction of multiple particles of CdS with the TiO_2 particle surface. Thus, the suppression of recombination and the high efficiency of the photocatalytic process are achieved. Furthermore, the limitation of the use of TiO_2 under only the ultraviolet region, due to its wide band gap, can be overcome by using CdS with a band gap in the visible range[44-47].

Semiconductors have a large potential in photocatalytic systems, as they are considered one of the best materials for their properties either in their natural or amended states. Moreover, due to the simplicity of their processing technologies, these photocatalysts have a bright future regarding the economical aspect, in particular. In the early research for such materials, much attention was focused on water purification and then extended to air purification and other technologies, such as solar hydrogen. In the development of semiconductors for photocatalytic water splitting, there are some requirements regarding these materials; in order for them to be effective [19, 48], they must be

1- Photocatalytic active
2- Biologically and chemically stable
3- Resistant to photo-corrosion
4- Inexpensive
5- Activated by sunlight

6- For water photolysis specifically, the energy of the conduction band (E_{CB}) must be higher or more negative than the hydrogen evolution potential on the electrochemical scale and the energy of valence band (E_{VB}) must be lower (more positive) than the oxygen evolution potential.

Taking into account all these requirements, the developed semiconductor aims to achieve the maximum efficiency of sunlight absorption, a maximum rate of charge separation and an optimum quantum yield. The semiconductor that best meets most of these requirements is titanium dioxide (TiO_2). This photocatalyst is the main one used in this project.

1.5.2 Titanium dioxide (TiO_2)

The first application of titania (TiO_2) was reported in the solar energy conversion field[49] and then it was found to be a fascinating material in photocatalysis to solve environmental issues. Due to its whiteness, high stability, opacity, nontoxicity, and availability TiO_2, is used mainly as a pigment. Nowadays, it has many other valuable applications, which are economically and industrially promising, such as self-cleaning, anti fogging, and anticorrosion surfaces.

TiO_2 is considered the best candidate in solar hydrogen research because it has unique features that fit with all the requirements

mentioned above except that it absorbs only ultra violet radiation owing to its wide band gap.

Titanium dioxide does not exist as a pure material in nature, but can be extracted from a variety of ores located throughout the world, such as ilmenite, which may contain 40-70% TiO_2. Two processes produce TiO_2 products: the first is the chloride process, as the titanium ore reacts with chlorine gas, while in the second, sulphuric acid is introduced to these ores. The European market produces 70% of TiO_2 by the sulphuric process.

Anatase, rutile, and brookite are the three main types of TiO_2. Rutile is the most stable (the particles size are above 35 nm), while anatase (below 11 nm) and brookite (11 - 35 nm) are stable for fine grained natural and synthetic samples [50]. At high temperatures, anatase and brookite are transformed into rutile, the stable phase. Most studies have focused on anatase and rutile, as brookite is rarely available. There are some differences between anatase and rutile phases in terms of specific gravity, hardness and refractive index, and other physical and chemical behaviours[51].

These two polymorphic phases crystallize in a tetragonal lattice. Their structure is a chain of TiO_6 octahedrals, which are more distorted in anatase than in rutile. However, anatase is a less closely packed structure than is rutile. Figures 1.9 and 1.10 represent the crystal structure of anatase and rutile, respectively.

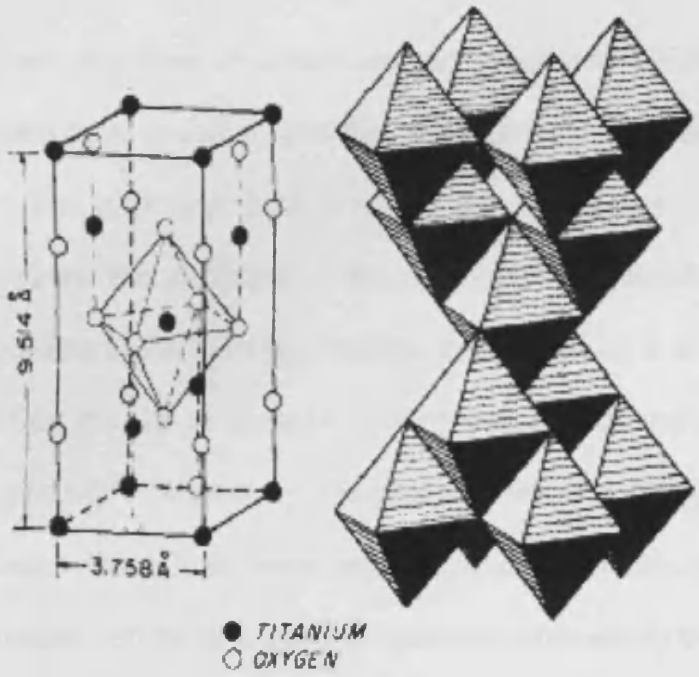

Figure 1.9: Crystal structure of anatase.

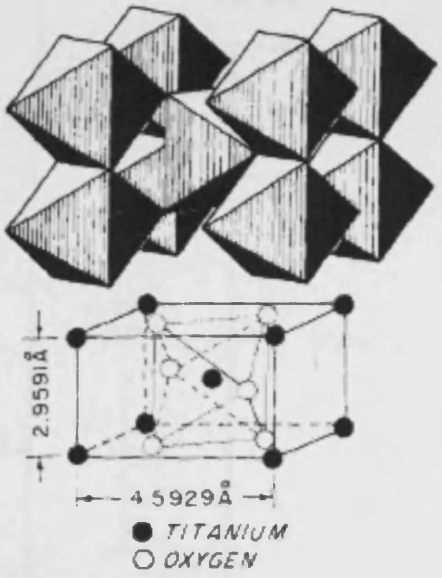

Figure 1.10: Crystal structure of rutile.

The electronic structure of semiconductors plays a significant role in their activities in photocatalytic reactions. UV-visible spectroscopic studies have revealed that the band gaps of anatase and rutile are 3.23 eV (384 nm) and 3.02(411 nm) eV, respectively [43, 49]. Figure 1.11 illustrates the positions of the VB and the CB of anatase and rutile. According to the density of states, their VB width is similar but different for the CB, the CB of anatase is narrower and its energy is larger than the CB of rutile[52]. Moreover, it is expected that it is difficult to reduce anatase because the CB is more negative than the H^+/H_2 potential. Therefore, hydrogen can be produced on anatase more easily than on rutile but less efficiently owing to the wider band gap.

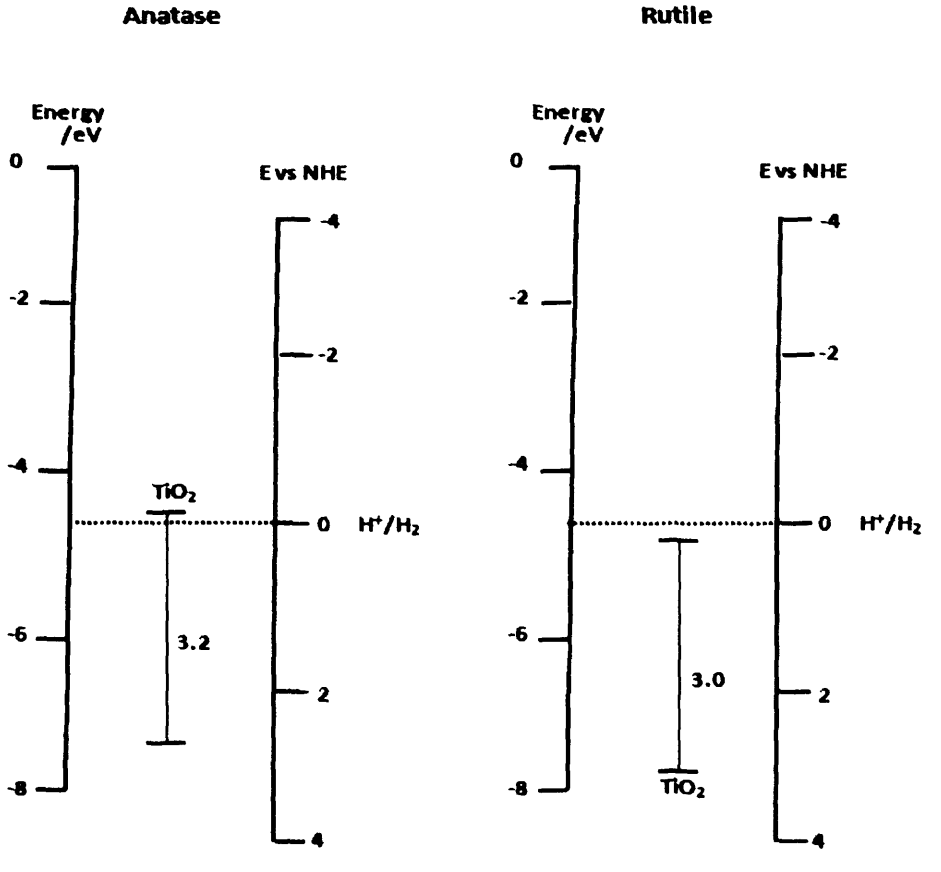

Figure 1.11: Energies for anatase and rutile TiO_2 in water PH = 1.

To increase the rate of electron-hole separation and, hence, the efficiency of photoreaction, a new photocatalyst was prepared, comprising 70% of anatase and 30% of rutile (or 80% anatase, 20% rutile). It is called Degussa P25 TiO_2 in which anatase reacts positively with rutile [53, 54]. TEM showed that TiO_2 P25 is formed from anatase and rutile separately[55]. It was found that the photocatalytic activity of TiO_2 P25 is more than that of anatase or rutile alone[56]. Titanium dioxide is among semiconductors, which has received considerable attention from researchers in the field of hydrogen production from photocatalytic water splitting [57-59]. The photocatalytic activity of TiO_2 depends on many factors, such as the anatase/rutile ratio, preparation method, particle size, specific surface area and so on. For example, on the one hand, decreasing the particle size of TiO_2 increases the surface area; in turn, this increases the number of active sites that can absorb the desired species. On the other hand, the small particles increase the rate of migration of photogenerated charge carriers from the bulk to the surface and, therefore, the photocatalytic reaction increases.

Most research deals with the photodegradation of organic compounds as one of the applications of TiO_2. TiO_2, as a photocatalyst, plays an important role in the decontamination of water and air. This is attributed to the high oxidation power of photoinduced holes. Photogenerated hole is as OH^- or $OH^\cdot$ chemisorbed radicals which was proved by ESR measurements[60].

The first use of TiO_2 in photocatalytic water splitting was in Fujishima and Honda's work. Because it is difficult to find a photocatalyst that absorbs light under the visible region and at the same time is photostable, the efficiency of solar hydrogen conversion is low. This problem has meant researchers have viewed the development of titania in different ways.

1.6 The objectives

Study of the reforming of methanol on Pd and Au loaded on TiO_2 (P25) is the first objective of this project in Chapter Three. The factors that affect the activities of these photocatalysts are investigated, such as metal loading, methanol concentration, and wavelength. Additionally, the results obtained from the liquid phase are compared with those of the gas phase. In this chapter, the reforming of higher alcohols, and glycerol in particular, which is one of the solutions for converting huge amounts of glycerol from the manufacture of biodesiel have been studied.

Doping titania with a non metallic atom, such as nitrogen, is tested in photocatalytic hydrogen production. Such a photocatalyst, which absorbs visible radiation, is characterised. These results are discussed in Chapter Four.

Chapter Five deals with the splitting of pure water over titania and palladium and gold-loaded titania to understand the mechanism more

clearly. Moreover, the concept of a back reaction between hydrogen and oxygen over these photocatalysts is studied.

Finally, the concluding chapter summarizes the results obtained from all the experiments, which gives the optimum rate of hydrogen production.

1.7 References

[1] John and M. Gribbin in *The Greenhouse Effect Vol.* **06 July 1996**.

[2] W. Cui, L. Feng, C. Xu, S. Lu and F. Qiu, *Cuihua Xuebao* **2003**, *24*, 937-941.

[3] L. Millard and M. Bowker, *Journal of Photochemistry and Photobiology, A: Chemistry* **2002**, *148*, 91-95.

[4] C. E. Taylor, R. P. Noceti, J. R. D'Este and D. V. Martello, *Studies in Surface Science and Catalysis* **1996**, *101*, 407-416.

[5] N.-L. Wu and M.-S. Lee, *International Journal of Hydrogen Energy* **2004**, *29*, 1601-1605.

[6] M. Granovskii, I. Dincer and M. A. Rosen, *International Journal of Hydrogen Energy* **2006**, *31*, 337-352.

[7] R. Kikuchi, *Environmental Impact Assessment Review* **2006**, *26*, 206-218.

[8] M. Ball and M. Wietschel, *International Journal of Hydrogen Energy* **2008**, *In Press, Corrected Proof.*

[9] K. Schoots, F. Ferioli, G. J. Kramer and B. C. C. van der Zwaan, *International Journal of Hydrogen Energy* **2008**, *33*, 2630-2645.

[10] Z. Chen, J. R. Grace, C. Jim Lim and A. Li, *International Journal of Hydrogen Energy* **2007**, *32*, 2359-2366.

[11] W. Yu, T. Ohmori, S. Kataoka, T. Yamamoto, A. Endo, M. Nakaiwa and N. Itoh, *International Journal of Hydrogen Energy* **2008**, *33*, 685-692.

[12] N. Gao, A. Li, C. Quan and F. Gao, *International Journal of Hydrogen Energy* **2008**, *33*, 5430-5438.

[13] P. Ji, W. Feng and B. Chen, *Chemical Engineering Science* **2009**, *64*, 582-592.

[14] D. Sivaramakrishna, D. Sreekanth, V. Himabindu and Y. Anjaneyulu, *Renewable Energy* **2009**, *34*, 937-940.

[15] M. Li, Y. Zhao, Q. Guo, X. Qian and D. Niu, *Renewable Energy* **2008**, *33*, 2573-2579.

[16] T. Bak, J. Nowotny, M. Rekas and C. C. Sorrell, *International Journal of Hydrogen Energy* **2002**, *27*, 991-1022.

[17] L. R. Millard in *'The Photocatalytic Production of Hydrogen', Vol. PhD* University of Reading, **2003**.

[18] A. J. Dickinson in *"Photocatalytic Hydrogen Production", Vol. PhD* Reading University, **1997**.

[19] A. Mills and S. Le Hunte, *Journal of Photochemistry and Photobiology A: Chemistry* **1997**, *108*, 1-35.

[20] K. Honda and A. Fujishima, *Nature* **1972**, *238*, 37-38.

[21] T. Ohno, Y. Masaki, S. Hirayama and M. Matsumura, *Journal of Catalysis* **2001**, *204*, 163-168.

[22] P. Boarini, V. Carassiti, A. Maldotti and R. Amadelli, *Langmuir* **1998**, *14*, 2080-2085.

[23] H. Hennig and R. Billing, *Coordination Chemistry Reviews* **1993**, *125*, 89-100.

[24] G. Xiao, X. Wang, D. Li and X. Fu, *Journal of Photochemistry and Photobiology A: Chemistry* **2008**, *193*, 213-221.

[25] S. Devipriya and S. Yesodharan, *Solar Energy Materials and Solar Cells* **2005**, *86*, 309-348.

[26] A. P. Davis and C. P. Huang, *Water Research* **1990**, *24*, 543-550.

[27] C. Galindo, P. Jacques and A. Kalt, *Chemosphere* **2001**, *45*, 997-1005.

[28] H. D. Burrows, M. Canle L, J. A. Santaballa and S. Steenken, *Journal of Photochemistry and Photobiology B: Biology* **2002**, *67*, 71-108.

[29] S. Licht, S. Ghosh, H. Tributsch and S. Fiechter, *Solar Energy Materials and Solar Cells* **2002**, *70*, 471-480.

[30] S. Licht, B. Wang, S. Mukerji, T. Soga, M. Umeno and H. Tributsch, *International Journal of Hydrogen Energy* **2001**, *26*, 653-659.

[31] S. Licht, *Electrochemistry Communications* **2002**, *4*, 790-795.

[32] Y. V. Kuzminskii and G. Y. Kolbasov, *Solar Energy Materials and Solar Cells* **1998**, *56*, 93-115.

[33] S. Licht, *International Journal of Hydrogen Energy* **2005**, *30*, 459-470.

[34] A. I. Kryukov, S. Y. Kuchmii and V. D. Pokhodenko, *Theoretical and Experimental Chemistry* **1995**, *30*, 141-157.

[35] P. Somasundaran, *Encyclopedia of Surface and Colloid Science* CRC Press, **2006**, p. 2312.

[36] A. Hameed, M. A. Gondal and Z. H. Yamani, *Catalysis Communications* **2004**, *5*, 715-719.

[37] G. R. Bamwenda, K. Sayama and H. Arakawa, *Journal of Photochemistry and Photobiology A: Chemistry* **1999**, *122*, 175-183.

[38] G. R. Bamwenda, T. Uesigi, Y. Abe, K. Sayama and H. Arakawa, *Applied Catalysis A: General* **2001**, *205*, 117-128.

[39] A. Sclafani, L. Palmisano and E. Davì, *Journal of Photochemistry and Photobiology A: Chemistry* **1991**, *56*, 113-123.

[40] T.-Y. Wei, Y.-Y. Wang and C.-C. Wan, *Journal of Photochemistry and Photobiology A: Chemistry* **1990**, *55*, 115-126.

[41] M. Bideau, B. Claudel, L. Faure and H. Kazouan, *Journal of Photochemistry and Photobiology A: Chemistry* **1991**, *61*, 269-280.

[42] M. Bideau, B. Claudel, L. Faure and H. Kazouan, *Journal of Photochemistry and Photobiology A: Chemistry* **1992**, *67*, 337-348.

[43] M. I. Litter, *Applied Catalysis B: Environmental* **1999**, *23*, 89-114.

[44] J. C. Tristão, F. Magalhães, P. Corio and M. T. C. Sansiviero, *Journal of Photochemistry and Photobiology A: Chemistry* **2006**, *181*, 152-157.

[45] P. Chatchai, Y. Murakami, S.-y. Kishioka, A. Y. Nosaka and Y. Nosaka, *Electrochimica Acta* **2009**, *54*, 1147-1152.

[46] H. Yang, L. Guo, W. Yan and H. Liu, *Journal of Power Sources* **2006**, *159*, 1305-1309.

[47] A. L. Linsebigler, G. Lu and J. T. Yates, *Chemical Reviews* **1995**, *95*, 735-758.

[48] A. Mills and S.-K. Lee, *Journal of Photochemistry and Photobiology A: Chemistry* **2002**, *152*, 233-247.

[49] A. Fujishima, X. Zhang and D. A. Tryk, *Surface Science Reports* **2008**, *63*, 515-582.

[50] M. R. Ranade, A. Navrotsky, H. Z. Zhang, J. F. Banfield, S. H. Elder, A. Zaban, P. H. Borse, S. K. Kulkarni, G. S. Doran and H. J. Whitfield, *Proceedings of the National Academy of Sciences of the United States of America* **2002**, *99*, 6476-6481.

[51] R. Hengerer, B. Bolliger, M. Erbudak and M. Grätzel, *Surface Science* **2000**, *460*, 162-169.

[52] A. Bouzoubaa, A. Markovits, M. n. Calatayud and C. Minot, *Surface Science* **2005**, *583*, 107-117.

[53] A. R. Gandhe and J. B. Fernandes, *Journal of Molecular Catalysis A: Chemical* **2005**, *226*, 171-177.

[54] B. Sun and P. G. Smirniotis, *Catalysis Today* **2003**, *88*, 49-59.

[55] A. K. Datye, G. Riegel, J. R. Bolton, M. Huang and M. R. Prairie, *Journal of Solid State Chemistry* **1995**, *115*, 236-239.

[56] T. Ohno, K. Sarukawa, K. Tokieda and M. Matsumura, *Journal of Catalysis* **2001**, *203*, 82-86.

[57] J. Nowotny, T. Bak, M. K. Nowotny and L. R. Sheppard, *International Journal of Hydrogen Energy* **2007**, *32*, 2609-2629.

[58] M. Hepel and I. D. Kumarihamy, *International Journal of Hydrogen Energy* **2007**, *32*, 2693-2702.

[59] R. Dholam, N. Patel, M. Adami and A. Miotello, *International Journal of Hydrogen Energy* **2008**, *33*, 6896-6903.

[60] L. Sirghi, Y. Hatanaka and T. Aoki, *Applied Surface Science* **2005**, *244*, 408-411.

CHAPTER TWO

Experimental

2.1 Introduction

The photocatalytic reactions in this project have been carried out in Pyrex vessels whether in liquid and gas phase and in an inert atmosphere. In all the experiments, the catalysts were irradiated by a xenon arc lamp. The hydrogen was detected by gas chromatography (GC).

In this chapter, the experimental set-up, the preparation and characterization of the catalysts are discussed.

2.2 The experimental set-up

The experimental arrangement used in this project was devised by Dickinson[1] which was similar to Domen's apparatus[2] with some modifications. Bowker's group used Dickinson's device for photocatalytic hydrogen production in the liquid and gas phase[3-5] as shown in figure 2.1. Some parts of the reactor were modified in this work as discussed in the following sections.

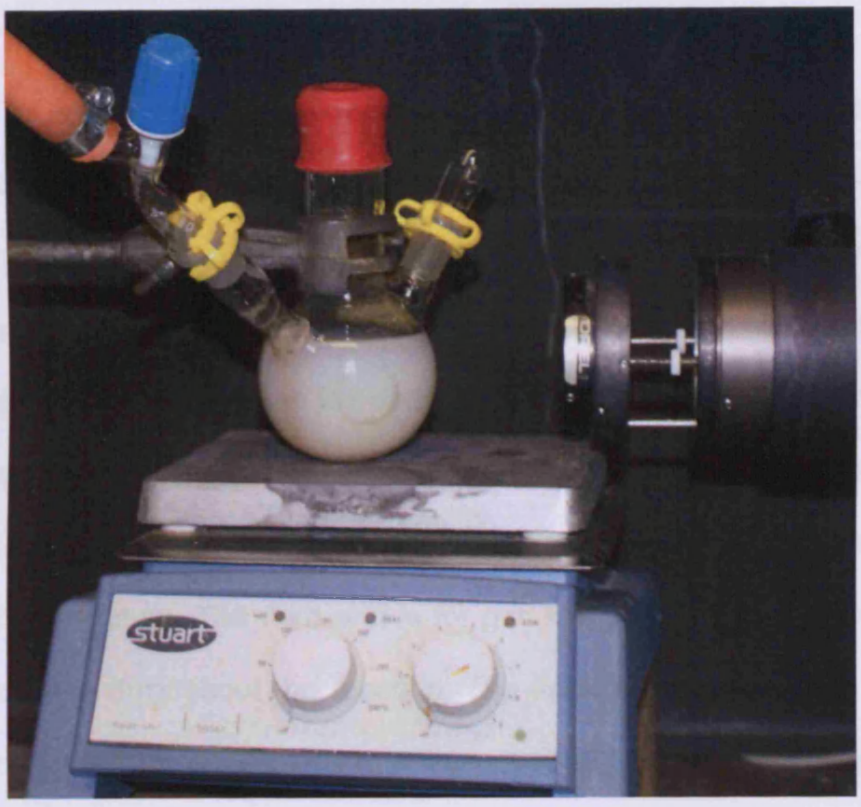

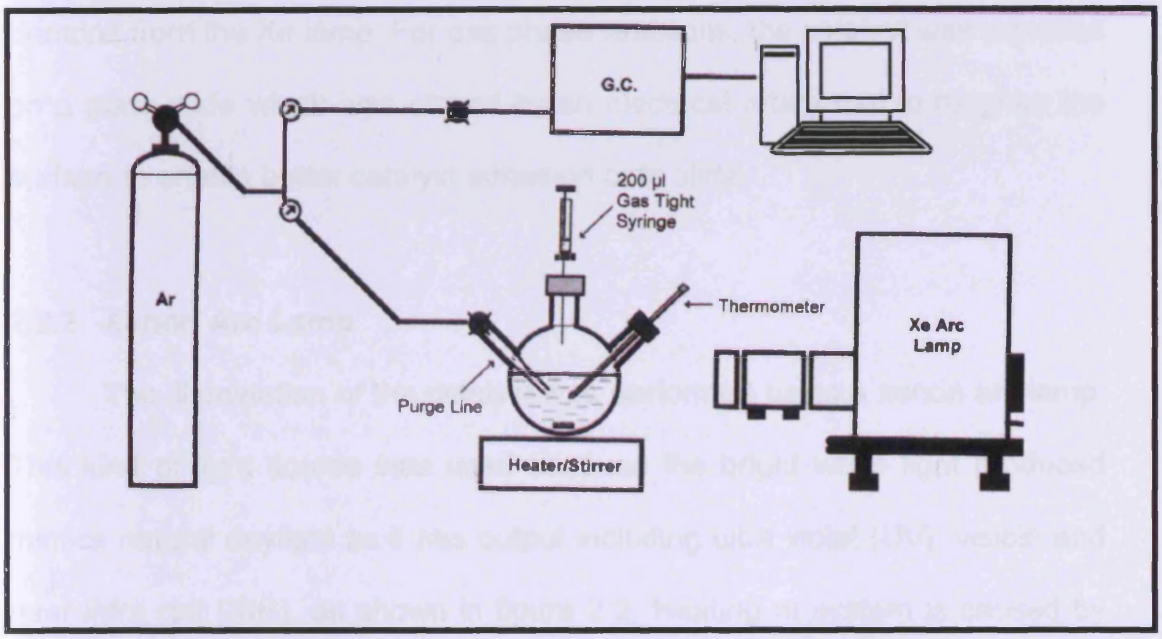

Figure 2.1: Reactor layout and photograph of reactor.

2.2.1 The photoreactor

The photoreactor is a three-armed, round bottomed, Pyrex flask. One arm is for purging the catalyst suspension with argon, and this is connected to an argon cylinder via a rubber line. This purge is used to remove any dissolved gases in the mixture, which may affect the rate of hydrogen production. Another arm can be used for different tasks, e.g. for measuring the temperature during the reaction by fitting a thermometer or thermocouple or for measuring the pH by introducing a pH electrode, but is otherwise sealed by a rubber septum. The third arm is for gas sampling. This arm was sealed with a septum throughout the reaction. The flask was placed on a magnetic stirrer for liquid phase reactions to ensure that all the particles of the catalyst are suspended in the solution and to give them uniform illumination by the photons from the Xe lamp. For gas phase reactions, the catalyst was mounted on a glass slide which was etched by an electrical rotary tool to roughen the surface to enable better catalyst adhesion onto slide.

2.2.2 Xenon Arc Lamp

The illumination of the catalyst was performed using a xenon arc lamp. This kind of light source was used because the bright white light produced mimics natural daylight as it has output including ultra violet (UV), visible and near infra red (NIR), as shown in figure 2.2. Heating of system is caused by the NIR and can be removed by the inclusion of a water filter (Oriel corporation model 61945) or using a dichroic mirror as in 3.2.6, which is designed to transmit visible wavelengths while reflecting NIR heat. However, all the experiments in this project were carried out without using any filter.

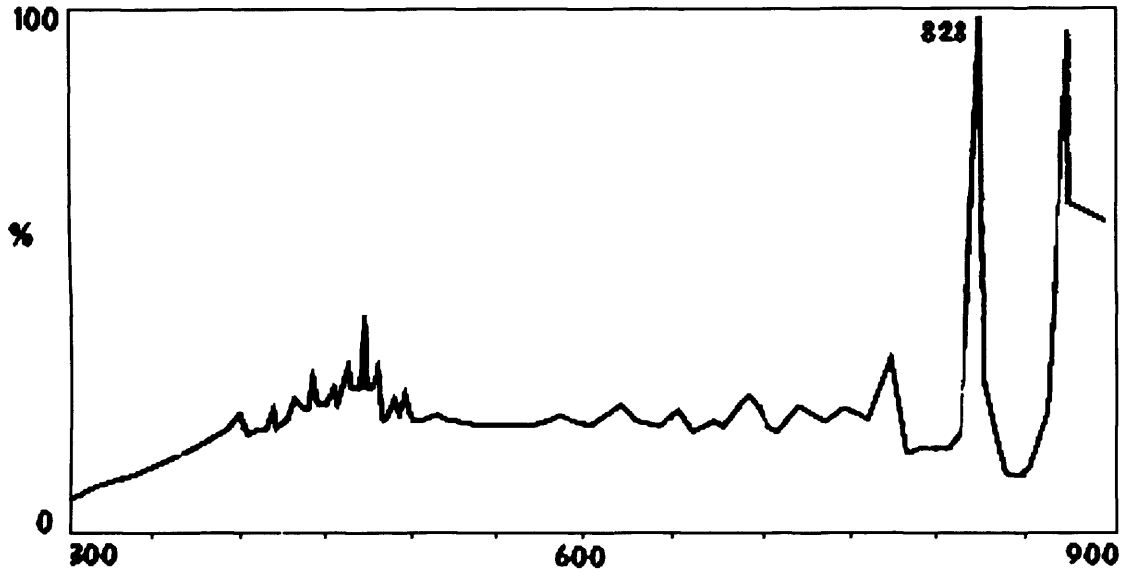

Figure 2.2: Xe arc lamp irradiance spectrum and transmission of light through Pyrex flask.

The transmitted wavelength range of light can be controlled by placing a filter between the Xe arc lamp and the flask. The filters cut out certain wavelengths (e.g. $\lambda > 258$, 380 or 400 nm). In this project, two kinds of Xe arc lamps were used (400 W). A 400 W Xe arc lamp, Oriel corporation model 66084 was used in some experiments mentioned in chapter three. This kind of lamp produces ultraviolet radiation at wavelengths of $\lambda < 300$ nm. The shortwave ultraviolet radiation photolyses oxygen to produce ozone, O_3. Ozone is a health hazard and can cause nasal dryness, nausea and irritation of the mucous membrane. Additionally, it can damage non-stainless metals due to its corrosive nature. According to OSHA, the maximum concentration allowed for workers 0.1 ppm for eight hours. To eliminate this risk, an ozone eater was used when this kind of lamp was used. This part of the reactor is a

housing containing a fan and catalytic filter elements such as manganese dioxide. since this material is not consumed in the transformation of ozone to oxygen; the life of this catalyst is indefinite. The fan collects air through a flanged-end hose and forces it through the filter elements where any ozone present is converted back into oxygen.

To simplify the design of the lamp source, a Xe ozone-free arc lamp (model 6271) was used in the rest of all the experiments in this project. Such kind does not emit wavelengths below 260 nm due to lamp's envelope consisting of doped quartz.

2.2.3 Gas chromatography

Hydrogen produced from the photocatalytic reaction was analysed and identified using gas chromatography with a Varian GC 3900. A small amount of sample (0.2 ml) was extracted from the reactor and injected into GC by a gas syringe through the hot injector port to make sure that all components of the sample (such as water vapour) are in gaseous phase and then pushed into the column by the carrier gas, (argon). The components of the sample are separated within the column due to the differences in their abilities to partition between the mobile and stationary phases in the column. After the separation process, the individual analytes are transferred to the thermal conductivity detector (TCD) by the carrier gas at different times. The electrical signals generated from each analyte in the detector are recorded using Varian's Galaxy program. Figure 2.3 shows the components of gas chromatograph.

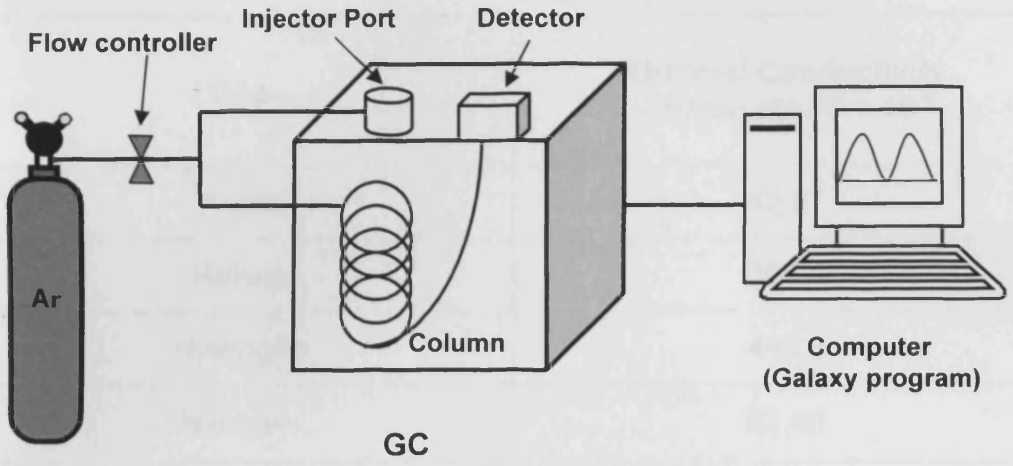

Figure 2.3: The diagram of the components of gas chromatography.

The components of gas chromatograph are discussed briefly as follows:

Carrier gas

. Moving the analytes from the injector to the column and then the detector is performed by a mobile phase which does not interact with the components of the samples. The carrier gases usually used in GC are nitrogen, helium, hydrogen and argon. In our case, the carrier gas used was argon due to the great difference in the thermal conductivity from that of hydrogen which is the main target of the analysis in the gases produced. Table 2.1 shows a comparison between thermal conductivities for various gases[6].

Table 2.1: Thermal conductivities for various gases at 26.7 °C.

Gas	Thermal Conductivity Cal/sec.cm.°C × 10^{-6}
Argon	42.57
Helium	360.4
Hydrogen	446.3
Nitrogen	62.40
Oxygen	63.64

The flow rate of the carrier gas has a significant role in determining the retention times of the different gases and hence affects the resolution via the separation time between the peaks of the elutes. The flow rate of argon used here was 30 ml/min in the case of GC (Varian 3900). If the flow rate is faster than that, the retention time decreases and the integrated peaks can interfere with one another. While at slower rate, the peak areas are larger and the analysis of the sample takes more time due to the slower retention times.

At a flow rate 30 ml/min, it was found the peak of hydrogen was the first as appears at approximately 1.5 minutes in the chromatogram, then oxygen at 2.2 minutes and nitrogen was eluted at 3 minutes. Although oxygen and nitrogen do not come from the photoreaction, their peaks were seen in every analyzed sample. This happens as a result of the presence of some air in the needle of the syringe. With flushing of the syringe before sampling, that peaks diminished clearly.

Injector

The sample is injected through a septum into the injection port by a Aldrich gas-tight syringe. In general, the temperature of the injector, which is hollow-heated cylinder, is controlled to ensure the sample remains in the gas phase. If the temperature is low, broad peaks and poor separation occurs. In contrast, at higher temperature, the sample may decompose or its structure may change. The end of the injector is connected with the column as the volatilized sample is swept to the column directly by the carrier gas which is continually flowing from the gas cylinder regulator through the injector into the column. The kind of the injector used was splitless and the entire sample injected was analysed.

Column

The column is considered the heart of the GC system as the separation of the components of the sample is performed inside this part of the GC. There are two types of gas chromatography columns: capillary and packed. Both types are coated with a stationary phase which seperates the compounds and the structure of stationary phase affects the retention time. Capillary columns are thin fused-silica in which the stationary phase is coated on the inner surface of column. Packed columns are typically glass or stainless steel coils which are filled by the stationary phase. Although the capillary column (typically 10 - 100 m in length) has higher separation efficiency than packed column (typically 1 - 5 m in length), they are more easily overloaded by sample.

The kind of column used in this work was a MS13X molecular sieve packed column (pore size of 10 Å in diameter, 2 m in length). This type detects hydrogen, oxygen and nitrogen. The column was usually placed inside ovens to control the temperature constantly and hence the retention times.

When the sample is brought to the column by the mobile phase, the components of the sample take different amounts of time (the retention time) to pass through the column depending on the extent of the interaction between these components and the stationary phase. The components that do not adsorb well on the packing will elute from the column more rapidly. On the other hand, the components that adsorb more strongly will take more time to elute. Hence the components of the sample are separated before eluting from the end of the column. Figure 2.3 shows an example chromatogram in which hydrogen was eluted first, then oxygen and finally nitrogen.

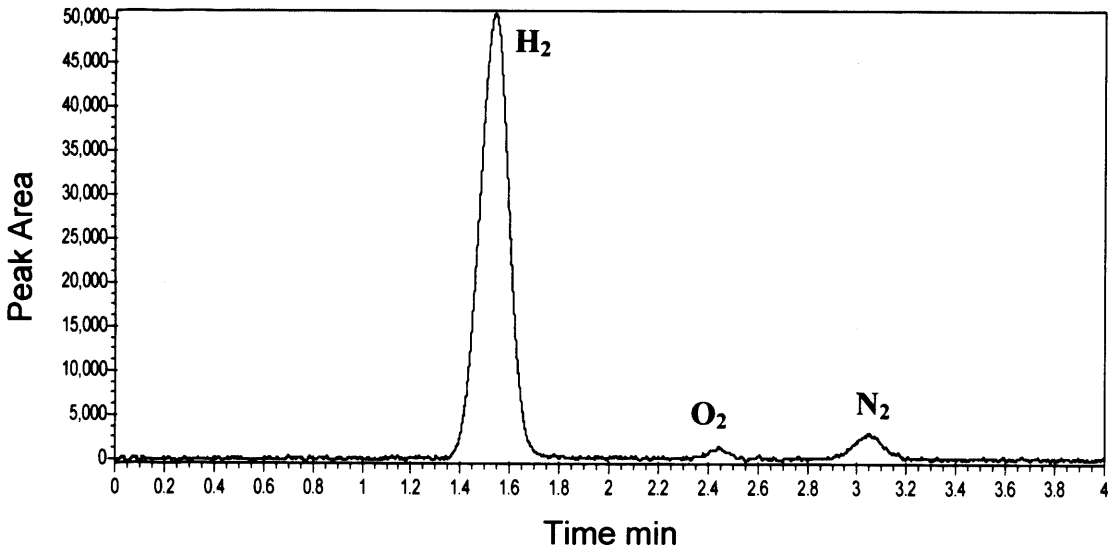

Figure 2.3: An example of chromatogram.

Detector

There are many kinds of detector and they are chosen according to the compounds to be detected and the sensitivity required. Among these is the thermal conductivity detector (TCD) which was used in this research.

TCD compares the thermal conductivities between the carrier gas flow and the carrier gas plus the column effluents since it contains four filaments made from tungsten-rhenium arranged in a bridge circuit known as a "Wheatstone bridge" as shown in figure 2.4. The temperature of these filaments should be constant. When the mixture of the sample with the reference gas pass one the pair of filaments and at the same time, the pure reference gas flows over the second pair, there is a difference in the cooling abilities of the two gas mixtures. As a result the power changes to keep the temperature of the four filaments constant. The power difference is measured and recorded as a peak by the Galaxy program.

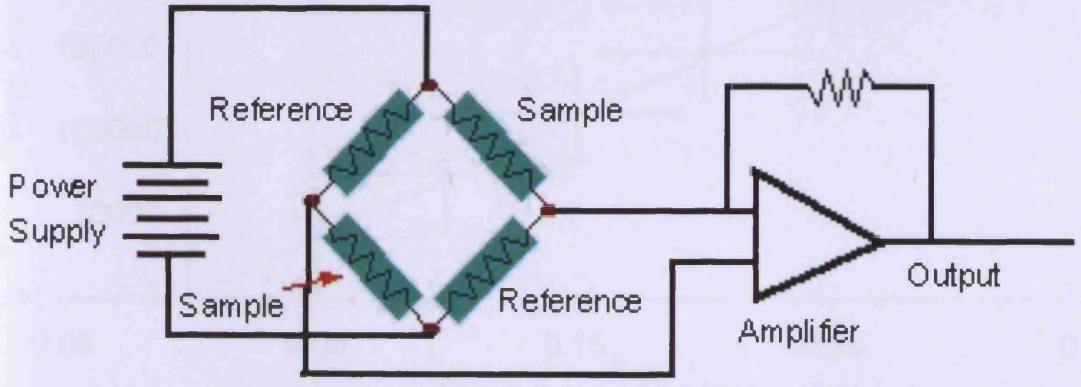

Figure 2.4: Schematic of a bridge circuit of TCD.

After the brief description of the components of gas chromatograph, the conditions of the GC set in our work were as follows:

Flow rate of the carrier gas (Argon)	30 ml/min
Injector temperature	50 °C
Column temperature	50 °C
TCD temperature	120 °C
Filament temperature	170 °C

2.2.4 Calibration

The GC was calibrated by injecting exact volumes of pure hydrogen gas into the packed column. The peak areas at different volumes were plotted against that of the known volumes (figure 2.5).

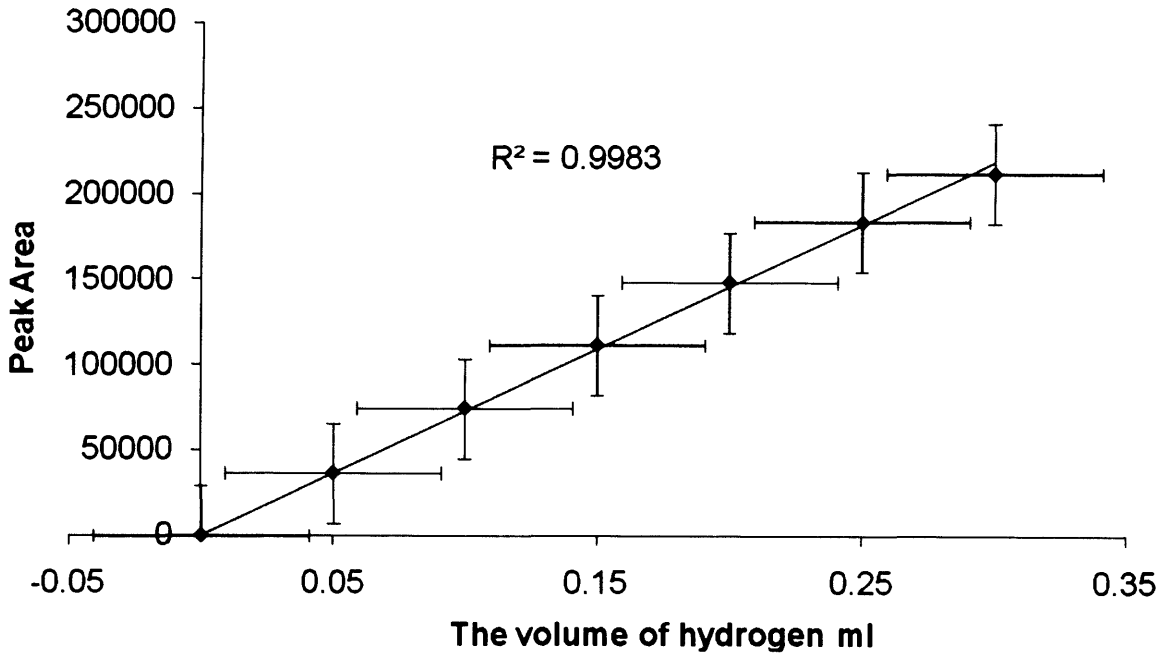

Figure 2.5: Calibration Plot for hydrogen.

From figure 2.5, the slope of this relationship was calculated which was used in determining the volume of hydrogen produced from the photocatalysis reaction in the flask. Before these calculations were done, the total volume of gas in the reactor should be known. For the liquid phase reactions, the volume of the reaction mixture was 100 ml and the capacity of the vessel was 165 ml, so the gas phase of the Pyrex flask was 65 ml.

From the calibration curve and the volume of the gas phase in the reactor as well as the volume of sample injected into the GC (0.2 ml), the volume of hydrogen produced from the reaction can be calculated from the following relations:

Volume of H_2 in the syringe = Peak area integral / slope of calibration

Total H_2 volume in the flask = (volume of H_2 in the syringe/syringe volume) × gas volume in the flask

These calculations were used for the gas phase reactions as well as the liquid. The only difference between this phase and of that in the liquid phase was the gaseous flask volume. The volume of the solution was 15 ml in this case, much less than of that of the liquid phase in order to avoid contact with the catalyst mounted on the glass slide as shown in figure 2.6. Thus, the gas phase volume over the solution in this case was 150 ml.

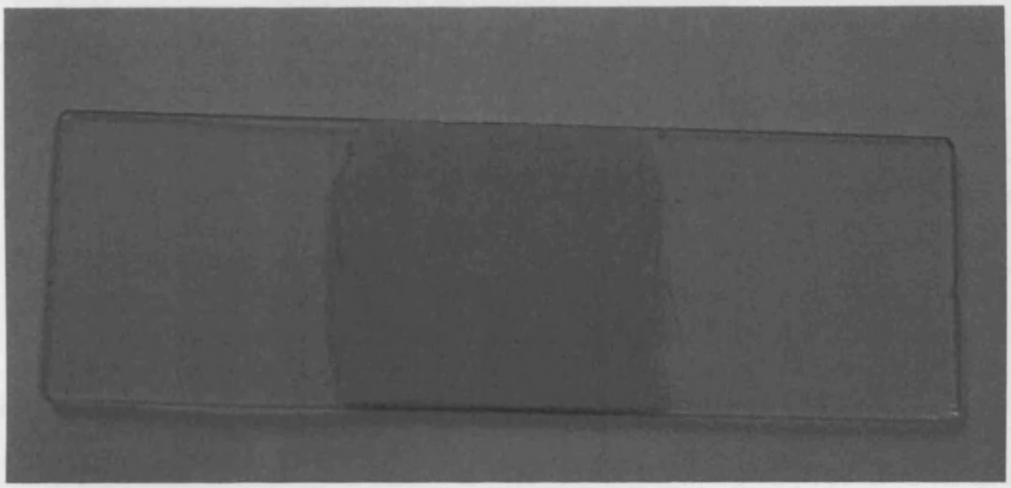

Figure 2.6: The catalyst mounted on the glass in the reactor of gas phase reaction.

2.3 Methodology

The reaction mixture in the liquid phase typically contains 0.2 g of the catalyst, 100 ml deionised water and 100 µl of anhydrous methanol. This mixture was purged with argon for 30 minutes to remove any dissolved gases. Then the lamp source was switched on and the reaction mixture was continually stirred.

For gas phase reactions, 50 mg of the catalyst was mounted on a part of glass slide, its size was 28 × 25 mm. This area of the slide was etched to ensure that the catalyst adheres quite strongly to it.

The hydrogen produced from this reaction was detected by withdrawing 0.2 ml from the gas phase over the solution using a tight gas syringe every 30

minutes this then inserted in the septum of the injector of the GC to get the peak of hydrogen.

2.4 Catalyst preparation

There were several types of catalysts used in this project and they were prepared by different methods, as described below.

2.4.1 Pd/TiO_2

The normal catalyst used was Pd loaded onto titanium dioxide, (TiO_2, P25 Degussa), and it was prepared by incipient wetness impregnation. To prepare this catalyst, the amount of liquid, which fills all the pores of the support, was determined and it was found that 1.5 ml of water was sufficient to fill the pores. The preparation of 2 g of 0.5% w Pd/TiO_2 is as follows:

The mass of Pd required = (0.5 × 2)/100

= 0.01 g

The assay for the $PdCl_2$ (the metal salt used) was 59.82 %

The actual mass of $PdCl_2$ required = (0.01× 100)/59.82

= 0.0166 g

0.0166 g of $PdCl_2$ was dissolved in 1.5 ml of deionised water to get the required percentage weight of metal salt solution. A few drops of concentrated hydrochloric acid were added with slight heating (~ 35 °C) to obtain a clear solution since $PdCl_2$ is slightly soluble.

This volume of metal salt solution was added gradually to the dry TiO_2 with stirring by glass rod to impregnate 2 g of titania and to ensure all the pores of the support were filled. The paste formed was dried at 120 °C in an oven for 2 hours to remove all the water, and then calcined at 500 °C for 2 hours. XPS studies revealed that the oxidation state of Pd deposited on the surface of the TiO_2 after calcination was zero. After calcination, the catalyst was ground in a pestle and mortar and sieved through a stainless steel mesh as 53 μm typically.

2.4.2 Au/TiO_2

The preparation of this catalyst is similar to that mentioned in the case of Pd/TiO_2 (the incipient wetness method) but the precursor used in the preparation of gold salt solution was chloroauric acid, $HAuCl_4.3H_2O$. Due to its hygroscopic nature, the stock solution was prepared by dissolving 1 g of this salt with 10 ml of deionised water was which used in the preparation of the desired catalyst.

The change of the colour of Au/TiO_2 during the calcination process is ascribed to the conversion of the gold from Au^{+3} to the reduced state of Au^0. The colour change was from yellow (gold salt) to a blue-grey colour.

Although the activity of Au/TiO_2 calcined at 300 °C was twice that after calcination at 500 °C, the catalyst (used in section 3.2.9) was calcined at 500 °C. This was done in order to be able to compare easily the activities of Pd/TiO_2 and Au/TiO_2 for the reforming of glycerol under the same conditions, and prepared by the same methods.

2.4.3. Pd / mesoporous titania

Mesoporous titanium dioxide was used as a support rather than titania (P25) as it has a high surface area and thus affect the efficiency of photocatalytic hydrogen production. This prepared material was received from National Chemical laboratory, India, and tested in our reactor. The sol-gel method was adopted to prepare the template free meso-TiO_2 due to the ease to control its texture, chemical and morphological properties. Figure 2.7 displays the steps of preparation of mesoporous TiO_2 through template free sol-gel method[7].

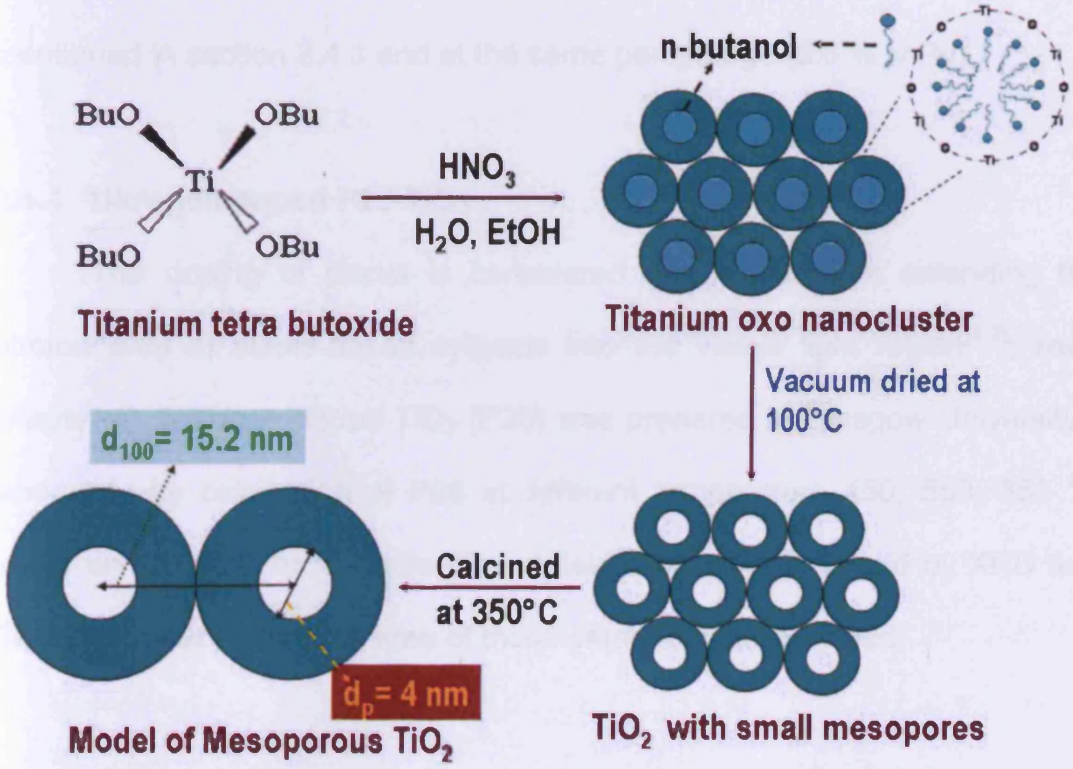

Figure 2.7: Schematic model of preparation of template free mesoporous TiO_2.

Titanium tetra-butoxide $Ti(OBu)_4$ was the precursor of the titania. The desired amount of $Ti(OBu)_4$ was stirred in absolute ethanol to make a solution (0.33 M) for 3 hours. During the vigorous stirring, 0.6 ml of 0.14 M HNO_3 was added step-by-step and then left for further 2 hours with stirring. The gel formed was dried at room temperature, ground to a fine powder and vacuum dried around 100 °C for overnight. Finally, the material was calcined at 350 °C for 4 hours.

This support was tested with and without loading of palladium. Loading method of Pd on mesoporous TiO_2 was similar to that on titania P25 mentioned in section 2.4.1 and at the same percentage (0.5 % w Pd).

2.4.4 Nitrogen doped P25-TiO_2

The doping of titania is considered one solution for extending the photoactivity of titania-based systems into the visible light region[8,9](seen chapter 4). Nitrogen doped TiO_2 (P25) was prepared in Glasgow University's laboratory by calcination of P25 at different temperature 450, 550, 650 °C under an NH_3 flow for 5 hours. This catalyst was characterised by XRD and SEM. The specific surface area of these catalysts was identified.

2.5 Catalyst characterisation

Numerous techniques have been used to characterise the catalysts including: Brunauer, Emmett and Teller surface area (BET), X-ray Diffraction (XRD) and Scanning Electron Microscopy (SEM). These techniques enable us

to understand more about the mechanism of photoreactions and their potential applications and how the efficiency of these catalysts can be developed. In the following sections, each technique is briefly discussed individually.

2.5.1 BET Surface Area

The surface area of a catalyst is an important attribute which dictates the activity and sometimes stability of the materials. There are different methods to achieve this measurement which can be single or multipoint methods. The standard method is the multipoint BET method. BET stands for Brunauer, Emmett and Teller and their paper regarding the determination of surface area was published in 1938 [11]. The technique depends on the gas sorption (adsorption and desorption) by clean powder materials.

Adsorption is a consequence of the additional energy of the atoms on the surface of materials, which are not surrounded by others in all directions compared with those in the bulk. However, these atoms can attract other atoms or molecules (adsorbates). Two types of adsorption are recognised according to the nature of the interaction between the surface molecules and the gas molecules; physical and chemical adsorption. In chemical adsorption (chemisorption), the gas molecules are bonded to the surface of the adsorbent by chemical bonds which means there is a sharing or exchanging of electrons between the gas molecules and the solid surface. As a result, a monolayer of gas molecules will be formed on the surface. This kind of adsorption is not easily reversible and needs significant energy input to

release the gas molecules adsorbed from the surface. In contrast, for physical adsorption (physisorption), the bonding attraction between the adsorbate and the adsorbent is weak and of the van der Waals type.

The determination of BET surface area of all kinds of catalysts is based on the Langmuir physical adsorption isotherm theory. To apply this theory on the multilayer adsorption in BET surface area measurements, some assumptions should be considered such as:

- The physisorption of gas molecules on the surface is as infinite layers.
- There is no interaction between the adsorbed layers.
- Langmuir theory can be applied to each layer.

For BET measurements, the weighed catalyst is heated and degassed to form a clean surface, then cooled and re-weighed. After that, the sample is exposed to nitrogen gas (an inert gas available in high purity) in controlled amounts and over a wide range of pressures. The amount of adsorbed or desorbed gas molecules is determined by the pressure variations. Knowing the area of adsorbed gas molecule, the surface area of the material can be calculated via the following equation:

$$\frac{1}{\upsilon\left[(P_0/P)-1\right]} = \frac{c-1}{\upsilon_m c}\left(\frac{P}{P_0}\right) + \frac{1}{\upsilon_m c}$$

υ = the total volume of molecules added

υ_m = the volume of gas molecules corresponding to the monolayer.

P = the pressure

P_o = the saturation vapour pressure

C = the constant related to the adsorption heating.

Equation 1 is an adsorption isotherm and can be plotted as a straight line with $1/ (\upsilon(Po/P)-1)$ on the y-axis and P/Po on the x-axis, as shown in figure 2.8. Knowing the slope and intercept, the surface area can be calculated from equation 2, as follows:

$\upsilon_m = 1/(S+I)$

$C = 1 + (S/I)$

So, A_{BET} (surface area)= $(\upsilon_m . N)/V$ (2)

Where N= Avogadro's number

V = molar volume of adsorbent gas

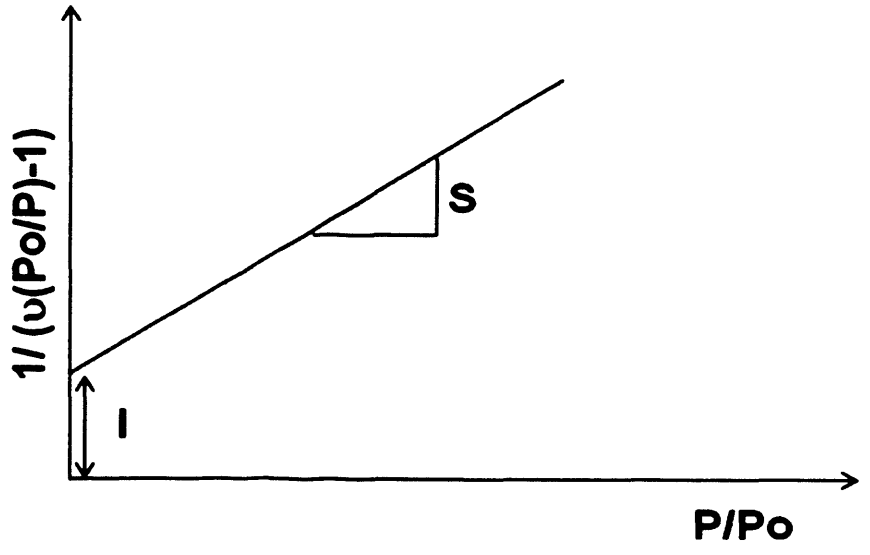

Figure 2.8: Adsorption isotherm for BET surface area measurements.

2.5.2. Scanning Electron Microscope (SEM)

Light microscopes have a limitation whether in their resolution of objects (> 0.2 μm). This led to the development of scanning of the surface of fine materials (down to 50 nm in size) by a beam of high energy electrons rather than the light. The interaction between the beam and sample produces images which provide some great information of the surface sample in terms of topography (its features), composition (which elements and compounds are present), morphology (the shape and size of the particles) and crystallographic information (the arrangement of atoms in the sample).

Max Knoll obtained the first SEM image for silicon steel in 1935 and many workers have developed and improved the performance of this technique for many last years.

The diagram in figure 2.9 shows the general structure of the SEM instrument and helps to explain how it works. The electron beam is produced from a tungsten filament cathode heated by applying a voltage. The anode attracts these electrons and they are focussed into a beam by a condenser lens. The scanning coils create a magnetic field that deflects the beam passed through it back and forth and then the objective lens focusses the scanned beam on the sample as a very fine point (not in the diagram). When the electrons hit the sample, electrons from the sample are ejected. The secondary electrons and backscattered electrons, (elastically scattered electrons), are collected by a detector which convert them into signals and then images.

Due the vacuum conditions used in this technique, the sample should be dried to remove any water before introducing the sample to the beam of electrons in SEM instruments. In the past non conducting samples were coated with a thin layer of conducting material but in modern instruments this is usually no longer necessary.

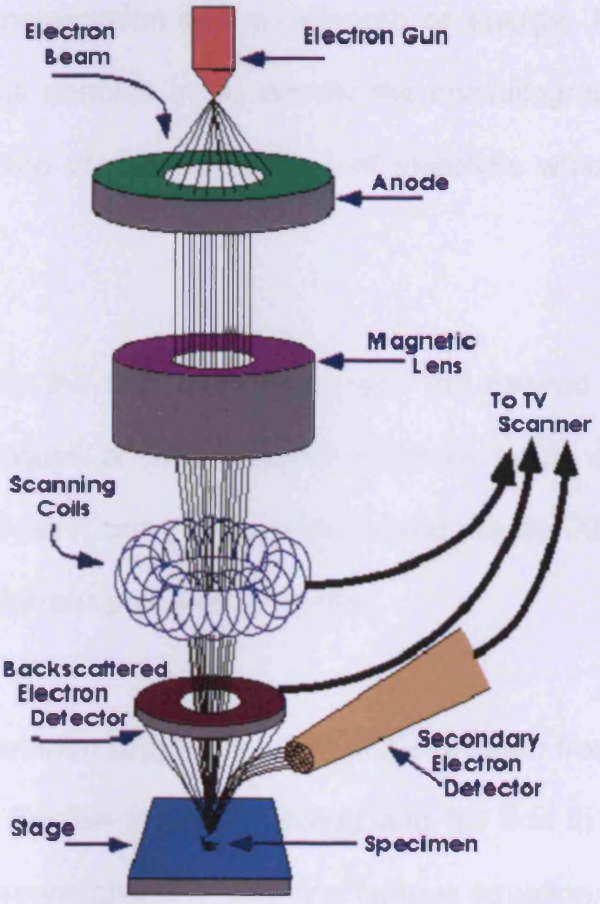

Figure 2.9: diagram of SEM instrument.

2.5.3 X-Ray diffraction (XRD)

A useful non-destructive analytical techniques is X-ray diffraction which is abbreviated as XRD. In 1912, it was discovered that crystalline substances act as three-dimensional diffraction gratings for X-ray.

In general, this technique is based on the relationship between the intensity of scattered x-ray beam hitting the sample and the incident and scattered angle, polarization and wavelength or energy. The data obtained from XRD analysis enables us to identify the crystallographic structure, the composition and the physical properties of materials which are powders or films.

According to the type of materials and the desired information, there are several techniques of XRD analysis, such as single crystal XRD, high-resolution XRD, X-ray rocking curve analysis and powder XRD. The latter was used to characterise our powdered samples.

The phenomenon of the diffraction of X-ray beam from the crystals was explained by the English physicists Bragg and his son in 1912. They were presented this observation in the following famous equation:

$$n\lambda = 2d \sin\theta$$

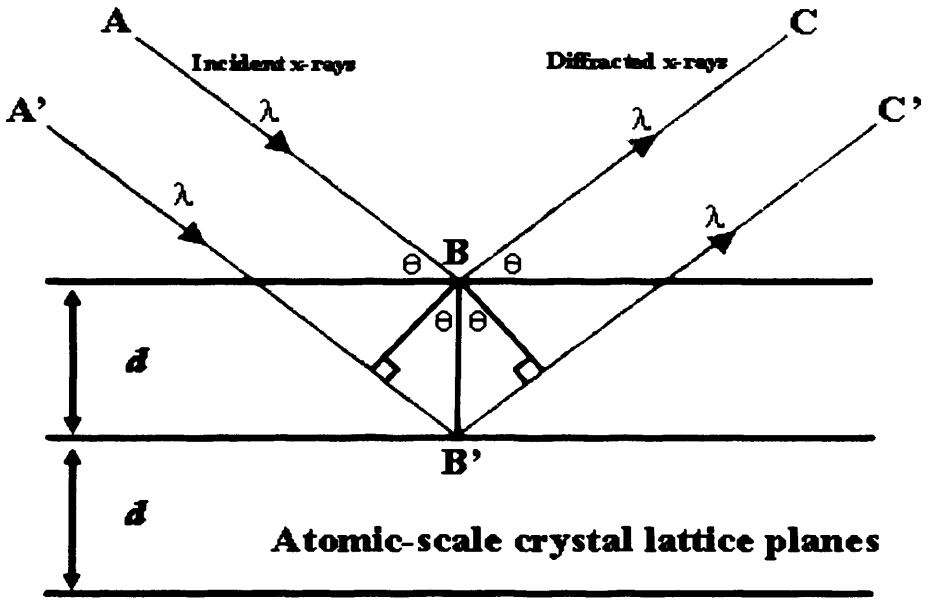

Figure 2.10: Schematic diagram for Bragg's law.

According to the diagram drawn in figure 2.7, the symbols in Bragg's equation can be defined as follow:

d = the distance between different plane of atoms in the crystal lattice,

θ = the angle of diffraction,

n = an integral number of wavelengths, and

λ = the wavelength of X-rays.

The atoms or molecules in a crystal are arranged forming a crystal lattice. These arrangements may be found in different directions, horizontally, vertically or diagonally which give the form of lattice planes. The planes are parallel to each other and the distance between the planes is called the lattice plane distance, d. When the parallel X-rays strike a pair of parallel lattice planes, the atoms within the planes scatter the incident waves at an angle θ which is half the angle between the incident beam and the diffracting beam.

2.6 The references

[1] A. J. Dickinison in *'Photocatalytic Hydrogen Production', PhD, Vol.* The University of Reading, **1997**.

[2] Karunarl Domen, Shulchl Nalto, Takaharu Onlshl and Kenrl Tamaru, *J. Phys. Chem.* **1982**, *86*, 3657-3661.

[3] J. Greaves in *Photocatalytic Hydrogen Production using Gold on Titania, Vol. PhD* The University of Reading, **2005**.

[4] L. Millard and M. Bowker, *Journal of Photochemistry and Photobiology, A: Chemistry* **2002**, *148*, 91-95.

[5] D. W. James in *'The Photocatalytic Reforming of Methanol', MSc Vol.* The University of Reading, **1998**.

[6] R. C. Weast, *Handbook of Chemistry and Physics*, CRC Press, 1974-1975, p. E2.

[7] D. Kulkarni, A. Murugan, A. Viswanath and C. Gopinath, *Journal of Nanoscience and Nanotechnology* **2009**, *9*, 371-377.

[8] C. Belver, R. Bellod, A. Fuerte and M. Fernندez-Garcيa, *Applied Catalysis B: Environmental* **2006**, *65*, 301-308.

[9] T. Ihara, M. Miyoshi, Y. Iriyama, O. Matsumoto and S. Sugihara, *Applied Catalysis B: Environmental* **2003**, *42*, 403-409.

[11] S. Brunauer, P. H. Emmett and E. Teller, *Journal of the American Chemical Society* **1938**, *60*, 309-319.

CHAPTER THREE

Photocatalytic Methanol and Glycerol Reforming on Metal-TiO_2 Catalyst

3. Photocatalytic Methanol Reforming on Metal-TiO_2 catalysts

3.1 Introduction

Extensive research has focused on the hydrogen economy during the past few decades. The efficient conversion of liquid water to gaseous hydrogen and oxygen (water splitting) is still an intellectual challenge. Thus much attention has been paid to the enhancement of the energy efficiency to at least 10% of the solar energy available.

The experiment of Fujishima and Honda[1] is one of the major discoveries of the 20th century. Their photoelectrochemical cell decomposed the water into hydrogen and oxygen when a titanium oxide electrode was connected with a platinum black electrode. The direction of the current shows that the oxidation reaction (oxygen evolution) occurs at the titanium oxide electrode and the reduction (hydrogen evolution) occurs at the platinum black electrode. After their success with TiO_2, a huge amount of work has been carried out to develop the solar-hydrogen system with increasing conversion efficiency of solar energy into chemical energy[2-4].

For hydrogen production using sunlight and water as available abundant raw materials, there are different ways to split the water into hydrogen and oxygen. Use has been made of photoelectrochemical cells as

mentioned in Fujishima and Honda' work and later works[5-7], of powdered semiconductor photocatalysts loaded with various metals, using dye sensitizers to alter the wavelength response of the semiconductor and of sacrificial systems where either the oxidation or reduction half-reaction is targeted.

Loading of noble metals such as Pd, Pt, and Au on TiO_2 has a great interest in the field of the hydrogen photoproduction. These metals can change the surface properties of semiconductors, which in turn promote the efficiency of the photocatalytic reaction[8, 9]. The enhancement arises from the suppression of electron-hole recombination as the excited electron transfers to the metal leaving a hole in TiO_2 [10, 11].

It was found that Pd/TiO_2 is the most active in terms of the hydrogen evolution from water and methanol system compared to the other metals (Ir, Fe, Co, Ni, Rh, Ru, Pt and Au) loaded TiO_2[12]. However, it is generally believed that Pt/TiO_2 is the most efficient catalyst for the reaction due to its low overpotential for hydrogen production. In general, comparisons between the activities of the metals are complicated, due to greatly varying conditions of the reaction, the preparation method, and the state of the water (gas or liquid phase)[13-18].

The yield of hydrogen produced is usually still low due to the reverse reaction between hydrogen and oxygen. The addition of some organic compounds such as methanol, ethanol, and EDTA enhances the rate of

hydrogen production considerably, to much higher yields than for water alone[2, 19]. These substrates are called sacrificial electron donors. That means they increase the time for recombination of photogenerated electron and hole. The photodecomposition of organic compounds and water leads to the formation of hydrogen like carbon dioxide. However, the mechanism is not completely known.

Methanol as a hole scavenger was chosen as a model molecule to simplify the study as it contains only one functional group (hydroxyl). One of the mechanisms of the photooxidation of methanol over the photocatalyst suggested[2, 19-21] that this reaction is stepwise including stable intermediates as follows:

$$CH_3OH + 2h^+ \longleftrightarrow HCHO + 2H^+ \quad (3\text{-}1)$$

$$HCHO + H_2O + 2h^+ \longleftrightarrow HCOOH + 2H^+ \quad (3\text{-}2)$$

$$HCOOH + 2h^+ \longleftrightarrow CO_2 + 2H^+ \quad (3\text{-}3)$$

Hydrogen is formed by reducing the hydrogen ions by the photogenerated electrons:

$$2H^+ + 2e^- \longleftrightarrow H_2 \quad (3\text{-}4)$$

The overall reaction is:

$$CH_3OH\ (l) + H_2O(l) \longleftrightarrow CO_2(g) + 3H_2(g) \quad (3\text{-}5)$$

According to this mechanism, the hydrogen was produced from methanol reforming and water splitting simultaneously. Table 3.1 shows the rate of

hydrogen production over different catalysts in the presence of different sacrificial reagents.

Table 3.1: The rates of hydrogen production over different catalysts.

Catalyst	H_2 production rate µmol/h	Conditions	References
Pt/TiO_2	4675	Gas phase 29 % methanol (v/v)	[18]
Cu/TiO_2	1350	Liquid phase 1:1 methanol/water Pyrex reactor	[17]
$AgO+TiO_2$	1700	Liquid phase 1000 ml Methanol	[22]
Graphite silicon $GS+TiO_2$	22.3	40 vol % methanol UV irradiation	[23]
NiO/TiO_2	162.6	Liquid phase 200 ml Methanol Pyrex reactor	[24]
$HLaNb_2O_7$:In	36	10 vol % Methanol (5 mol% In)	[25]
2% Rh/TiO_2	449	Gas phase 10% wt NaOH Quartz cell	[26]
0.3% Pt/TiO_2	78	Liquid phase 0.76 mol Na_2CO_3 Quartz reactor	[27]

The aim of this work

The work in this chapter concerns an investigation of several factors on methanol reforming over Pd/TiO_2. These factors include the amount of catalyst, methanol concentration, Pd loading in liquid and gas phase, and wavelength of the light. Moreover, reforming of glycerol over Pd/TiO_2 and Au/TiO_2 is investigated and comparison of the results with those for methanol

is made. This chapter also deals with supports with high surface area, such as mesoporous TiO_2, and compares its activity with Pd/TiO_2. Pd/TiO_2 and Au/TiO_2 were prepared and tested in the apparatus for this reaction as described in chapter two. All of the catalysts were made using P25 Degussa TiO_2 as a photoactive support except $Pd/MTiO_2$ where the mesoporous TiO_2 was the support.

3.2 Results and Discussion

3.2.1 The concentration of the catalyst

As shown in figure 3.1, the volume of H_2 produced increases nearly linearly with time. The relationship between the rate of hydrogen production and the amount of the catalyst (in 100 ml of deionised water and 100 µl of methanol) is illustrated in figure 3.2 which shows that the rate (the amount of hydrogen evolved divided by 60, 120 or 240 mins) increases sharply at low catalyst concentrations and then declines above 0.2g.

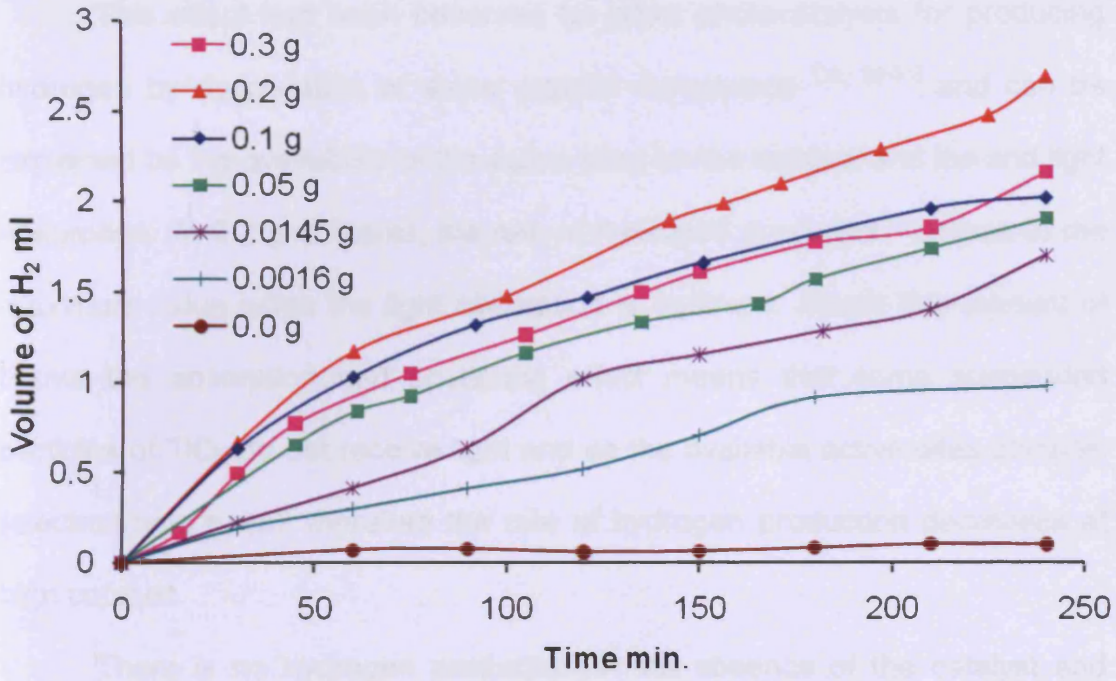

Figure 3.1: The effect of the catalyst amount on the hydrogen production.

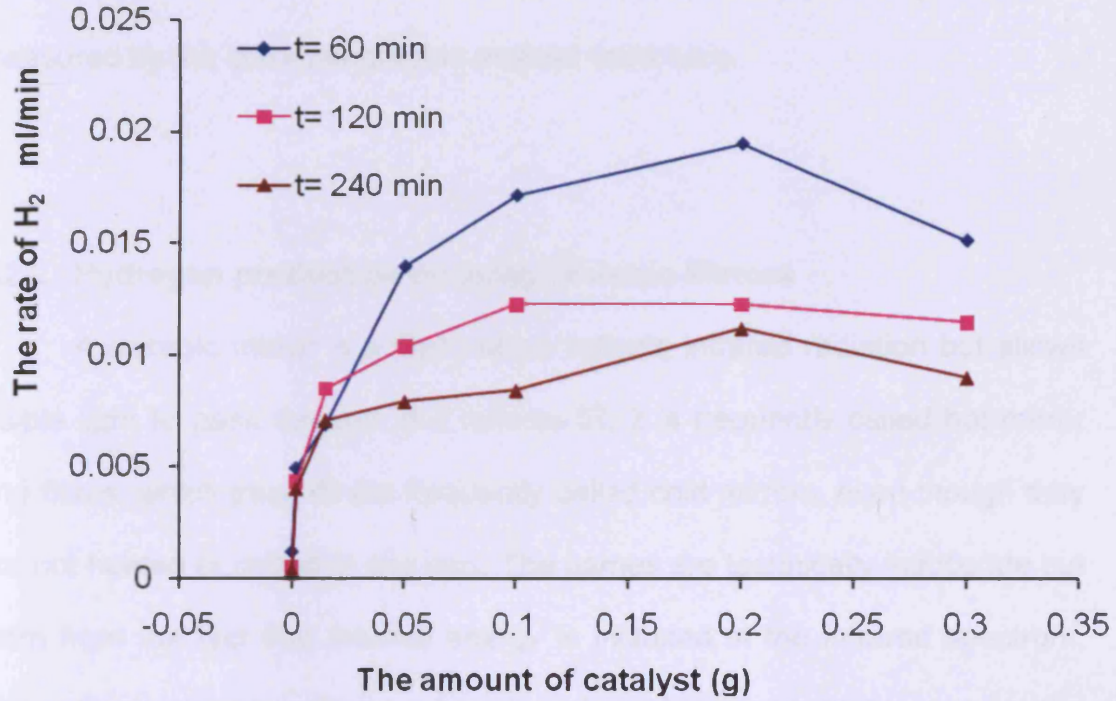

Figure 3.2: Hydrogen production rate from different concentrations of 0.5% Pd/TiO_2 catalyst in water.

This effect had been observed for other photocatalysts for producing hydrogen by degradation of some organic compounds [12, 28-31] and can be explained by the availability of the active sites on the catalyst and the and light absorption. At 0.2 g of titania, the rate of hydrogen production reaches to the maximum value when the light absorption is optimum. Above this amount of titania the absorption and scattering effect means that some suspended particles of TiO_2 do not receive light and so the available active sites diminish (electron/hole pairs); therefore the rate of hydrogen production decreases at high catalyst.

There is no hydrogen production in the absence of the catalyst and argon. Therefore, the production of hydrogen by this technique is a catalytic reaction. As will be shown later CO_2 is also produced, though it is not measured by the chromatographic method used here.

3.2.2 Hydrogen production by using Dichroic Mirrors

A dichroic mirror is a filter, which reflects infrared radiation but allows visible light to pass through. If it reflects IR, it is frequently called hot mirror and filters, which pass IR are frequently called cold mirrors, even though they are not heated or chilled in any way. The names are technically inaccurate but stem from the fact that thermal energy is included in the infrared spectrum. The optimum wavelength was when there is no filter used, as approved in the earlier work[31], i.e. the all wavelength transmitted from the lamp source from IR to visible region was focused on the reactor. The effect of dichroic mirrors on the rate of hydrogen production and the temperature of the reactor was

investigated. A thermocouple placed in the right arm of flask revealed that the temperature of the system reduced from 95 to ~50°C. Figure 3.3 displays the volumes of hydrogen produced from illumination of 0.2 g of 0.5% Pd/TiO_2 in the liquid phase with 100 ml deionised water and 100 µl methanol using three different wavelengths range of dichroic mirrors and compared these results with that reaction which did not use filters. The rate of that reaction with 280-400 nm of filter was quite similar to that of standard reaction (without using a filter) while 260-320 and 350-450 nm were lower than the wider range of wavelengths. From these results, the presence of dichroic mirrors does not enhance the rate of hydrogen production, which is considered the main aim of this chapter. However, this mirror may be useful if the photocatalytic reaction occurred at room temperature is required and gives the same rate of the hydrogen production in the same time.

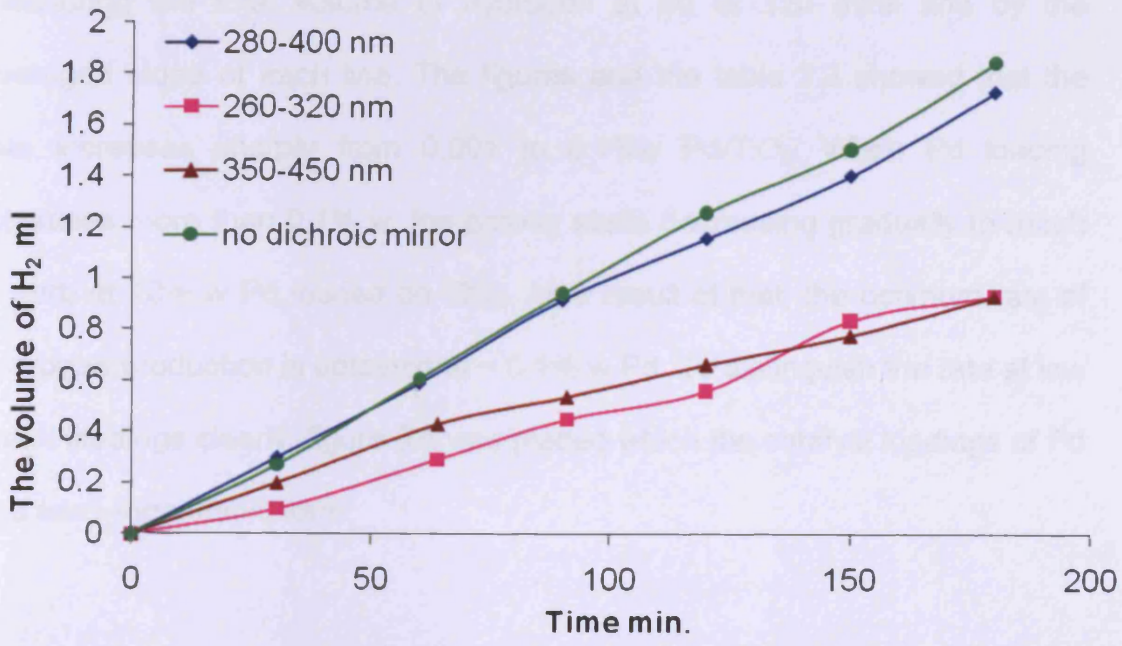

Figure 3.3: The effect of different wavelengths by using dichroic mirror.

3.2.3 Metal loading dependence in liquid phase

The aim of this set of investigations was to determine the dependence between metal loading and the rate of hydrogen production. A series of catalysts of different weight loading of palladium on titania were prepared. These were 0.001, 0.01, 0.1, 0.5, 2.0, 5.0, 7.0 and 10.0%w Pd on Degussa titania. The reaction was tested by using 0.2 g of the catalyst in 100 ml deionised water and 100 µl methanol.

As shown in figure 3.4, the amount of hydrogen evolved depends strongly on the Pd loading and it is also observed that there is an initial induction period for the highest loadings of Pd. This dependence is clearer when the rate of hydrogen evolution was calculated and plotted versus the different metal loadings in figure 3.5. The rate was calculated both by measuring the total volume of hydrogen at 60 or 120 mins and by the averaged slope of each line. The figures and the table 3.2 showed that the rate increases sharply from 0.001 to 0.1%w Pd/TiO_2. When Pd loading increases more than 0.1% w, the activity starts decreasing gradually to reach to zero at 10% w Pd loaded on TiO_2. As a result of that, the optimum rate of hydrogen production is obtained at ~ 0.1% w Pd. To distinguish the rate at low metal loadings clearly, figure 3.6 was plotted which the catalyst loadings of Pd in a semi-logarithmic form.

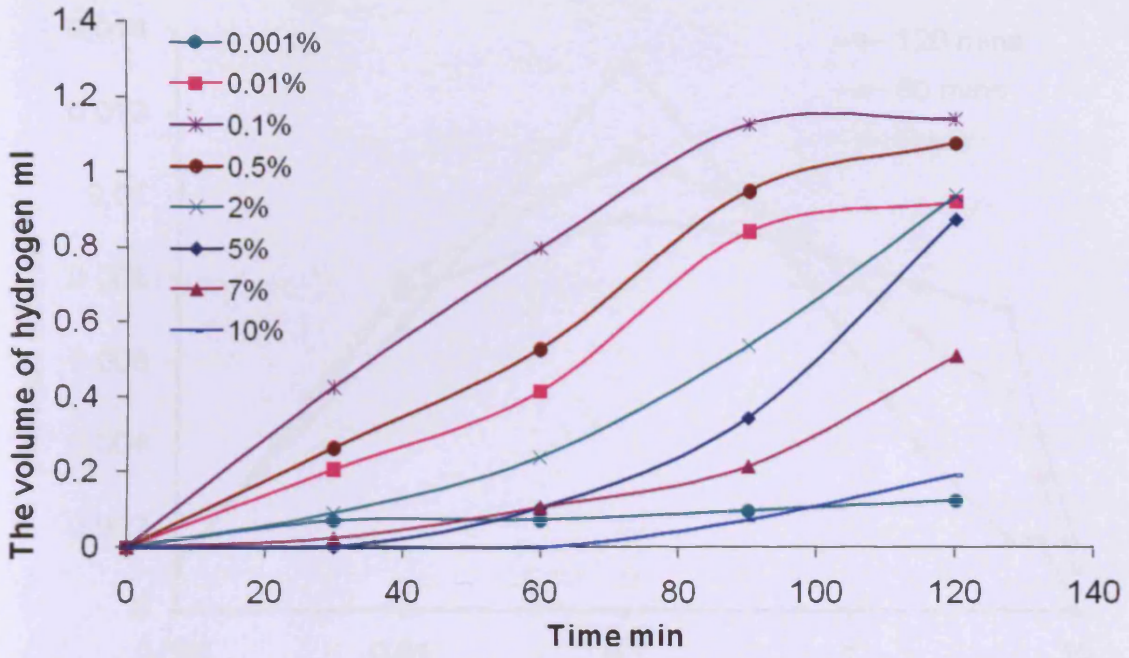

Figure 3.4: The effect of Pd loadings on the hydrogen production.

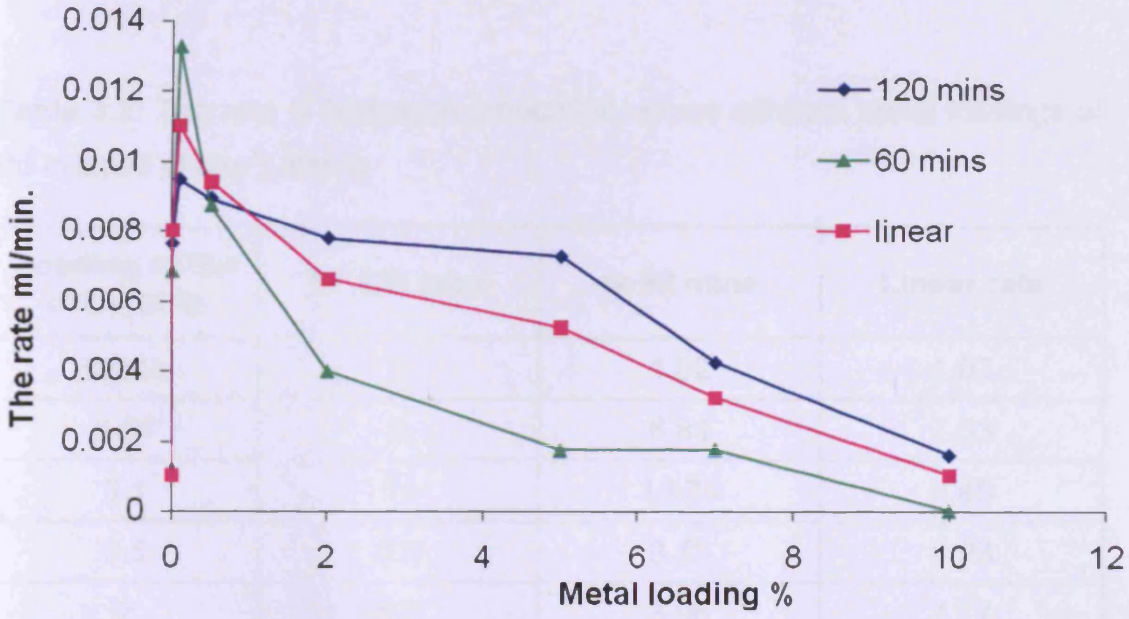

Figure 3.5: Hydrogen production rate versus Pd metal loadings.

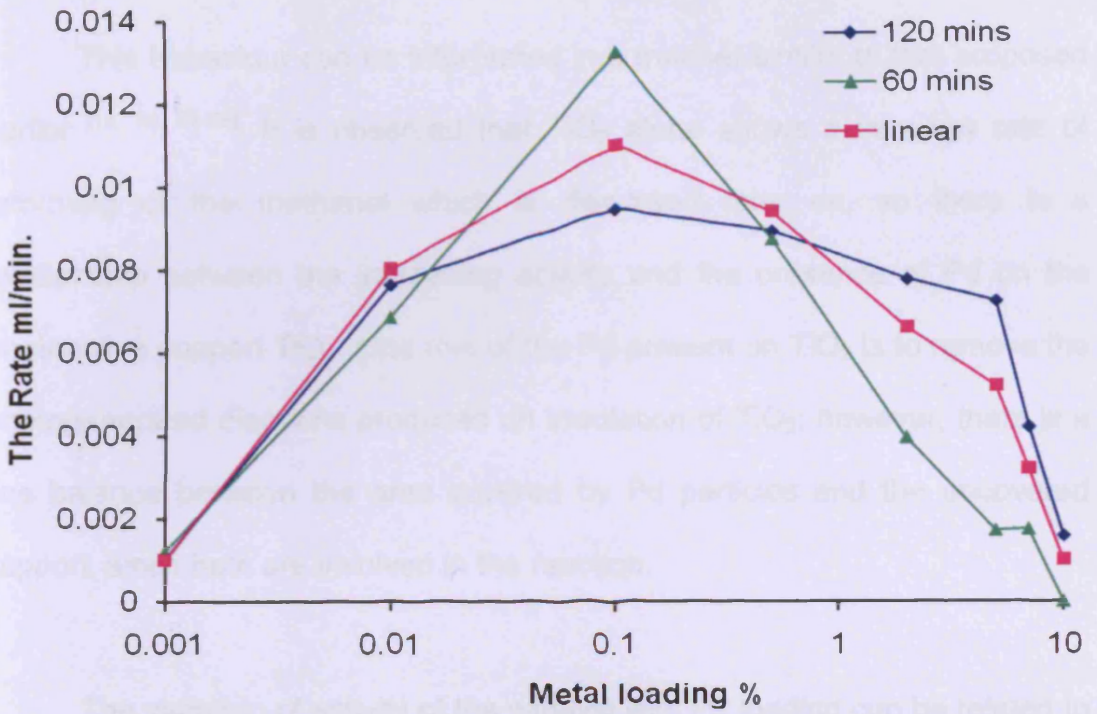

Figure 3.6: A semi-logarithmic plot of hydrogen production rates versus Pd metal loading.

Table 3.2: The rate of hydrogen production versus different metal loadings of Pd in liquid phase (µl/min).

Loading of the catalyst /g	T= 120 mins	t= 60 mins	Linear rate
0.001	1	1.02	1.02
0.01	8	6.84	7.63
0.1	11	13.25	9.46
0.5	9.4	8.73	8.93
2	6.6	3.96	7.77
5	5.2	1.72	7.25
7	3.2	1.75	4.22
10	1	0	-

This behaviour can be interpreted in a manner similar to that proposed earlier [12, 15, 32-36]. It is observed that TiO_2 alone shows a very low rate of reforming of the methanol which is discussed later on, so there is a relationship between the increasing activity and the presence of Pd on the photoactive support TiO_2. One role of the Pd present on TiO_2 is to remove the photogenerated electrons produced on irradiation of TiO_2; however, there is a fine balance between the area covered by Pd particles and the uncovered support, since both are involved in the reaction.

The variation of activity of the catalyst with Pd loading can be related to the active sites which are proposed to be at the boundary between the metal particles and the support, that is, at the interface between the metal and semiconductor[37]. As presented in figure 3.7, at low loading, the particles are separated over the surface of the support. With increasing the metal loading, the particle size increases and so the boundary length increases. As the palladium particles become big enough to almost touch, the rate of hydrogen production reaches the maximum value, where the perimeter is maximised. With increasing the coverage of TiO_2 by more palladium, the particles begin to merge which leads to a reduction of the active sites until all the surface is completely covered by the palladium when the activity reduces to zero.

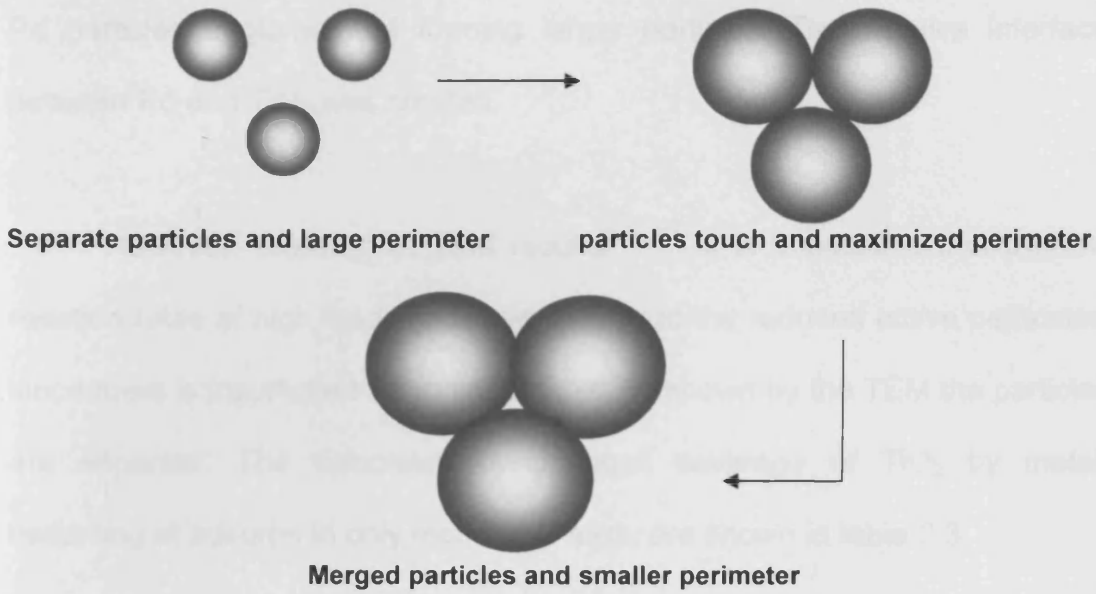

Figure 3.7: The proposed relationship between the particle growth and the rate of hydrogen production.

TEM measurements revealed the particles of Pd at highest loading were separate before and after the photoreaction. The size of Pd particle of 5% Pd/TiO_2 was ~ 3 nm for the fresh catalyst while after 5 hours of irradiation, it increased to around 6 nm[31]. The presence of large particles after reaction was attributed to the sintering process occurring during the course of the reaction. The induction time at high Pd loading may be also interpreted in the light of this process. At 10% wt Pd/TiO_2, there is no hydrogen evolved in the initial of the part of the reaction due to overlapping of Pd particles. Then hydrogen started evolving because of the sintering process, which means that

Pd particles agglomerated forming larger particles. Thus, active interface between Pd and TiO_2 was created.

However, referring to TEM results[31, 32], it is impossible that the low reaction rates at high loadings is due directly to the reduced active perimeter, since there is insufficient Pd to enable this, as shown by the TEM the particles are separate. The calculated percentages coverage of TiO_2 by metal, assuming at adsorbs in only monolayer form, are shown in table 3.3

Table 3.3: The percentage coverage of palladium on TiO_2 in monolayers at different loadings.

% wt Pd loading	Percentage coverage in monolayers
0.001	0.011371213
0.01	0.113712135
0.1	1.137121345
0.5	5.685606726
2	22.7424269
5	56.85606726
10	113.7121345

The values in table 3.3 were calculated as follows:

Number of surface atoms of TiO_2 per m^2 = 1×10^{19} atoms

Number of surface atoms of TiO_2 for 0.2 g = 1×10^{19} × 50 m^2/g (surface area of titania) × 0.2 g = 1×10^{20} atoms

Mass of Pd of 0.2 g of 0.1%Pd/TiO_2 = 2×10^{-4} g

Number of moles of Pd = Pd mass/atomic weight of Pd = $2\times10^{-4}/106$ = 1.88×10^{-6} moles

Number of atoms of Pd = number of moles × Avogadro's number

$$= 1.88\times10^{-6} \times 6.02\times10^{23} = 1.1 \times 10^{18} \text{ atoms}$$

Then, the percentage of coverage for 0.1%Pd/TiO_2 = $1.1 \times 10^{18}/1\times10^{20}$

$$\sim 1\%$$

That means that the optimum Pd loading which gave the highest rate of hydrogen production, it only covers a very small part of the surface. Therefore, the active perimeter theory could not explain the activity of catalysts with different metal loadings. Therefore, it is proposed that the active region is somewhat remote from the particles. So the active sites, which are responsible of the reaction are located remotely from the actual metal-titania interface. Thus, these remote boundaries, which surround each particle, when the metal loading increase (after the optimum loading), start overlapping at much smaller particle size. Subsequently, the rate of reaction reduces at lower loading of Pd (figure 3.8). The existence of active region remote from the metal surface could be due to the electronic depletion zone around the

particles, which in turn leads to that the carbon monoxide spills over and builds up at the interface between the metal and titania.

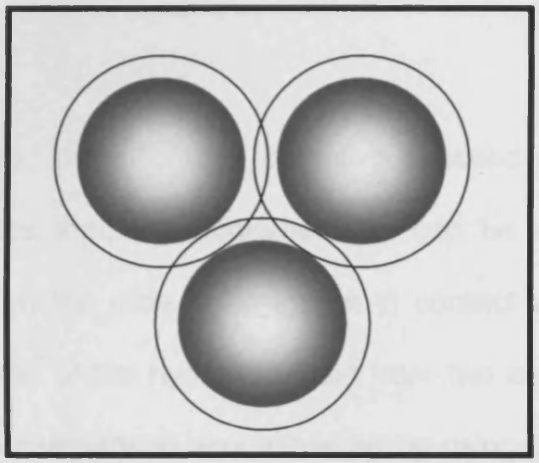

Figure 3.8: The overlapping of the boundaries of the active regions surrounded the Pd particles overlap.

3.2.4 Pd loading dependence in gas phase:

Many studies have been carried out for liquid phase for methanol reforming over Pd or Au/TiO_2 [12, 32, 33]. In the stirred aqueous solution, the chance of illumination of all the particles at the same time is non equal which means that the nearest particles from the light may mask those which are further away from the light source. Consequently, the rate of hydrogen production is affected. To avoid these problems, the reaction has also been investigated in the gas phase. In this phase, the catalyst is mounted on a thin

layer on a slide, as described in chapter two. All the slides were mounted with 50 mg of different loadings of Pd on TiO_2. It should be considered that, for all the gas phase experiments, the catalyst on the slide was suspended above 15 ml of deionised water and 100 µl methanol and was not immersed in the liquid.

By this way, more of the particles exposed to the light can be illuminated. Besides that, the agglomeration can be avoided because the catalyst mounted on the slide is no longer in contact with liquid. Figure 3.9 shows a comparison of the hydrogen yield from two experiments (liquid and gas phases). This comparison was achieved by using the free-ozone Xe arc lamp. It was observed that the optimum rate over (0.1 % wt. Pd/TiO_2) in the gas phase was more of that in liquid phase (0.5% wt. Pd/TiO_2) by 30% (78 and 47 µl/min, respectively), even though much less catalyst was used (0.05 and 0.2 g, respectively)

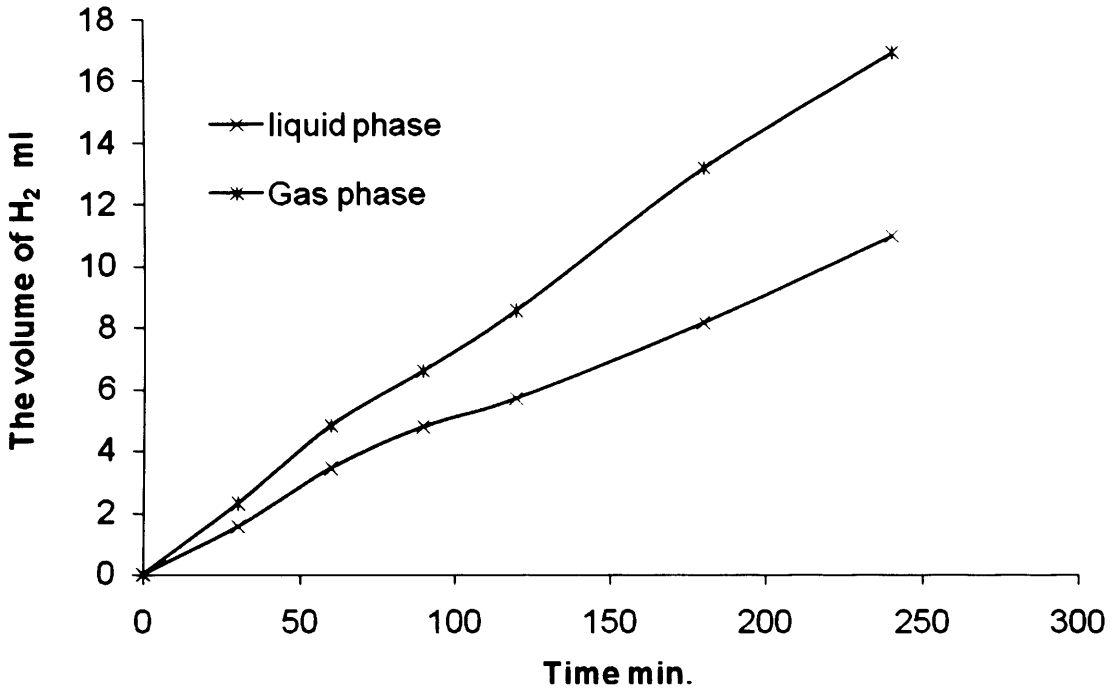

Figure 3.9: Comparison of H_2 yield from gas and liquid phase over 0.5% Pd/TiO_2.

To produce the hydrogen in this way, the water and methanol must be in the gaseous state, but it is uncertain in which form the reactants reach the catalyst. It is possible, for instance, that water and methanol condense on to the catalyst surface and that the reaction occurs in this liquid-like layer. During the reaction, the temperature was measured by inserting thermocouple through the side arm of the reactor (attached with the slide) and it was ~95° C, and it is felt that condensation is unlikely.

In figure 3.10, the amount of hydrogen evolution is similar to that in the liquid phase but is more linear, and is for only ¼ of the amount of catalyst. Even small quantity of palladium on TiO_2 (0.001%w Pd) caused a significant increase in the amount of hydrogen evolved but adding Pd above 0.1% (0.5-20%), the hydrogen production decreased. In figure 3.11, 3.12 and table 3.4, 0.1% loading appears to be about the optimum loading and with further Pd the rate decreased. 20% gives nearly the same rate for that TiO_2 alone.

In gas phase, there are a number of differences from the liquid phase experiments:

i) Higher maximum rate

ii) TiO_2 alone appears to have significant activity.

iii) Higher activity at high loading with no induction period.

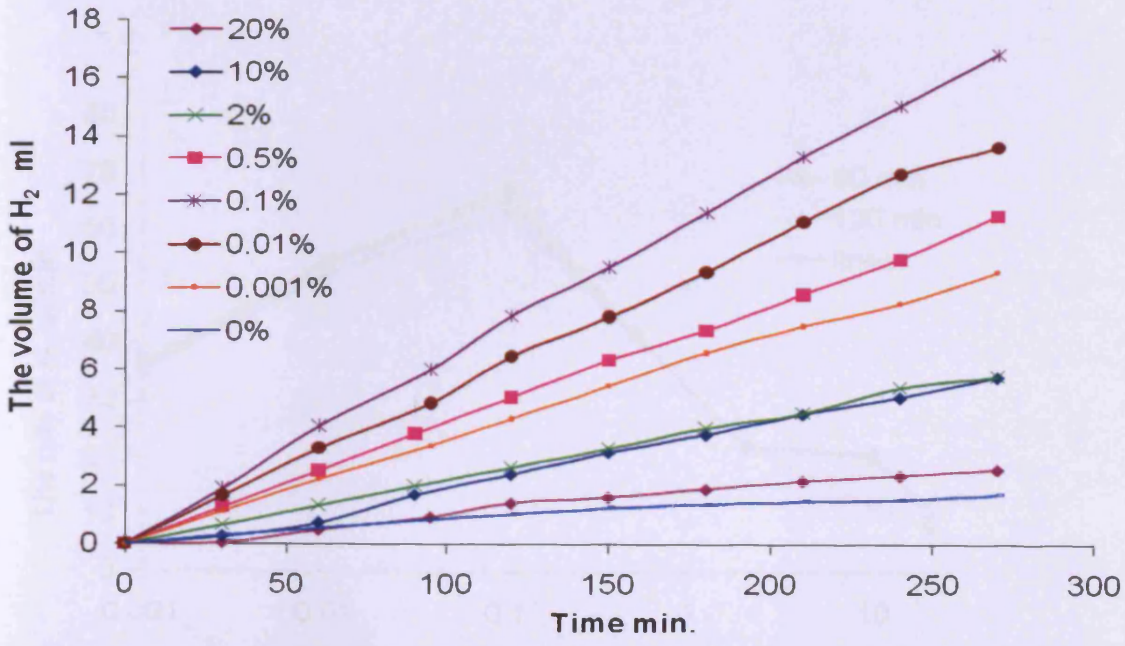

Figure 3.10: The effect of Pd loadings on the hydrogen production in gas phase.

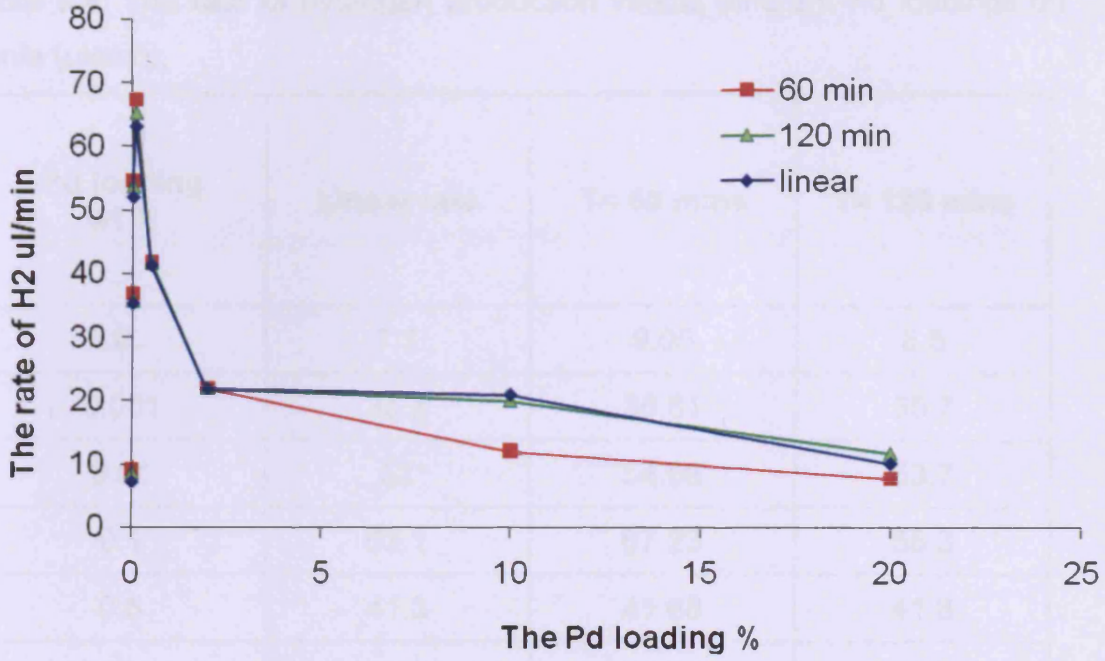

Figure 3.11: The rate of hydrogen production versus the Pd loading.

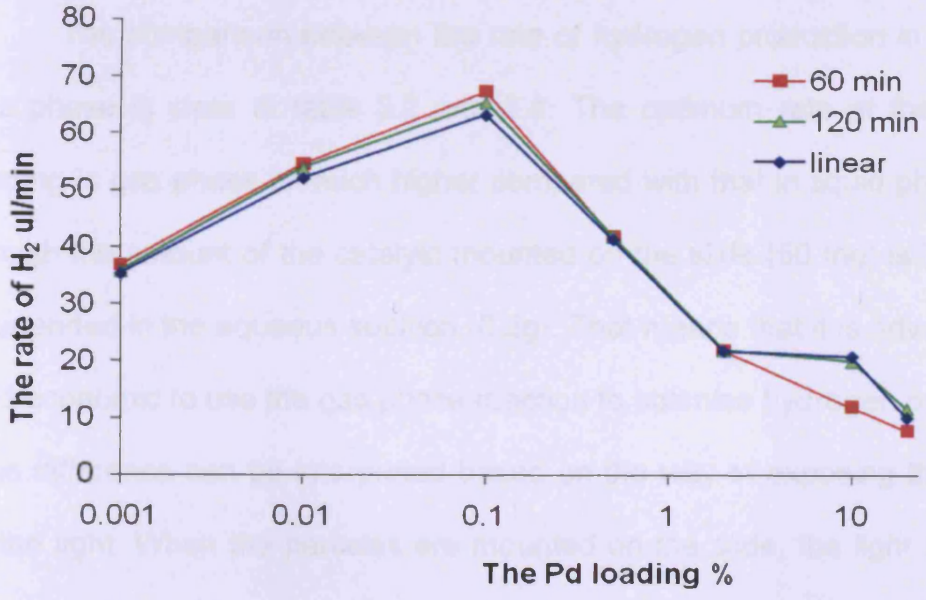

Figure 3.12: A logarithmic plot of the rate of H_2 over different Pd loadings.

Table 3.4: The rate of hydrogen production versus different Pd loadings on titania (µl/min).

Pd loading wt %	Linear rate	T= 60 mins	T= 120 mins
0	7.1	9.05	8.5
0.001	35.3	36.81	35.7
0.01	52	54.56	53.7
0.1	63.1	67.23	65.3
0.5	41.3	41.68	41.8
2	21.8	21.85	21.9
5	24.5	23.815	24.7
10	20.8	11.98	19.9
20	10	7.7	11.6

The comparison between the rate of hydrogen production in liquid and gas phase is clear in table 3.2 and 3.4. The optimum rate at the optimum loading in gas phase is much higher compared with that in liquid phase, even though the amount of the catalyst mounted on the slide (50 mg) is lower than suspended in the aqueous solution (0.2g). That means that it is advantageous and economic to use the gas phase reaction to optimise hydrogen production. This difference can be interpreted based on the way of exposing the catalyst to the light. When the particles are mounted on the slide, the light is focused better on the catalyst than it is on the suspended particles, and thus the illumination efficiency is higher.

3.2.5 The effect of optical density

The number of photons come from the Xe lamp can be controlled by using filter which transmits a part of photons coming from the lamp source. 2 g of 0.5% Pd/TiO_2 suspended in 100 ml of deionized water and 100 µl of methanol was illuminated by different quantities of photons using three filters which differ in the transmittance (10, 25, 50%) and as well as the same reaction was carried out without a filter (the standard reaction). Such reaction is considered photocatalytic reaction as it was not observed any hydrogen in the absence of light.

Figure 3.13 and 3.14 showed that the highest rate was in the case which there was no filter. Moreover, in this figure, there was a significant difference of H_2 yields. When the transmittance increases, the number of photons increases and hence the rate of hydrogen production increases. The increase of quantity of photons means the number of illumnated of TiO_2 particles increases and hence the rate of hydrogen production. However, Not all the photons produced from the lamp source go through the reactor due to the transmittance of the Pyrex flask was above 300 nm, as mentioned in chapter two.

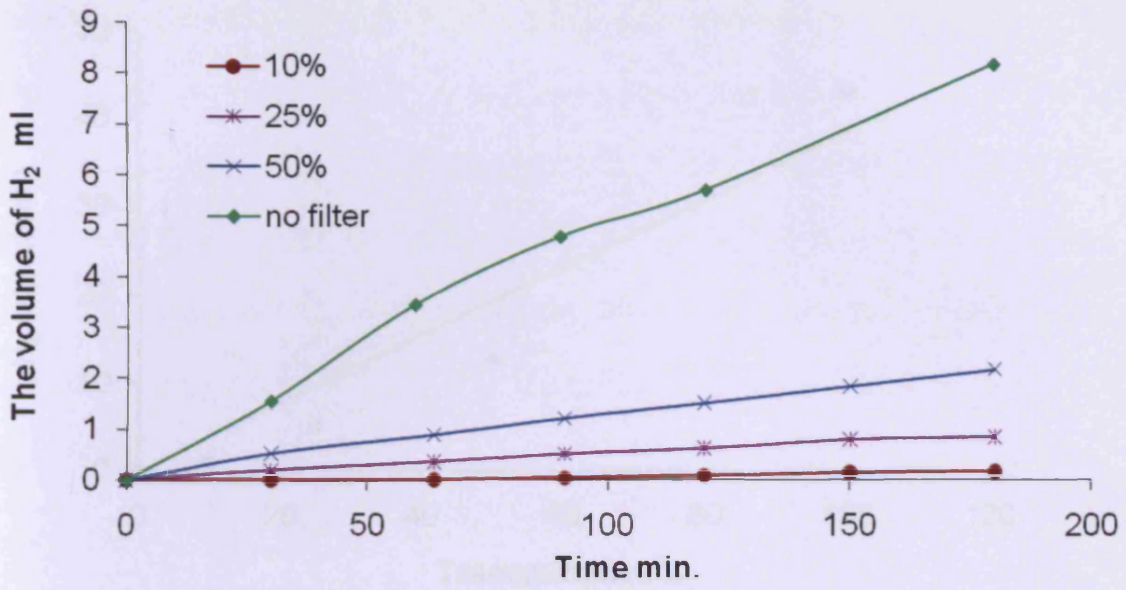

Figure 3.13: The effect of optical density on the hydrogen production.

In figure 3.14, it is observed that there was a marked effect on the rate of hydrogen formed after placing a filter. The production of hydrogen decreased by 3 times when 50% of photons were transmitted compared to that no filter used. In addition of that, the increase of H_2 production rate is linear with increase of the photons which means the reaction is approximate first order with respect of light.

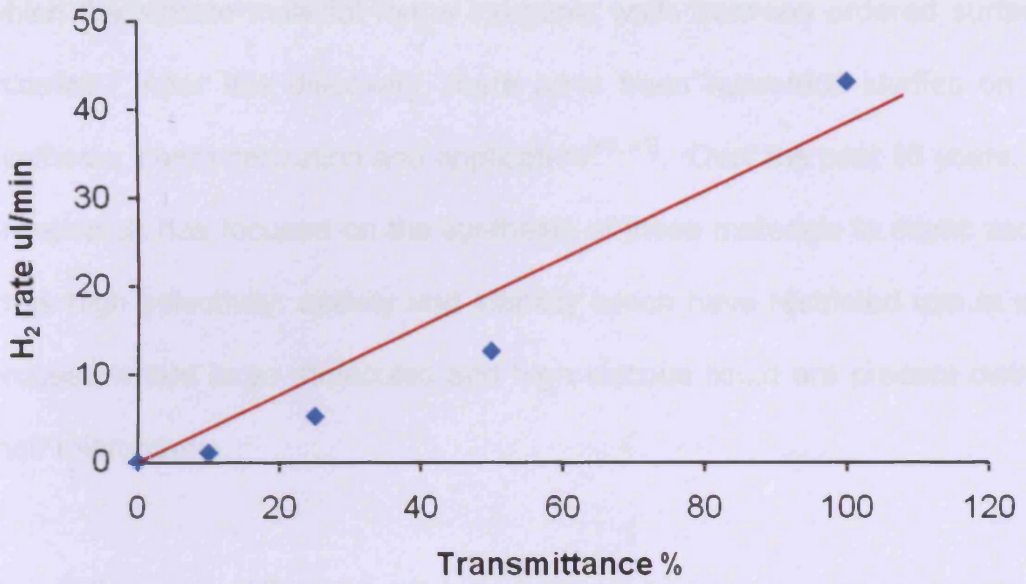

Figure 3.14: Hydrogen production rate versus different percentage transmittance.

3.2.6 Hydrogen production over mesoporous TiO_2 ($MTiO_2$)

According to IUPAC notation, porous materials were divided into several kinds by their pore diameter. Microporous materials have pore diameters of less than 2 nm and macroporous materials have pore diameters of greater than 50 nm; the mesoporous category thus lies in the middle. Their large internal surface area, as high as 1,000 m^2/g, and large uniform pores, make them useful for applications in catalysis, separation and absorption. Mobil Corporation invented the successful method of ordered mesoporous molecular sieve (M41S)[38, 39]. They proposed that the formation of these materials takes place by means of a liquid-crystal 'templating' mechanism, in

which the silicate material forms inorganic walls between ordered surfactant micelles. After this discovery, there have been numerous studies on their synthesis, characterization and application[40, 41]. Over the past 10 years, a lot of research has focused on the synthesis of these materials to mimic zeolites in its high selectivity, activity and stability which have restricted use in some process where large molecules and high viscous liquid are present owing to their micropores.

There are different synthesis methods to form mesoporous materials, among of them is the templating as mentioned in Mobil work. By another way, a typical synthesis starts with formation of organic micellar species in aqueous solution, then polycondensation of an inorganic matrix and finally removal of the organic template. Yao *et al.* reported the first new templateless procedure which is based on the synthesis of the mesoporous structure in the absence of surfactant to avoid calcination or extraction method as well as use the large amount of expensive and toxic materials serving as template[42]. The mesoporous materials prepared by this method were mesoporous silica-alumina materials with narrow pore size distribution and large specific surface area.

By the typical approach, many porous non-silica oxides were synthesized[43, 44]. Mesoporous titanium dioxide is among those materials which has a great role in a lot of photocatalytic reactions. The first successful attempt for synthesizing mesoporous amorphous titanium dioxide was by Antonelli using alkyl phosphate as surfactant in the modified sol-gel

synthesis[43]. The calcinations or solvent extraction is generally used to remove the phosphorous from the template to get high surface area's catalyst. However, it was difficult to achieve that completely in the case of preparation of titanium dioxide because phosphorous is bound strongly to the molecular sieve[45]. Subsequently it affects the catalytic properties of TiO_2. Liu *et al.* reported a novel simple, template-free synthetic approach for preparing of mesoporous titanium oxide[46]. This route, considered an inexpensive synthesis, involved HNO_3-catalyzed hydrolysis and polymerization of TBT (titanium (IV) n-butoxide) in ethanol without using a structure-directing template.

In this work, mesoporous titanium dioxide $MTiO_2$ was prepared through template-less method in the National Chemical Laboratory in Pune, India by Gopinath *et al* was used as photocatalyst to investigate the rate of photocatalytic hydrogen production. The preparation method was described in chapter two.

To investigate the activity of mesoporous TiO_2 in photocatalytic hydrogen production, 0.5, 2 and 10% wt. Pd/$MTiO_2$ were prepared by the impregnation method. Figure 3.15 shows the comparison between the activities of $MTiO_2$ and commercial Degussa P25 at the same Pd loading, in liquid phase. Pd/TiO_2 (P25) was twice as active as Pd/$MTiO_2$. This could have been due to too low a Pd loading. So this led us to prepare 2 and 10% wt. Pd/$MTiO_2$ to clarify more regarding the effect of metal loading on its activity.

These high loadings were tested in gas phase. Figure 3.16 showed that none of these loadings gave hydrogen more than over 0.5%Pd/TiO_2.

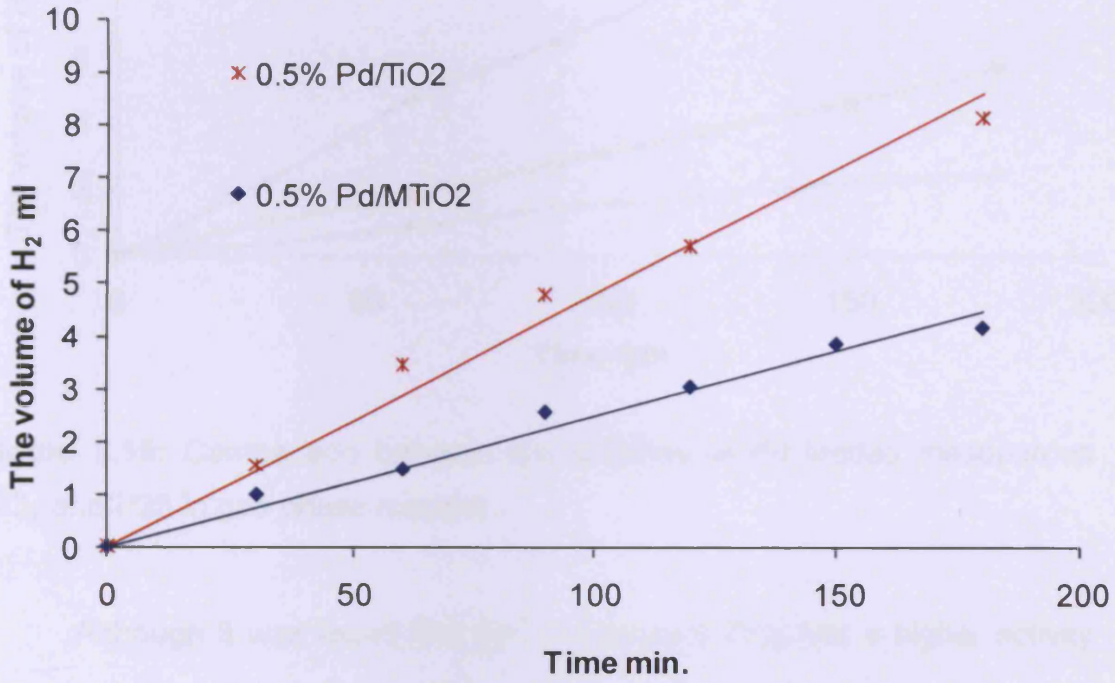

Figure 3.15: Comparison between the activities of 0.5% Pd loaded mesoporous TiO_2 and P25 in liquid phase reaction.

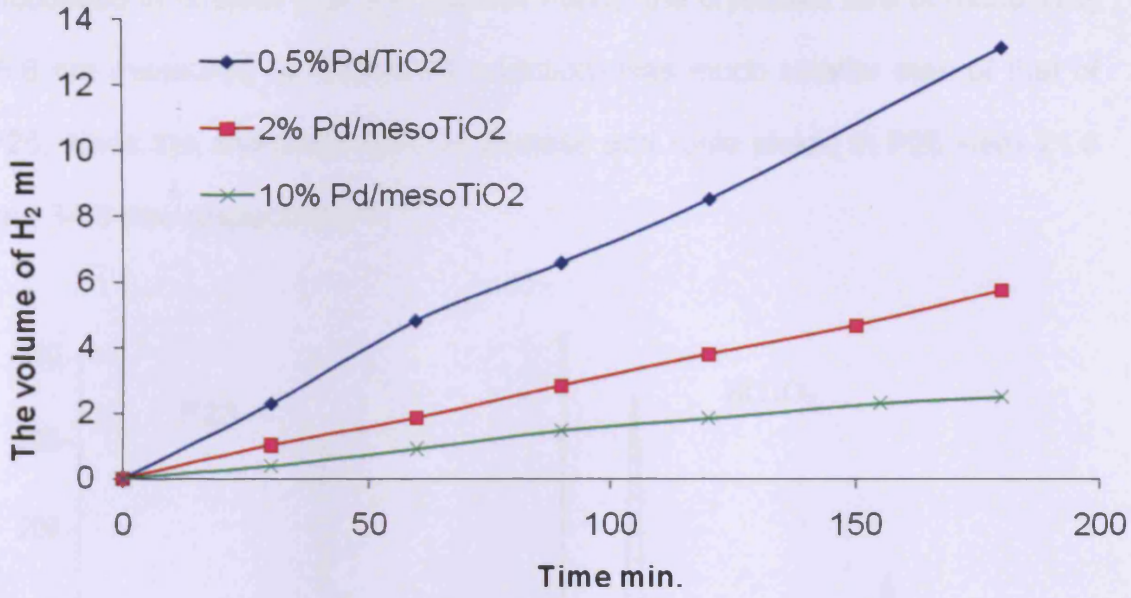

Figure 3.16: Comparison between the activities of Pd loaded mesoporous TiO_2 and P25 in gas phase reaction.

Although it was found that the mesoporous TiO_2 has a higher activity than Degussa in the oxidation of formaldehyde and acetone[47], their activities alone without Pd loading in production of hydrogen were the opposite in our work. There was no hydrogen from methanol at all in the case of mesoporous TiO_2 that has high surface area while some hydrogen was detected over TiO_2 P25, as a shown later in chapter 5.

When P25 and meso-TiO_2 were characterised by XRD, a significant difference was obtained in terms of the kind of the phase and the crystallite size, which was calculated by Scherrer's equation. Figure 3.17 displays diffraction peaks at 2θ = 25.3, 38.0, 48.1 and 55.3°, which means the meso-TiO_2 was composed of the anatase phase only. However, the P25 was anatase phase with some rutile, which in turn increases the activity of TiO_2 as

disccused in chapter four. On another hand, the crystallite size of meso-TiO_2 (6.8 nm measured by Scherrer's equation) was much smaller than of that of P25, since the crystallite sizes of anatase and rutile phase in P25 were 21.6 and 34.6 nm, respectively[33, 48].

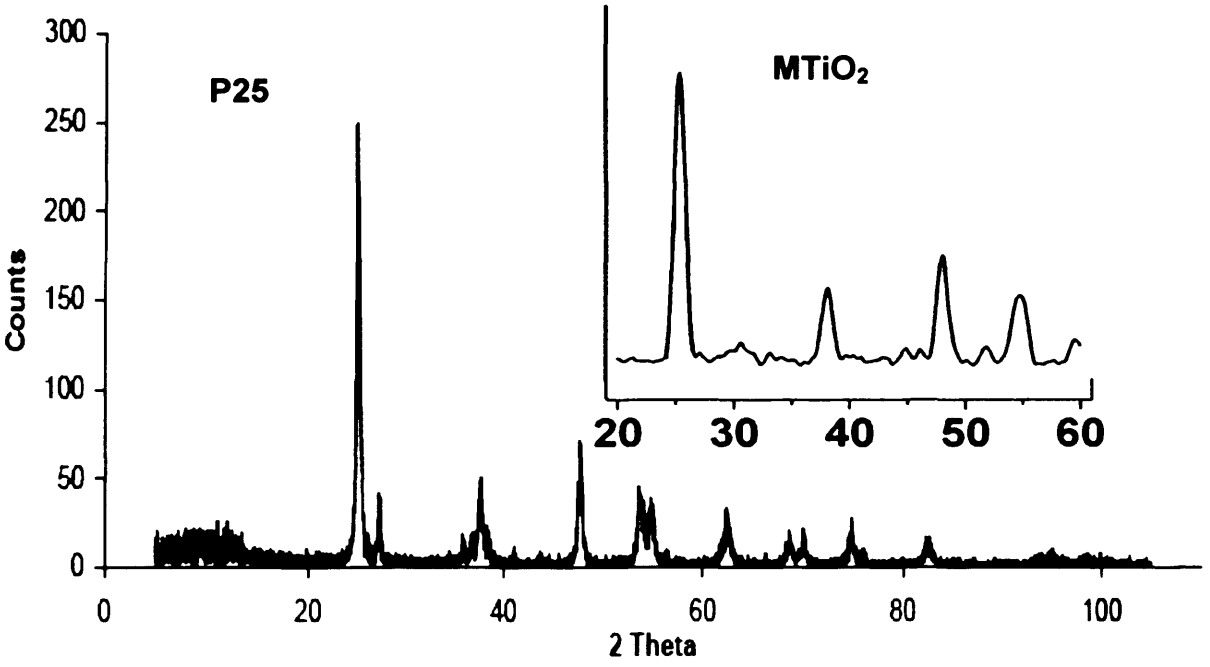

Figure 3.17: XRD analysis of TiO_2 P25 and mesoporous titanium dioxide $MTiO_2$ prepared by template free method.

3.2.7 The effect of methanol concentration

As mentioned previously, the addition of sacrificial reagents such as alcohols and other organic materials inhibit the hydrogen/oxygen reaction and

increase the rate of hydrogen production [2, 3, 35, 49]. Moreover, these materials are able to reduce the recombination of photogenerated electrons and holes.

Dickinson investigated sets of different concentrations of methanol on the rate of H_2 production[32]. The effect was clear between the rate of H_2 production with or without methanol. The hydrogen production increased with increasing the methanol concentrations, though the greatest rate was more apparent at low concentration. When the rate of hydrogen production per gram of methanol used was calculated and plotted against methanol concentration, the correlation displayed that the optimum rate was at low methanol concentration. This study demonstrated that the rate of hydrogen evolution had little dependence on the concentration of methanol. Similar results in the case of gas phase that methanol concentration had a roughly zeroth order effect on the rate[12].

However, the methanol concentration range was rather limited in Dickinson's study, and so here very low volumes 0, 3, 10, 30, 50, 100, 200 and 300 µl methanol were added to 100 ml of deionised water with 0.2 g of 0.5%w Pd/TiO_2, in order to elucidate the dependence clearly. Figure 3.18 shows the evolution of hydrogen versus time. At low concentrations, the rate of reaction depends strongly on the volume of methanol added. With increasing the volume from 3 to 30 µl, the rate increases. Above 30 µl, there is little obvious change. This behaviour is a typical kind of Langmuirian catalytic reaction, which is manifested in figure 3.19 as the rate of hydrogen production against methanol concentration. In all the experiments, the conversion is low

and thus the rate of hydrogen formation is not affected by reactant concentration changes during the time of the individual experiments.

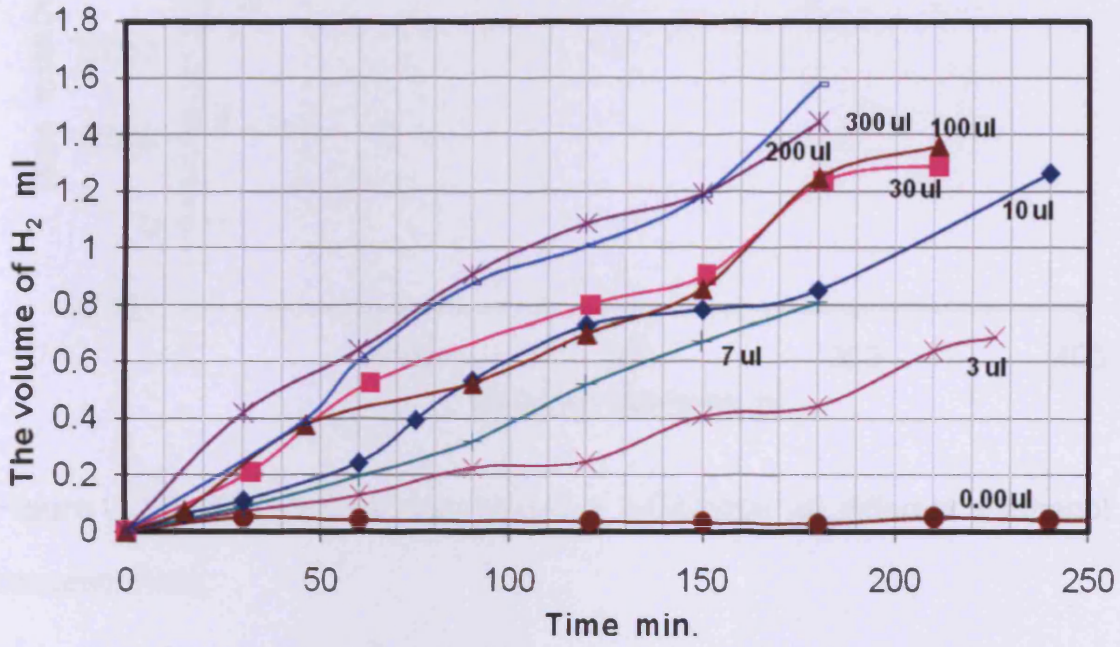

Figure 3.18: The effect of methanol amount on the hydrogen production.

The minimum amount of methanol required to cover the surface of the catalyst as a monolayer can be derived as follows:

Specific area of the catalyst = 59 m^2/g

The surface area of 0.2 g of 0.5%Pd/TiO_2 = 11.8 m^2

The number of the surface atoms ~10^{19} m^{-2}

Thus, the number of surface atoms in 0.2 g of 0.5%Pd/TiO_2 = 1.18 × 10^{20}

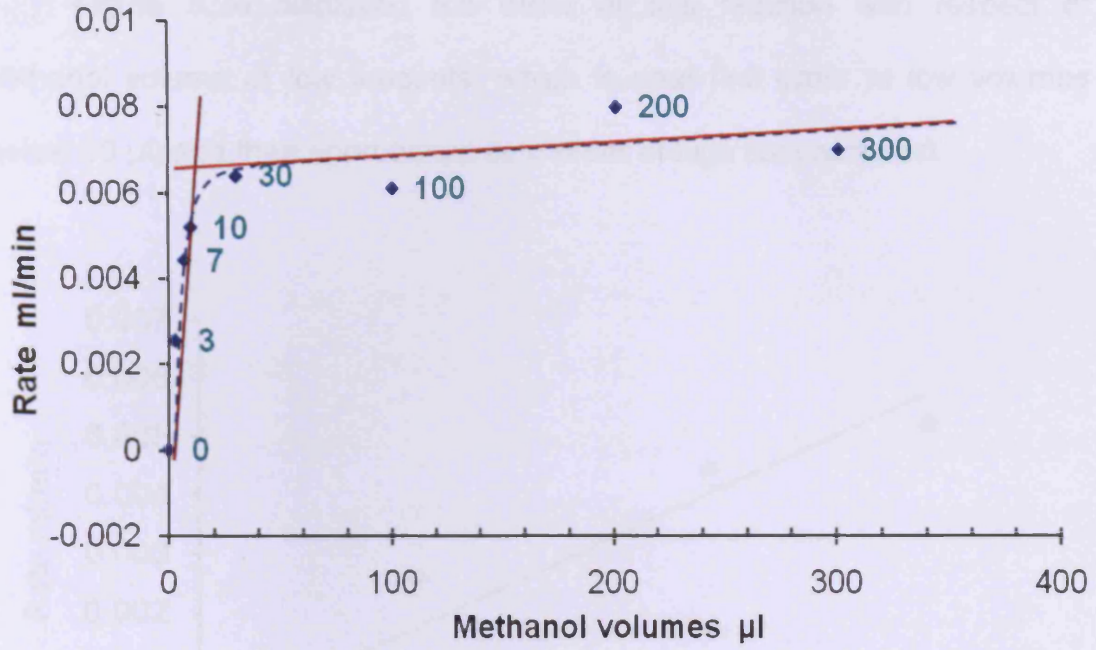

Figure 3.19: The rate of the hydrogen production at different methanol concentrations.

Figure 3.19 illustrated that the rate is maximized at ~ 10 µl of methanol, which corresponds with 1.4×10^{20} molecules. This number of methanol molecules are almost the same of the number of the surface atoms, though it must be noted that the 10 µl, from figure 3.19, extrapolated is rather approximate. However, the closeness of these two numbers indicates that at this point, all the active centres of the catalyst are saturated by the reactants (i.e. the monolayer is formed according to Langmuir model). As a result of that, the rate of hydrogen production increases with increasing of methanol concentration until the monolayer formed, and then there is no marked change thereafter as the methanol is in excess.

Figure 3.20 displayed the order of this reaction with respect of methanol volume at low amounts, which is near first order at low volumes (below 30 µl) and then approaches zero order at high concentration.

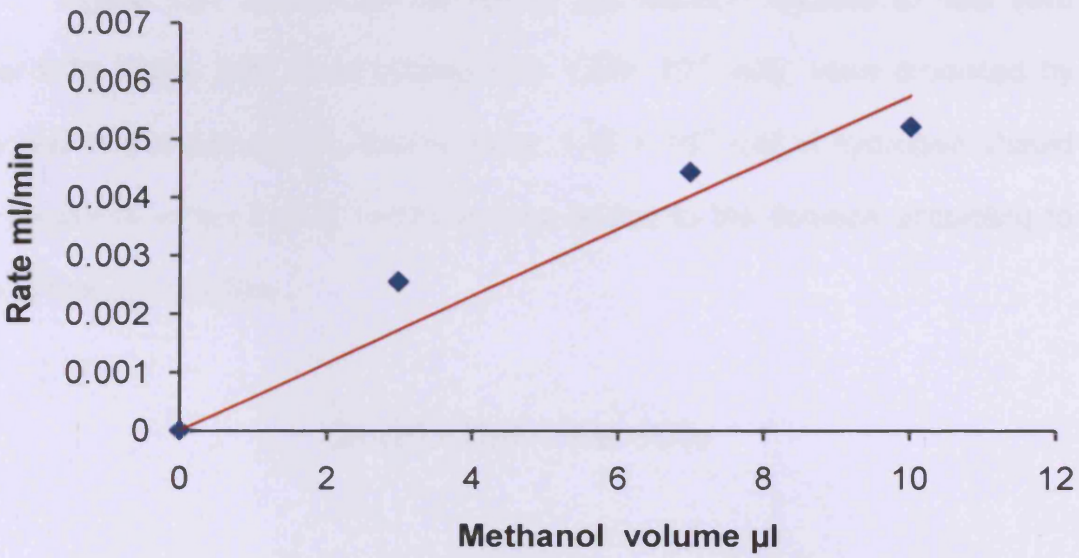

Figure 3.20: Dependence of hydrogen production rate on low methanol concentrations.

3.2.8 The reaction completion at low methanol concentration

In the most of the last experiments, it is observed that the rate of the reaction decreased slowly with the time. To study whether the decrease in the rate of hydrogen production due to the catalyst deactivating or consumption of methanol completely, a very small amount of methanol was used.

2 µl of methanol was added to 100 ml of deionised water mixed with 0.2 g of 0.5% w Pd/TiO_2. The mixture was irradiated with stirring and analyzed the gas produced every 30 minutes and was carried out for a very long time.

Figure 3.21 shows that the rate of the reaction reduced to near zero after 9.30 hours. 3.55 ml of hydrogen (= 1.48×10^{-4} mol) were produced by the end of the experiment. Theoretically, 1.48×10^{-4} mol of hydrogen should be produced when 2 µl of methanol was added to the solution according to the following equation:

$$CH_3OH + H_2O = 3H_2 + CO_2$$

So excellent compatibility between the theoretical and practical results is apparent, confirming the stoichiometry above.

To demonstrate further that the catalyst was not poisoned, three drops of methanol were added to the mixture after the reaction stopped and it was found the rate of hydrogen evolution increased once again. This increase proved that the catalyst was still effective for producing hydrogen from the reforming of methanol. Hence the ceasing of hydrogen production after a long time was because all the methanol molecules were consumed by reaction. This result demonstrated strongly that Pd/TiO_2 was stable in spite of a long period of illuminating the catalyst which is considered to be an important requirements of a useful photocatalysts.

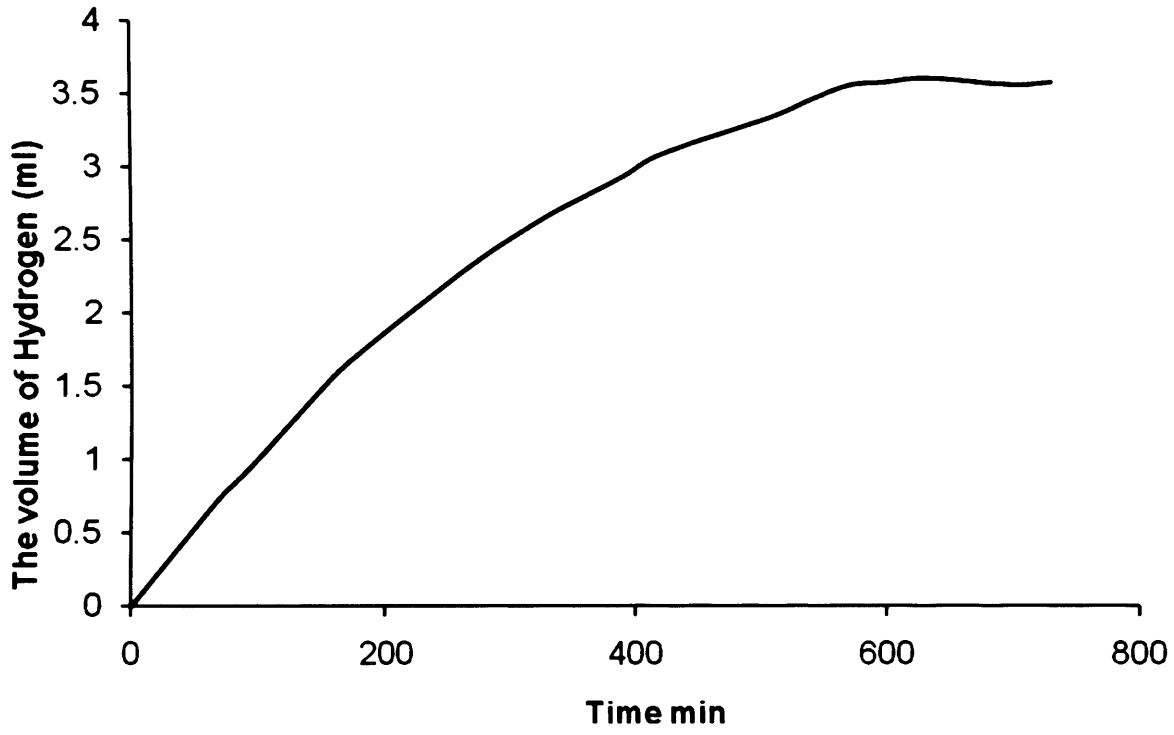

Figure 3.21: the completion reaction at low concentration of methanol.

3.2.9 Comparison between the photoreforming of methanol and glycerol

Since the energy crisis in 1970, there has been considerable interest in the development of alternative and renewable energy sources. Current concerns over finite natural oil reserves and the impending consequences of global warming has led to a considerable increase in the attention given to this area. The use of biodiesel appears to offer a means of reducing both net carbon dioxide emissions and air pollution, thus it is a renewable and environmentally friendly fuel. In specific definition, biodiesels are alkyl esters of fatty acids and are a fuel made from vegetable oils or animal fats. The transesterification route is the usual process to produce biodiesel. This

process is depicted as follows; 45 pounds of fat or oil (such as soybean oil) are reacted with 4.5 pounds of a short chain alcohol in the presence of a catalyst to produce 4.5 pounds of glycerol and 45 pounds of biodiesel. However, one of the issues of this technology is that for every tonne of biodiesel generated, 220.5 pounds (100 kg) of glycerol is produced and this has an adverse effect on biodiesel economics. There is therefore a need to identify new routes by which the side product glycerol can be converted into useful products. Recently, several approaches have been reported to produce high-value products from an abundant glycerol. Catalytic conversion processes are crucial to convert glycerol to useful chemicals. Scheme 1 shows several different approaches regarding to these conversions[50]. Pyrolysis and gasification of glycerol processes can be a source of hydrogen as liquid or gas fuel depending on the temperatures. However, the difference between these processes is the gasification is done in the presence of oxygen. A high H_2 yield was produced by the gasification of glycerol using supercritical water without a catalyst[51].

As known, the reforming process of glycerol represents steam reforming, catalytic partial oxidation, or autothermal reforming based on the source of heat and the kind of the reactants according to the general equation:

$$C_3H_8O_3 + x\ H_2O + y\ O_2 = a\ CO_2 + b\ CO + c\ H_2O + d\ H_2 + e\ CH_4 + ...$$

Dauenhauer and co-workers examined the autothermal reforming of glycerol and found that rhodium supported on alumina foams had a high fuel conversion and high selectivity to H_2[52].

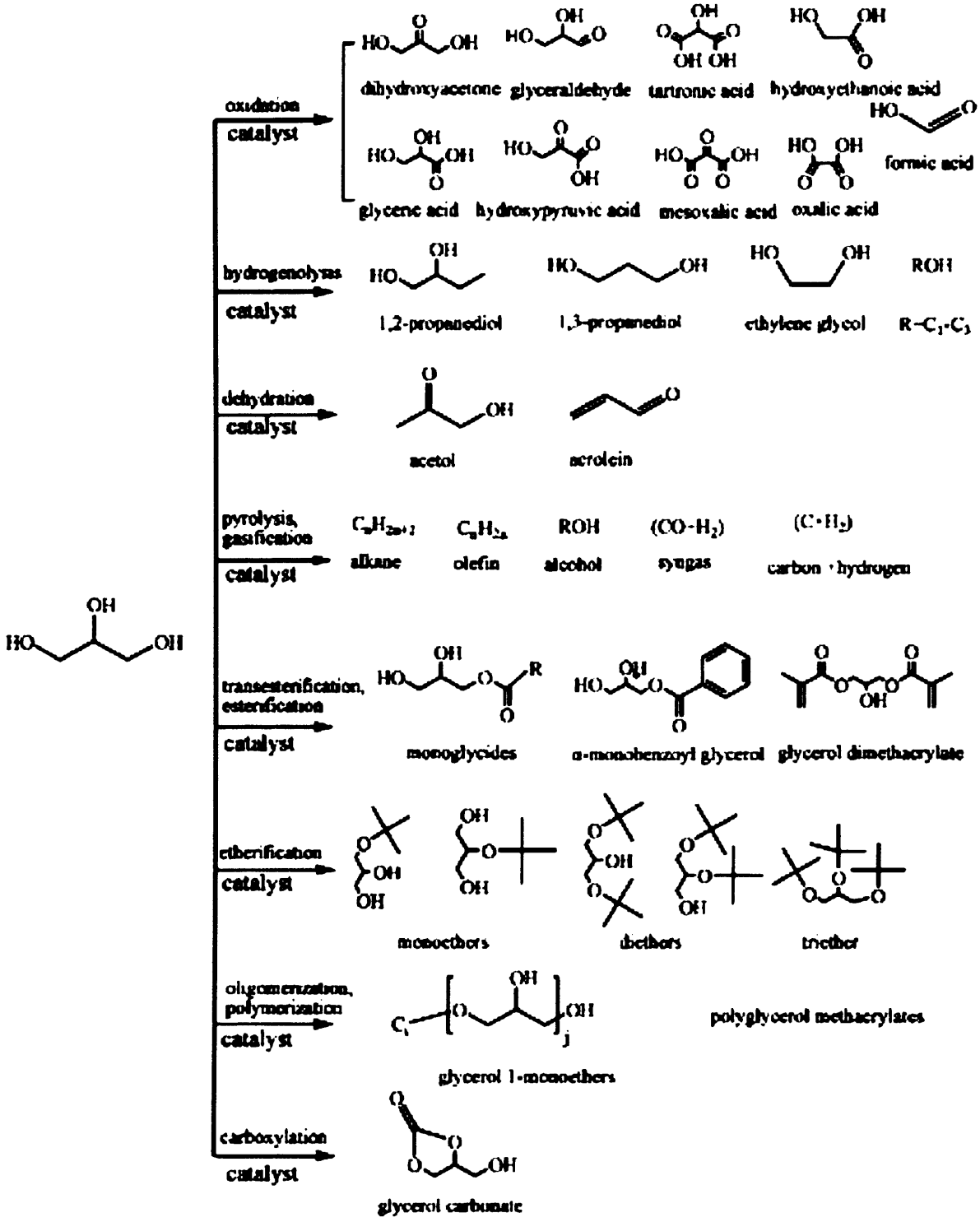

Scheme 1: processes of catalytic conversion of glycerol into useful chemicals.

Beside that, the conversion of glycerol to hydrogen by using the steam reforming process was studied recently by Douette *et al* [53]. This research used glycerol as reforming feedstock for hydrogen production using a fixed bed reactor of based-nickel catalyst. Oxygen to carbon ratio, steam to carbon ratio and temperature had an effect on the rate of the conversion of glycerol. The best yield of hydrogen produced (4.6 mol H_2 / mol glycerol) was when the steam to carbon ratio was 2.2 and the temperature was 760° C. This yield represented 65 % of the stoichiometric reforming of glycerol (7 mol H_2 / mol glycerol) as shown in the following equation:

$$C_3H_8O_3 + H_2O \rightarrow 7H_2 + 3CO_2 \quad (1)$$

Douette *et al* also investigated the use of the crude glycerol obtained from the biodiesel which contains NaCl, NaOH and another impurities. It was found the initial rates of reforming of crude glycerol is similar of that for pure glycerol then the rate decreased due to the deactivation of the catalyst. Na was responsible for reducing the activity. When it was added to the pure glycerol, the rate tended to the same behaviour as in the case of crude glycerol.

Photocatalysis may be an economical and an alternative approach to the conversion of glycerol, which overcomes the issue of using high temperatures and the catalyst poisoning. Reforming of glycerol photocatalytically can be performed in an analogous way to the reforming of methanol in this work. 100 ml of deionised water was stirred with 0.2 g of

catalyst (0.5% w Pd/TiO_2 or 2% w Au/TiO_2) and 100 µl of glycerol or methanol and illuminated to 3 hours. The gaseous products were analysed by GC and MS in the same time. These loadings of Pd and Au were chosen because they gave the optimum hydrogen production rate.

The rate of hydrogen evolution from oxidation of glycerol is depicted in figure 3.22 and is compared with the result with for methanol.

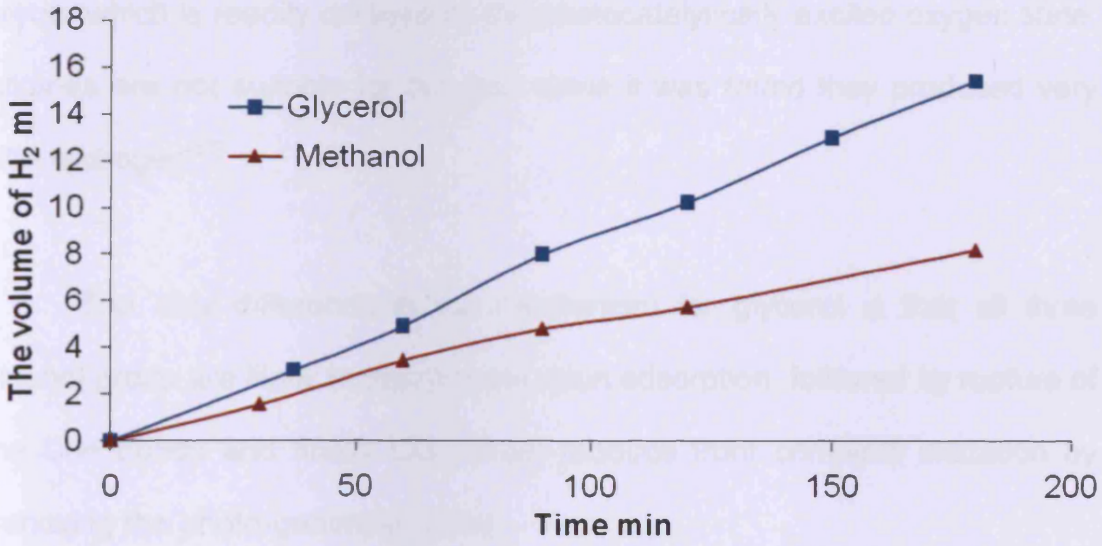

Figure 3.22: The rates of hydrogen production from the photocatalytic reforming of glycerol and methanol over a 0.5% Pd/TiO_2.

Hydrogen production rates of reforming of glycerol and methanol were constant with irradiation time and they were 85.3 and 45 µl/min, respectively. Subsequently, these results indicate that the rate from glycerol was double of

that of methanol. The stoichiometric reactions prove the rates observed through equation 3-6 and 3-7, since glycerol contains three hydroxyl groups compared to that of methanol,

$$C_3H_8O_3 + H_2O \rightarrow 7H_2 + 3CO_2 \quad (3\text{-}6)$$

$$CH_3OH + H_2O \rightarrow 3H_2 + CO_2 \quad (3\text{-}7)$$

The present experiment confirms that the most important factor for hydrogen production from such molecules is the presence of an alcohol group, which is readily oxidised by the photocatalytically excited oxygen state. Alkanes are not suitable for this goal since it was found they produced very little hydrogen[33].

The only difference in the mechanism for glycerol is that all three alcohol group are likely to deprotonate upon adsorption, followed by rupture of the C-H bonds and finally CO_2 would produce from complete oxidation by removing the photo-generated holes.

The same reactions were carried out over 2% wt Au/TiO_2. 2% of Au was reported as an optimum loading[33]. Figure 3.23 showed that the same comparison between the reforming of methanol and glycerol over this catalyst. Like Pd/TiO_2, the rate of hydrogen production from reforming of glycerol was higher than from that of methanol (48 and 13 µl/min), respectively. However, the difference between the rates here was more than three times.

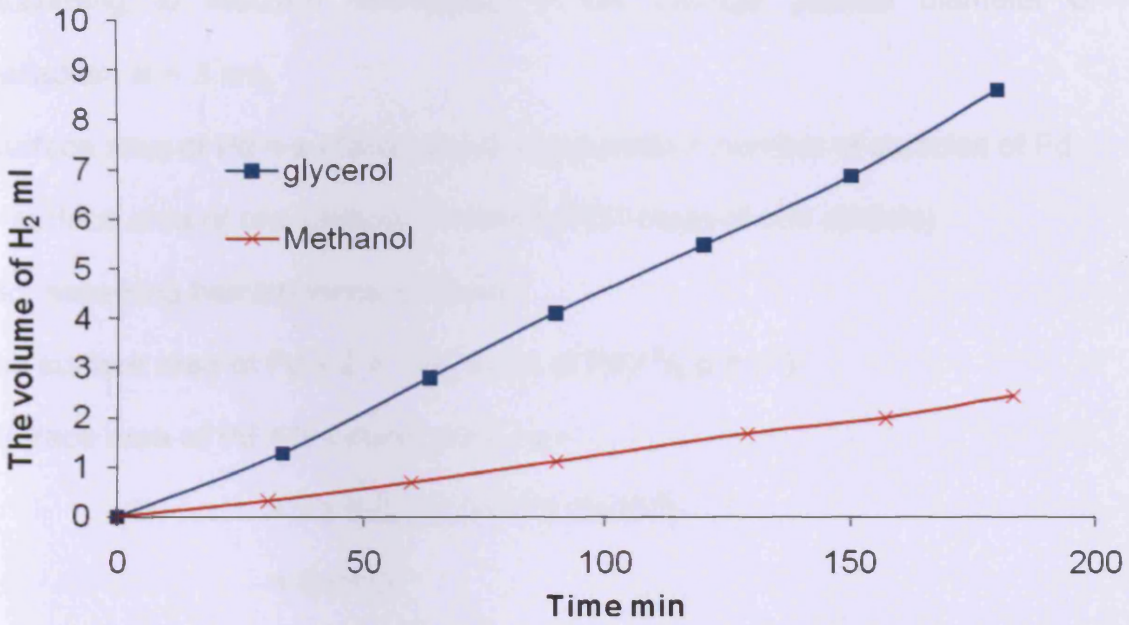

Figure 3.23: The rates of hydrogen production from the photocatalytic reforming of glycerol and methanol over a 2% Au/TiO_2.

Au/TiO_2 catalysts have shown photocatalytic activity for the evolution of hydrogen despite the fact that to be believed it was inactive in the catalytic reactions [14, 15, 54, 55]. Although this catalyst appeared to have good activity towards the hydrogen production, reforming of glycerol over Au was 1.7 times slower than over Palladium.

Based on the diameter of the metal particles, their surface area can be calculated.

In the case of 0.5% w Pd/TiO_2:

The mass of Pd for 2 gram of titania = 0.01 g

The density of palladium = 12 g/cm^3

According to electron microscopy[32], the average particle diameter of palladium is ~ 3 nm.

Surface area of Pd = surface area of one particle × number of particles of Pd

= surface area of one particle × (mass of Pd / mass of one particle)

So, assuming hemispherical particles,

the surface area of Pd = $2 \pi r^2 \times$ (mass of Pd / $^2/_3 \rho \pi r^3$)

Surface area of Pd = 3 × mass of Pd / p r

$= 3 \times 0.01 / (12 \times 10^6).(3 \times 10^{-9})$

$= 0.83\ m^2$

So, the surface composition is 1.66% Pd, since the surface area of TiO_2 (P25) is 50 m^2.

Secondly, 2% w Au/TiO_2 was used in the reforming of methanol and glycerol. To compare the surface composition by optimum loading of Pd with of that of Au, the same calculations mentioned above was used as follows:

The mass of gold for 2 g of titania = 0.04 g

The density of gold = 19.3 g/cm^3

According to XRD results[33], the diameter of gold particle is 37.6 nm.

Surface area of Au = 3 × mass of Pd / ρ r

$= 3 \times 0.04 / (19.3 \times 10^6).(37.6 \times 10^{-9})$

$= 0.165\ m^2$

So, the surface composition in the case of Au/TiO_2 is 0.33 %. Now the comparison between two optimum loading of these catalysts becomes more

apparent as the surface area per unit volume for Au/TiO_2 is much lower than of that in the case of Pd/TiO_2.

The mechanism of reforming of glycerol over Pd/TiO_2 and Au/TiO_2 can be proposed on the light of the mechanism of reforming of methanol over these catalysts[32, 33]. Figure 3.24 illustrates the mechanism of photocatalytic methanol reforming over Pd/TiO_2 as a catalytic cycle. Methanol adsorbs dissociatively on Pd metal forming CO and liberating two moles of hydrogen while on the surface of titania, water is reduced forming hydrogen gas. In the absence of light, CO strongly adsorbed would poisoned the metal (desorption temperature 450 K)[56] and the reaction would stop (a). When TiO_2 is exposed to UV light, the electron absorbs the photon and is excited from valence to the conduction band producing highly activated oxygen species, which it is possible as O^-. The excitation process takes place when the wavelength of light is equal or greater than the band gap of TiO_2 (3.2 eV) (b). The electrophilic species formed attacks CO adsorbed on the metal to form CO_2 leaving a hole on TiO_2 (h^+), which is filled by H_2O molecule, and surface vacancy on Pd (V) which is filled by another methanol molecule (c and d). Therefore, the reaction cycle restarts.

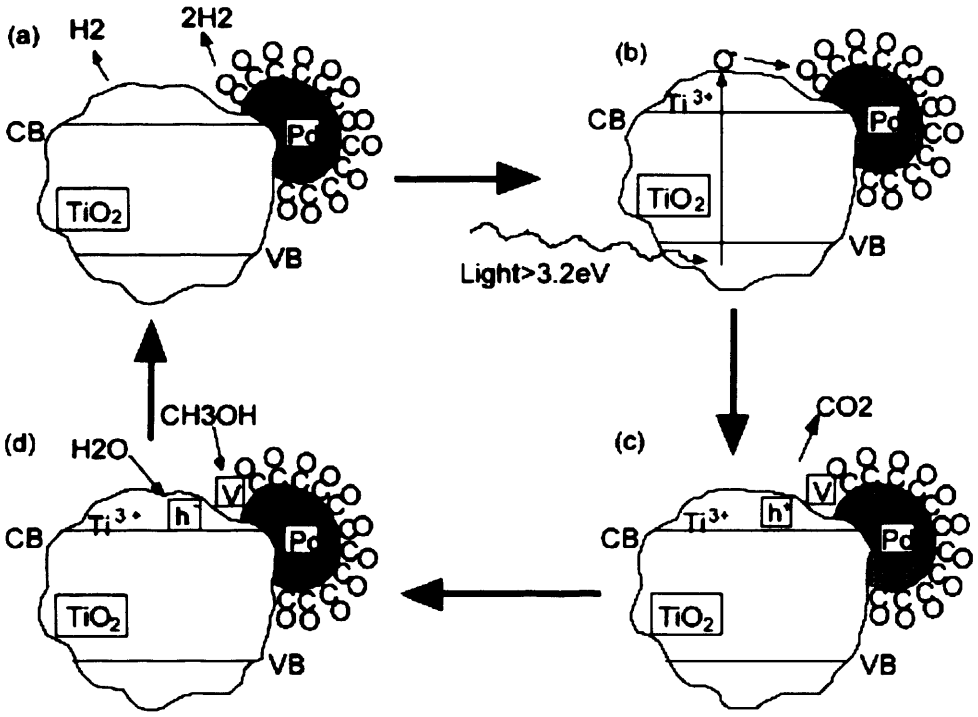

Figure 3.24: The mechanism of methanol reforming over Pd/TiO_2.

It was expected that the mechanism over Au/TiO_2 is similar to that over Pd/TiO_2 except the intermediate. Due to the weaken bonding of CO to the surface of gold than to the surface of Pd, the expected intermediate is the methoxy group that means the methanol molecules are partially dehydrogenated over gold and the reaction would stop at this step in the absence of light. Subsequently, the methoxy is oxidized by the electrophilic oxygen generated by photoactivation of TiO_2.

The only difference between methanol and glycerol is three hydroxyl groups, which are adsorbed on the surface of metal instead of one functional group in the case of methanol.

3.3 Conclusion

The generation of hydrogen from methanol reforming at different conditions was investigated. The results of these studies are summarised as follows:

- Among the factors studied which affect on the rate of hydrogen evolution were the quantity of the catalyst. The optimum rate was obtained when 0.2 g of Pd/TiO_2.
- Loading TiO_2 with metals such as palladium had a varying effect on the rate whether in liquid or gas phase reactions. 0.1% wt. Pd gave the highest rates in both phases. If the Pd loading was lower or higher of these values, the rates were less than the optimum. On the another hand, hydrogen produced from gas phase photocatalysis increased by 30 % compared to the liquid phase reaction. The active regions around the Pd particles appear to play an important role in governing the activity of Pd/TiO_2 at different Pd loading.
- $Pd/MTiO_2$ has lower activity in terms of hydrogen evolution compared to Pd/P25, even though mesoporous TiO_2 has high surface area.
- Adding methanol to the reaction mixture enhances the rate significantly. Below 10 µl of methanol, the rate increases linearly with its concentration but after that, the reaction approaches zero order. Besides that, the hydrogen production stopped when all methanol molecules were consumed which was demonstrated by following up the reaction with a very small amount of methanol for a long time.

- Similar results were obtained when glycerol was used instead of methanol as a sacrificial reagent. Hydrogen and carbon dioxide were the only gases produced. since glycerol contains three hydroxyl groups, then the rates of hydrogen evolution over Pd/TiO_2 and Au/TiO_2 were much more than that in the case of methanol. Pd/TiO_2 was more active than Au/TiO_2 for both reactions.

3.4 References

[1] K. Honda and A. Fujishima, *Nature* **1972**, *238*, 37-38.

[2] T. Sakata and T. Kawai, *Chemical Physics Letters* **1981**, *80*, 341-344.

[3] T. Sakata, *Journal of Photochemistry* **1985**, *29*, 205-215.

[4] Z. Zou, J. Ye, K. S. and and H. Arakawa, *Nature* **2001**, *414*, 625-627.

[5] K. Ohashi and J. McCann, *nature* **1977**, *266*, 610-611.

[6] M. F. Weber and M. J. Dignam, *Journal of The Electrochemical Society* **1984**, *131*, 1258-1265.

[7] P. J. Sebastian, *International Journal of Hydrogen Energy* **2001**, *26*, 115-115.

[8] A. J. Bard, *J. Phys. Chem.* **1982**, *86*, 172.

[9] A. J. Bard and M. A. Fox, *Acc. Chem. Res.* **1995**, *28*, 141.

[10] A. J. Nozik, *Applied Physics Letters* **1977**, *30*, 567-569.

[11] G. Q. Lu, W. Chrzanowski and A. Wieckowski, *The Journal of Physical Chemistry B* **2000**, *104*, 5566-5572.

[12] L. R. Millard in *The PhotocatalyticProduction of Hydrogen*, *Vol. PhD* University of Reading, **2003**.

[13] J. Arana, J. M. Dona-Rodriguez, J. A. H. Melian, E. T. Rendon and O. G. Diaz in *Role of Pd and Cu in gas-phase alcohols photocatalytic degradation with doped TiO2*, *Vol. 174* **2005**, pp. 7-14.

[14] G. R. Bamwenda, S. Tsubota, T. Kobayashi and M. Haruta, *Journal of Photochemistry and Photobiology A: Chemistry* **1994**, *77*, 59-67.

[15] G. R. Bamwenda, S. Tsubota, T. Nakamura and M. Haruta, *Journal of Photochemistry and Photobiology A: Chemistry* **1995**, *89*, 177-189.

[16] T. Chen, Z. Feng, G. Wu, J. Shi, G. Ma, P. Ying and C. Li, *J. Phys. Chem. C* **2007**, *111*, 8005-8014.

[17] H.-J. Choi and M. Kang, *International Journal of Hydrogen Energy* **2007**, *32*, 3841-3848.

[18] W. Cui, L. Feng, C. Xu, S. Lu and F. Qiu, *Catalysis Communications* **2004**, *5*, 533-536.

[19] T. Sakata, T. Kawai and K. Hashimoto, *Chemical Physics Letters* **1982**, *88*, 50-54.

[20] A. A. Nada, H. A. Hamed, M. H. Barakat, N. R. Mohamed and T. N. Veziroglu, *International Journal of Hydrogen Energy* **2008**, *33*, 3264-3269.

[21] M. Antoniadou and P. Lianos, *Journal of Photochemistry and Photobiology A: Chemistry* **2009**, *204*, 69-74.

[22] J.-W. Park and M. Kang, *International Journal of Hydrogen Energy* **2007**, *32*, 4840-4846.

[23] M. Ikeda, Y. Kusumoto, S. Somekawa, P. Ngweniform and B. Ahmmad, *Journal of Photochemistry and Photobiology A: Chemistry* **2006**, *184*, 306-312.

[24] T. Sreethawong, Y. Suzuki and S. Yoshikawa, *International Journal of Hydrogen Energy* **2005**, *30*, 1053-1062.

[25] Y. Wei, J. Li, Y. Huang, M. Huang, J. Lin and J. Wu, *Solar Energy Materials and Solar Cells* **2009**, *93*, 1176-1181.

[26] K. Yamaguti and S. Sato, *J. Chem. Soc., Faraday Trans.1* **1985**, *81*, 1237 - 1246.

[27] K. Sayama and H. Arakawa, *Chem. Lett.* **1992**, 253.

[28] S. Chen and Y. Liu, *Chemosphere* **2007**, *67*, 1010-1017.

[29] J. Lea and A. A. Adesina, *Journal of Photochemistry and Photobiology A: Chemistry* **1998**, *118*, 111-122.

[30] J. C. Garcia and K. Takashima, *Journal of Photochemistry and Photobiology A: Chemistry* **2003**, *155*, 215-222.

[31] D. W. James in *'The Photocatalytic Reforming of Methanol', MSc Vol.* The University of Reading, **1998**.

[32] A. J. Dickinison in *'Photocatalytic Hydrogen Production', PhD, Vol.* The University of Reading, **1997**.

[33] J. Greaves in *Photocatalytic Hydrogen Production using Gold on Titania, Vol. PhD* The University of Reading, **2005**.

[34] S.-C. Tsai, C.-C. Kao and Y.-W. Chung, *Journal of catalysis* **1982**, *79*, 541-461.

[35] S. Teratani, J. Nakamichi, K. Taya and K. Tanaka, *The chemical Society of Japan* **1982**, *55*, 1688-1690.

[36] L. Millard and M. Bowker, *Journal of Photochemistry and Photobiology, A: Chemistry* **2002**, *148*, 91-95.

[37] M. Bowker, D. James, P. Stone, R. Bennett, N. Perkins, L. Millard, G. a. J. and A. Dickinson, *journal of catalysis* **2003**, *217*, 427-433.

[38] C. T. Kreasge, M. E. Leonowicz, W. J. Roth, J. C. Vartuli and J. S. Beck, *nature* **1992**, *359*, 710-712.

[39] J. S. Beck, J. C. Vartuli, W. J. Roth, M. E. Leonowicz, C. T. Kreasge, C. T. Schumitt, K. D. Chu, C. T.-W. Olson, D. H. Sheppard, E. W. McCullen, S. B. Higgins and J. B. Schlenker, *J. Am. Chem. Soc.* **1992**, *114*, 10834.

[40] A. Corma, M. Iglesias and F. Sanchez, *F. Catal. Lett.* **1996**, *39*, 153.

[41] P. T. Tanev, M. Chibwe and T. J. Pinnavaia, *nature* **1994**, *368*, 321.

[42] N. Yao, G. Xiong, K. L. Yeung, S. Sheng, M. He, Y. Yang, X. Liu and X. Bao, *Langmuir* **2002**, *18*, 4111-4117.

[43] D. M. Antonclli and Y. J. Ying, *Cem, Mater.* **1996**, *8*, 874.

[44] P. V. Braun, P. Oscnar and V. Tohvev, *J. Am. Chem. Soc.* **1999**, *121*, 7302.

[45] D. Huang, Y. J. Wang, L. M. Yang and G. S. Luo, *Microporous and Mesoporous Materials* **2006**, *96*, 301-306.

[46] C. Liu, L. Fu and J. Economy, *J. Mater. Chem* **2004**, *14*, 1187-1189.

[47] J. Yu, M. Zhou, B. Cheng, H. Yu and X. Zhao, *Journal of Molecular Catalysis A: Chemical* **2005**, *227*, 75-80.

[48] D. Kulkarni, A. Murugan, A. Viswanath and C. Gopinath, *Journal of Nanoscience and Nanotechnology* **2009**, *9*, 371-377.

[49] A. Patsoura, D. I. Kondarides and X. E. Verykios, *Catalysis Today* **2007**, *124*, 94-102.

[50] C.-H. Zhou, B. J., Y.-X. Fan and G. Lu, *Chemical Society Reviews* **2008**, *37*, 527-549.

[51] X. Xu, Y. Matsumura, J. Stenberg and M. J. Antal, *Ind. Eng. Chem. Res.* **1996**, *35*, 2522-2253.

[52] P. J. Dauenhauer, J. R. Salge and L. D. Schmidt, *Journal of Catalysis* **2006**, *244*, 238-247.

[53] A. M. D. Douette, S. Q. Turn, W. Wang and V. I. Keffer, *Energy Fuels* **2007**, *21*, 3499-3504.

[54] H. Kanno, Y. Yamamoto and H. Harada, *Chemical Physics Letters* **1985**, *121*, 245-248.

[55] M. Albert, Y. M. Gao, D. Toft, K. Dwight and A. Wold, *Materials Research Bulletin* **1992**, *27*, 961-966.

[56] I. Z. Jones, R. A. Bennett and M. Bowker, *Surface Science* **1999**, *439*, 235-248.

CHAPTER FOUR

Hydrogen Production Over Non-Metal Doped TiO_2

4.1 Introduction

TiO_2 has attracted much attention due to its photostability, availability, electronic properties and high potential to oxidize a wide range of organic compounds. Thus, it has applications in several fields by irradiation with UV light. The most important requirements in the field of the application of photocatalysts are photostability and absorption under visible light. Unfortunately, the utilization of TiO_2 is limited to the ultraviolet region because of its wide band gap. Such a region represents only about 5% of the solar spectrum while 95% reaches the earth's surface in the range of visible light (400-600 nm). This limitation diminishes the efficiency of solar energy conversion using such photocatalysts. The development of titania with a high visible light response and high activity is one of the major current challenges in the energy and environment fields.

All the methods of development of semiconducting photocatalysts have sought to achieve two objectives:

a) enhancement of the photocatalytic performance

b) extension of the ability of photocatalysts to absorb under visible radiation. The second objective can be achieved by narrowing the band gap or introducing a new absorption band within the band gap which would have the same effect.

Doping TiO_2 with impurities is one of the most feasible methods of modification. Both cationic (transition metals) and ionic (for example, N, S, C) doping of titanium dioxide have exhibited promising effects in reducing the band gap of TiO_2 making it a susceptible material to absorb visible radiation with a reasonable quantum yield. Anionic and cationic doping induces new states in the band gap of semiconductors, which can act as donors or acceptors during the excitation. Hence, the visible photoresponse of such a photocatalyst increases. However, the doping of foreign atoms does not necessarily increase the photocatalytic activity because some of the states can act as sites of photogenerated electron-hole recombination. Asahi set three requirements for the doping TiO_2 [1] to result in activity under visible light:

1) The energy states of dopants should be located in the forbidden area of TiO_2 (band gap).
2) H_2/H_2O potential should be less positive than of that of the dopants generated in the midgap to ensure that the reduction process occurs easily.
3) There should be sufficient overlap between the dopants' states and the band states of TiO_2 in order to enable the photogenerated carriers to migrate to the reactive sites within a reasonable time.

From these requirements, in particular 2 and 3, it may be concluded that the doping of anions is preferable to that of cations since the latter form electron-hole recombination sites in their localized d states

deep in the band gap of TiO_2. Additionally, some cation-doped TiO_2 is thermal unstable [2, 3]. In recent years, non-metal doped TiO_2 has attracted much attention and has undergone rapid development, as non-metallic atoms form strong covalent bonds with titanium.

In 1986, Sato found that the use of NH_4OH in the preparation of titanium hydroxyl caused the presence of impurities such as NO_x. Therefore, when TiO_2 was prepared from titanium hydroxyl, NO_x-doped TiO_2 was formed. This photocatalyst showed some activity in the oxidation of carbon monoxide and ethane under visible wavelengths [4]. After 15 years, Asahi et al. drew researchers' attention to this work by demonstrating that nitrogen doped TiO_2 absorbed light at less than 500 nm and has an activity in the photodegradation of acetaldehyde and the decoloration of methylene blue solution [1]. Since then, numerous studies of non-metallic doping have been carried out and are considered promising pathways in the field of visible-responsive photocatalysts. However, it could also be said that the field suffers from a great dral of confusion as a result of different explanations and, a lack of full understanding of the photocatalytic process.

Carbon-doped TiO_2 is one of the visible responsive photocatalysts in which some of the lattice oxygen atoms are substituted by carbon. This substitution causes a lowering of the band gap. Khan et al [5] prepared carbon-doped rutile by the controlled combustion of Ti metal in a natural gas flame. The optical absorption spectra of the resulting compound

showed two absorption peaks in the visible region at 440 and 535 nm (band gap 2.82 and 2.32 eV, respectively), which indicates there may be two different compositions of n-$TiO_{2-x}C_x$. According to data obtained from this paper, this photocatalyst is active in the splitting of water stoichiometrically to H_2 and O_2 with a 2:1 ratio. They claimed that the maximum photoconversion efficiency is 8.35 %. However, the work has been criticised on a number of counts including the lack of evidence for the photoactivity of carbon-doped TiO_2 by visible illumination, and the unreasonably high photoconversion efficiency [6, 7].

Based on Khan's attempt to split water using carbon-doped TiO_2, many studies have investigated the efficiency of photocatalytic water-splitting under visible illumination using carbon-doped TiO_2 prepared by hydrocarbon-flame-oxidation methods or spray pyrolysis of an organometallic precursor in CO_2 / O_2 [8, 9]. They found no photoresponse under the desired region of light. Neumann et al. claimed that carbon might form defect states in the band gap of TiO_2, which may be the sites of undesirable recombination. It was thought this was reason for the reduction of activity of carbon-doped TiO_2 under UV light compared to the undoped TiO_2 ; they also reported that there was no remarkable activity under visible radiation [10].

Park et al [11] reported that water splitting efficiency over $TiO_{2-x}C_x$ under visible light irradiation (> 420 nm) was higher than the pure TiO_2. In addition, the presence of oxygen vacancies during the annealing of

TiO_2 in a carbonaceous gas mixture resulted in an increase in the charge carrier density[12]. Therefore, the formation of oxygen vacancies might be the reason for the increased activity, not the presence of carbon [13].

Another dopant that has been reported to narrow the band gap of TiO_2 (< 3.0 eV) effectively is sulfur. Given its large ionic radius, the substitution of sulfur as an anion into the TiO_2 lattice requires the more energy (4.1 eV) than does the substitution of nitrogen (1.6 eV) [1]. Nevertheless, sulfur was doped with anions and cations. Umebayashi et al. prepared S-doped TiO_2 by oxidation annealing of titanium disulfide (TiS_2) or by ion implantation followed by thermal annealing [14, 15]. In both these methods, sulfur was replaced by oxygen, which in turn, shifted the absorption band to a higher wavelength (visible region). According to the first-principles band calculations[15], the narrowing of the band gap of TiO_2 is a result of mixing of S 3p states with the valance band (VB) and thus broadening of the VB. This group proved that this material was able to decolour methylene blue solution during visible light illumination.

In contrast, sulfur-cation doped TiO_2 was prepared by mixing titanium isopropoxide with thiourea [16]. Ti^{4+} was substituted with S^{4+}, which was identified by XPS. This material exhibited a high activity in some applications under visible light. Additionally, the light absorption of S-cation doping was strong, compared to N, C or S-anion doped TiO_2. Recently, a highly active S-cation doped TiO_2 was prepared by an attractively simple method, involving, the hydrothermal treatment of a

solution of TiS_2 at a low temperature [17].

Nitrogen-doped TiO_2 is considered representative of the anion-doped photocatalysts. Asahi et al.'s report [1] opened a new gate in the world of photocatalysts, as it showed researchers that the doping of TiO_2 might form a promising material that absorbs in the visible region light and has a significant activity in the photocatalytic reactions and water splitting, in particular.

The incorporation of nitrogen in titanium dioxide has been achieved by several methods, including chemical and physical synthesis. Yates et al [18] classified those methods into three types:

1- Modification of TiO_2 by ion bombardment [19-22].

2- Modification of TiO_2 in the forms of powder [23], films [24], and single crystal[25] or TiN[26] via gas phase chemical impregnation.

3- Growth of TiN_xO_y from liquid [27] and gaseous [28] precursors.

The variation of preparation methods used may lead to a range of different N-doped TiO_2 compounds, which may be expected to show a range of optical and electronic properties. Unfortunately it is difficult to make a direct comparison between the results of such studies because of the variation of the photocatalysts prepared by these methods in terms of the kind of material formed (powder, film, single crystal) and its surface area. The variation of the methods used to test the effectiveness of N-doped TiO_2 is another problem since the rates of decomposition of the

materials are not identical, even if the photocatalysts are identical. This, in turn, impedes the ease of comparison. Therefore, it is necessary to consider some factors that affect the results of the testing approach, for example, the type of sample, the kind of light source, the surface area, and the sensitivity of the testing method. It should be noted that the pulse laser deposition method (PLD) is of high reproducibility in the preparation of crystalline thin films and is among the most widely used techniques due to its versatility[29, 30].

N-doped TiO_2 has been intensively investigated experimentally and theoretically in an attempt to obtain answers to some important questions. Among these is the reason for the shifting of the absorption wavelengths towards the visible region of photocatalysts after the doping of nitrogen, which is considered one of the most important aspects. Asahi has claimed that mixing N *2p* levels with O *2p* formed VB leads to an increase in the width of this band and thus a decrease in the energy of the band gap [1, 20]. However, other studies argue that the interaction of nitrogen with titanium dioxide forms localized states in the band gap above the VB [31-33].

As well as the existence of such states above VB, other states below the conduction band (CB) have been proposed relating to the oxygen vacancy formed as a consequence of the doping[34]. Consequently, it is rational that there is no change from n-TiO_2 to p-TiO_2 during N doping. The theoretical studies have demonstrated that there

are interactions between two such kinds of midgap states since N-states reduce the energy formation of oxygen vacancies and the latter increases the stability of the former. Scheme 4.1 shows the possibilities for the photoexcitation of visible light responsive TiO_2.

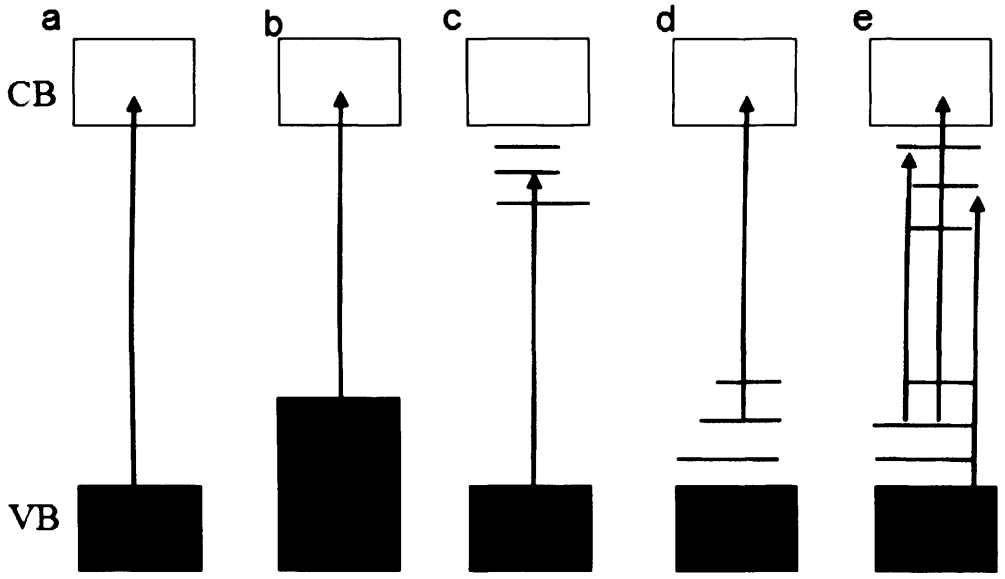

Scheme 4.1: The possibilities of band gap electronic structure of visible light responsive TiO_2. a) undoped TiO_2, b) narrowing of band gap of anion-doped TiO_2, c) the presence of localized states due to oxygen deficient, d) isolated and localized states in band gap due to N doping, and e) formation of N and states of oxygen vacancies in the midgap [35].

XPS studies have revealed there are two kinds of nitrogen doping: substitutional (400 eV peak) and interstitial (396 eV peak), the latter in TiO_2 being assigned to NO[34, 36]. The positions of their midgap states are different, as the interstitial nitrogen states have slightly higher energy levels than has the substitutional nitrogen. Solid state NMR (SSNMR),

studies, have proved that when nitrogen has a high oxidation state, the kind of nitrogen in N-doped TiO_2 is interstitial [37], but in general, the formation of one such kind of nitrogen depends on the preparation methods. It is assumed the two kinds are responsible for the absorption of visible light.

In general, most studies performed to date have focused on the feasibility of nitrogen doping on the photocatalytic activity of TiO_2 in visible light. Many authors have reported that the activity of TiO_2 was improved by adding nitrogen under the visible region[38, 39]. Table 4.1 shows attempts to achieve some photoreactions using N-doped TiO_2.

The reduction of photocatalytic activity of TiO_2 by N-doping in visible light might arise from several reasons. Firstly, oxygen vacancy states, which will be formed due to N doping, may act as trapping centres of photoelectrons, and thus prevent them reaching the surface where the reduction process occurs. Secondly, the trapping of photogenerated holes in the midgap states related to the nitrogen reduces their oxidative power. Thirdly, the doping of TiO_2 may cause lattice distortion and weakness of the bonds, which leads to a reduction in the stability of the structure[18, 40].

Table 4.1: Some photocatalytic reactions over N-doped TiO_2 (adapted)[35].

Description	Photocatalytic activity	Preparation method	Ref
Absorption onset: 500 nm; N1s peaks at 396 eV and 400 eV; nitrogen concentration: 1-1.4 atomic %.	Decompose methylene blue and acetaldehyde in visible irradiation, with similar activity in UV irradiation as non-doped TiO_2.	Sputtering deposition in N_2 /Ar, Or annealing TiO_2 powders in NH_3 at 873K	[1]
Absorption onset: 600 nm, N1s peak at 401.3 eV	Decompose methylene blue in solution by visible laser.	Nitriding TiO_2 nanoparticles with triethyl amine.	[41]
Absorption onset: 520 nm; a weak N1s peak at 404 eV	Degradation of 4-chlorophenol, benzene and acetaldehyde with visible light (λ>455 nm),	Hydrolyzing $TiCl_4$ in water with addition of ammonia, post-annealing at 673 K.	[42]
N-substituted for oxygen: 0.5-1.9%	Degradation of gaseous 2-propanol under visible light; UV light activity was weaker for doped samples than non-doped. Visible light activity was several times lower than UV light activity.	Annealing TiO_2 powders in NH_3	[32]
N1s peaks at 399.6 and 396.7 eV; increased absorption in the range of 2.4-3.0 eV.	Photodeposition of Ag from $AgNO_3$ solution in visible irradiation.	Annealing rutile (110) in NH_3 at 873 K.	[43]
N-substituted for oxygen: 2-16.5%; photo-response up to 550 nm.	Degradation of 2-propanol solution with visible irradiation; 6% N-substitution is the best.	RF Magnetron sputtering in N_2/Ar	[44]
Nitrogen atomic concentration: 1.5-5%	No visible light activity for degradation of stearic acid molecules; weak UV-activity.	Chemical vapor deposition in NH_3/N_2, using $TiCl_4$ and ethyl acetate as precursor.	[18]

Most of the studies conducted on anion-doped TiO_2, have been concerned with the degradation or decomposition of some organic compounds, (see Table 4.1). Hydrogen production using such photocatalysts has received much less attention and there have been few

attempts to produce hydrogen from water under visible radiation. However, since the mixing of the *2p* levels of the nitrogen with the *2p* levels of the oxygen leads to an upward shift of VB, while CB remains unchanged, N-doped TiO_2 may have the ability to employ the photoexcited electrons in CB in hydrogen production. The oxidative power of the photogenerated holes may be reduced, but since the potential for oxygen evolution is much less than that of the VB, the increase in the width of VB may not affect its oxidation ability[45].

In this chapter, different non-metals doped TiO_2 were tested in the photocatalytic hydrogen production process.

4.2. The catalysts

4.2.1. The preparation of catalysts

This chapter includes three sets of anion-doped TiO_2 photocatalysts. The first set is nitrogen-doped Degussa TiO_2 P25. The second is nitrogen-doped nanopowder TiO_2 anatase (Aldrich 99.7%). Both were prepared at the University of Glasgow by Justin Hargreaves, as discussed in Chapter 2. The third set of catalysts used in this chapter was prepared by Jawaad Darr at University College London. They doped nano-TiO_2 powder with a high surface area by different atoms (N, Ag or Sr). The titania was prepared from titanium (IV) bis (ammonium lactato) dihydroxide (TiBALD) using a continuous hydrothermal flow synthesis (CHFS). Then the nanopowder TiO_2 prepared with an anatase structure

was nitrided by an NH_3 (60%)/Ar(40%) gas flow (200ml/min) for 5 hours at 600°C.

To prepare the 2.5% Ag/TiO_2 and 2.5% Sr/TiO_2, catalysts Darr's group used a solution of TiBALD and metal (Ag or Sr) nitrates in the CHFS process. To distinguish between the nitrogen doped titania samples, they were labelled as follows:

- **N-D450**, **N-D550** and **N-D650** represent N-doped Degussa TiO_2 annealed at 450, 550 and 650°C under NH_3/Ar gas, respectively.

- **N-A450**, **N-A550** and **N-A650** represent N-doped Anatase TiO_2 annealed at 450, 550 and 650°C under NH_3/Ar gas , respectively.

- **N-T600** represents TiO_2 prepared by CHFS and then nitrided at 600°C under NH_3/Ar gas.

4.2.2. Methodology

All the experiments described in this chapter were carried out in a Pyrex flask and in a similar way to those discussed in Chapter 2. Most of these experiments were conducted in the gas phase due to the small quantities received of the original catalysts, as the standard amounts of catalysts used were 0.2 and 0.05g in the liquid and gas phases, respectively. The desired amount of catalyst was suspended in 100ml of deionised water, or mounted on a glass slide, which was held above 15ml of water depending on the kind of phase used; 100 µl methanol was

added in both cases as the hole scavenging reagent. After purging the suspension with argon gas for 30 minutes, the catalyst was irradiated by a 400W Xe arc lamp and then the gas phase flask was sampled and analysed by GC every 30 minutes.

4.3. Results and discussion

4.3.1. Characterisations of the photocatalysts

4.3.1.1. X-Ray Diffraction (XRD)

Figure 4.1 shows XRD patterns of N-doped TiO_2 P25 prepared at different temperatures (N-D450, N-D 550, and N-D 650), and compared to undoped TiO_2 P25. XRD was used to investigate any change that might happen in the phase structure of the titania after the doping process. As mentioned previously, in many studies [46, 47], the most intense peaks of the anatase and rutile phases in Degussa TiO_2 show at $2\theta = 25.25^{\circ}$ and $2\theta = 27.5^{\circ}$ respectively. It is apparent that nitrogen doping of TiO_2 P25 did not change its structure phase at 450, 550 and 650°C, except a new peak at $2\theta = 43^{\circ}$ appeared in N-D650, which is attributed to TiN[48, 49]. XRD analysis did not detect the nitrogen doped in the case of N-D450 and N-D550. There are some proposed reasons for the absence of the peak assigned to TiN in these samples. Firstly, there was the low content of nitrogen introduced in to the titanium oxide.

Secondly, the nitrogen atoms can exist in either the interstitial or the substitutional sites of the TiO_2 lattice[50]. Finally, the formation of TiN can only occur at a temp where Ti_3O_5 becomes unstable and at this point it decomposes to TiO and then TiN[51].

The heat treatment and surface defects are among the factors that affect the stability of the structure phase and thus the phase transformation from anatase to rutile [52, 53]. With the increase in temperature, the bonds and arrangement of atoms are affected; therefore, the transition phase from anatase to rutile takes place readily. The phase transition from anatase to rutile starts when the temperature rises above 600°C[54]. It was supposed that the doping of TiO_2 by nitrogen would not affect this behaviour [55].

Figure 4.1: XRD patterns of N-doped TiO_2 at different annealing temperatures (N-D450, N-D 550, and N-D 650) and of undoped TiO_2.

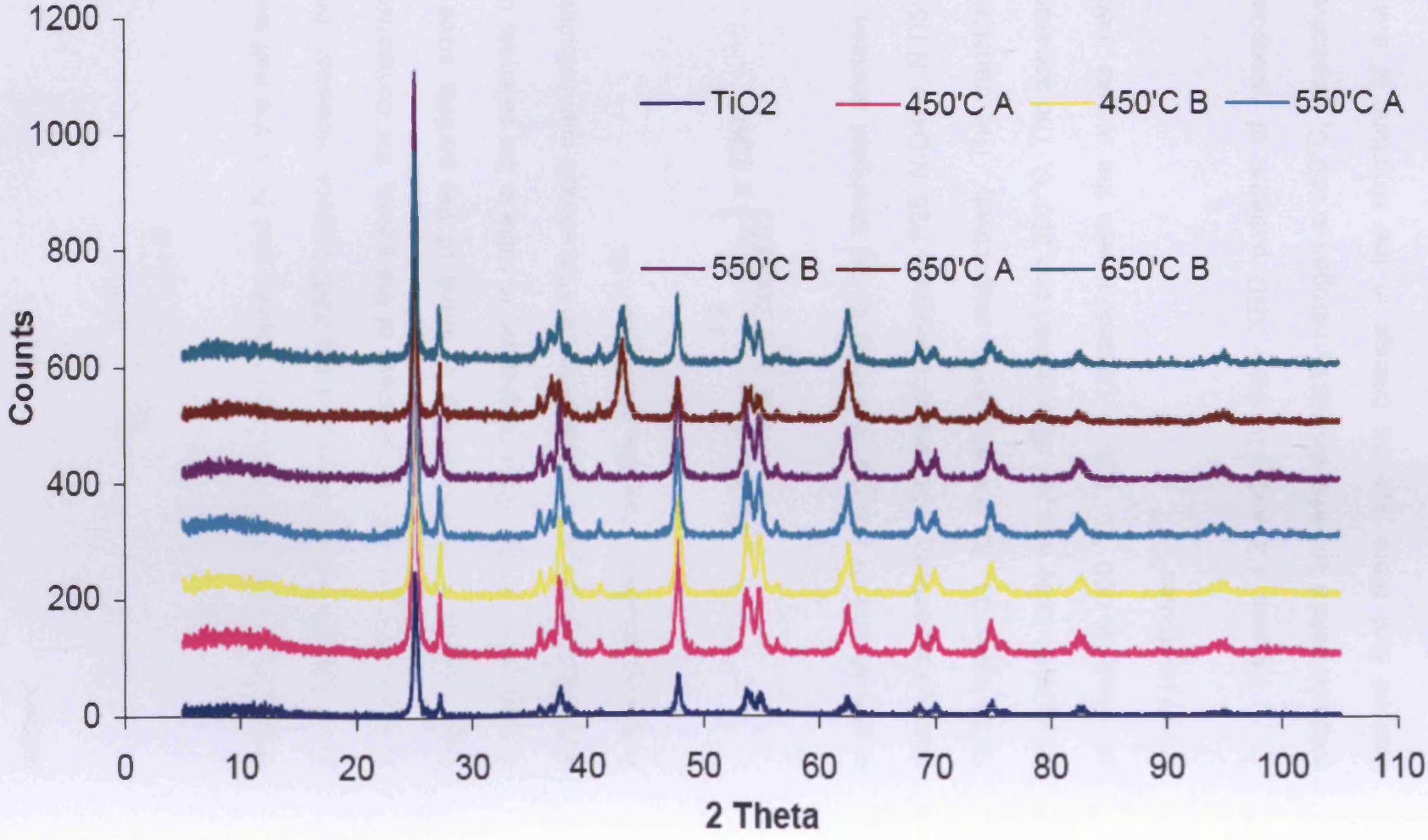

The average particle sizes, D, of anatase and rutile for all the samples can be calculated by Scherrer's formula, which is shown as follows:

$$D = \frac{0.9\lambda}{\beta_{1/2}\cos\theta}$$

where λ is the X-ray wavelength applied and $\beta_{1/2}$ is the half width of the most intense peak obtained in the XRD pattern. However, because of oxygen effects on the broadening of the peaks, the comparison in this case between these samples in terms of the particle sizes was not acceptable. For the ratios of anatase to rutile in the catalysts containing P25, the percentage of anatase in the P25 sample was calculated by the following equation using the XRD data[46, 56]:

$$(\%) = \left\{\frac{IA}{IA + 1.265\,IR}\right\} \times 100$$

where *IA* and *IR* are the intensities of the strongest anatase and rutile peaks, respectively. The ratio of anatase in P25, N-D450, N-D550 and N-D650 were 81, 82, 84 and 68%, respectively. The transformation of anatase to rutile was not clear at 450 and 550 °C. The apparent change occurred at 650 °C. This is consistent with the results mentioned in previous studies[38, 57].

Figures 4.2 and 4.3 show XRD patterns of nanopowder TiO_2 anatase before and after doping by nitrogen at 650°C, respectively. It was noticed that there was no change in the structure of anatase with

annealing at 450 and 550°C during doping by nitrogen, as seen in the case of N-D450 and N-D550. At 650°C, the peak at 43°C related to TiN was observed as in N-D650.

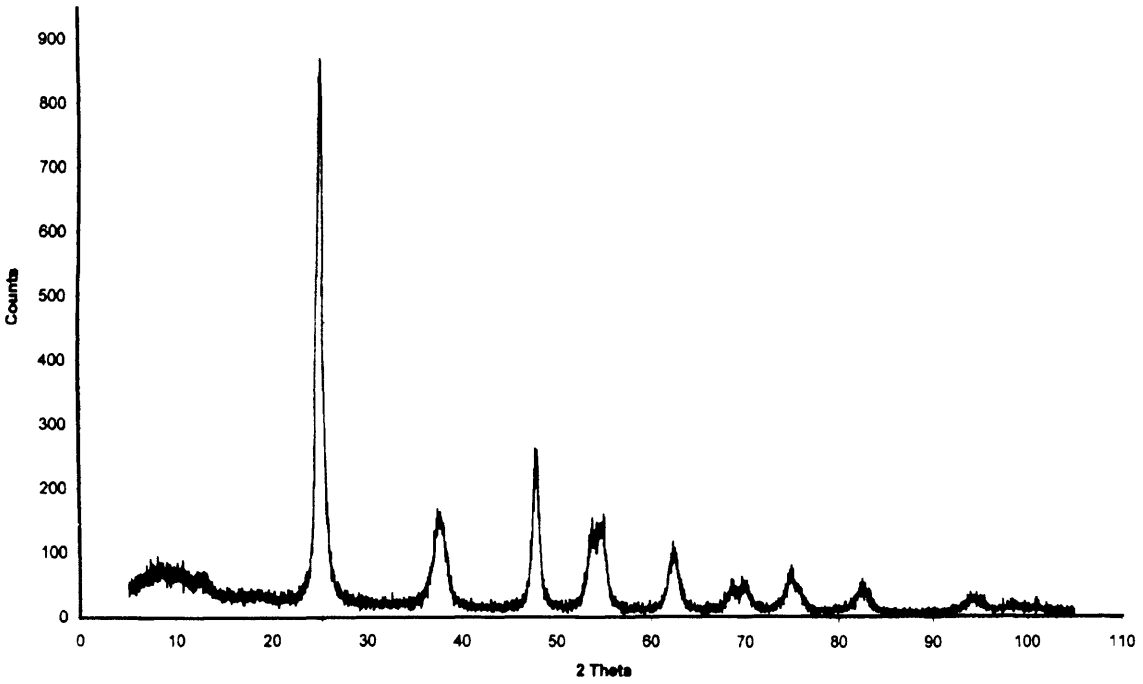

Figure 4.2: XRD pattern of N-nanopowder anatase.

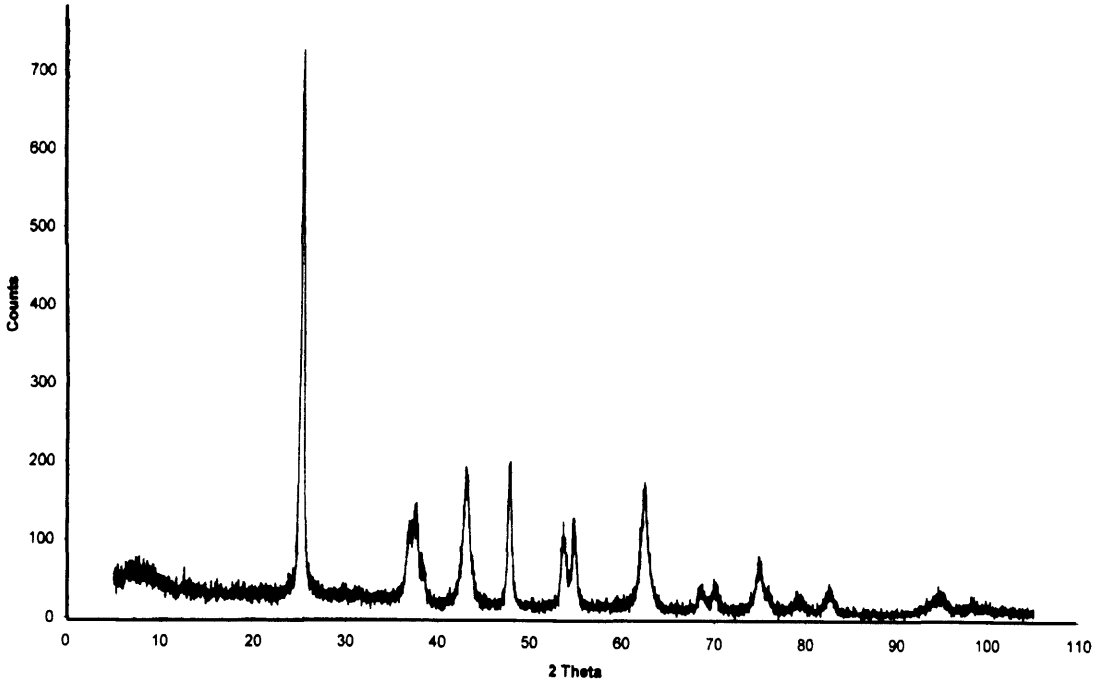

Figure 4.3: XRD pattern of N-A650.

Darr et al.[58] characterised N-TiO_2 annealed at different temperatures and found that TiN started forming above 700°C. The conversion of all the nanosized TiO_2 to cubic TiN was completed at 1000°C. According to the XRD patterns in their work, there was no peak of TiN observed in the case of N-T600. This is different to what happened in the case of N-D650 and N-A650, even though the nitridation processes undertaken were similar. Many factors might cause this difference, such as the precursor used, the surface area of the sample, and the time and rate of exposure of titania to the ammonia flow. The crystallite size of nanoparticles TiO_2 (estimated from XRD by Scherrer Equation) increased during nitriding as a result of agglomeration since the crystalline size of nano-TiO2 is 5 and increases to 42 nm at 600°C.

For Ag/TiO_2 and Sr/TiO_2, the same researchers above found that the XRD pattern revealed only the anatase phase structure, no peak for Ag or Sr metals observed. This may be ascribed to the small particle size of these metals in the sample, as the minimum limit of XRD detection for any crystallite metal is around 5nm[59]. In addition to the particle size, the low content of metals affects the exhibiting of their peaks in the XRD pattern.

4.3.1.2. Specific Surface Area BET

BET surface areas of N-doped TiO_2 anatase samples were measured and compared with those of undoped anatase shown in Table 4.2. The higher annealing temperatures during the preparation of N-doped anatase lowered their BET surface area significantly. This happened owing to the agglomeration of particles to make larger particles. In contrast, BET surface areas of N-doped P25 catalysts, (shown in the same table) did not change significantly. That means P25 is stable during doping. According to that, the change of BET surface area of these catalysts does not depends only on the annealing conditions, but also on the kind of precursor used[23, 60].

Table 4.2: The BET surface area of undoped and N-doped TiO_2 (anatase and P25).

Samples	S_{BET} (m^2/g)
Undoped P25	50
N-D450	48
N-D550	55
N-D650	57
Undoped Anatase	190
N-A450	131
N-A550	96
N-A650	71
N-T600	35

For N-T600, the adverse impact of heating on BET surface area was clearly drastic in this case, as there was a large difference between nanopowder TiO_2 prepared by CHFS ($290m^2/g$) and N-T600 ($35m^2/g$)[58].

Ag/TiO_2 and Sr/TiO_2 have large surface areas (259 and $237m^2/g$, respectively) compared with all the photocatalysts used in this project. CHFS is clearly a useful method for making photocatalysts with a high surface area.

4.3.1.3. Scanning Electron Microscopy (SEM)

SEM showed the changes caused by increasing the temperature and nitrogen doping characterised N-doped TiO_2 samples. Figures 4.4 and 4.5 show SEM images of nanoparticles of anatase and P25, respectively, before and after doping at 450, 550 and 650°C. It is difficult to identify any relationship between the effect of heating and the morphology of these materials; the BET area suggests that analyse samples at least should have agglomerated with the increase in temperatures. It appears that the effect of heating affects the morphology at a lower scale than is measured here. However, the P25 has an irregular shape and exists as a large cluster, while nanopowder anatase has a more definite shape than has P25.

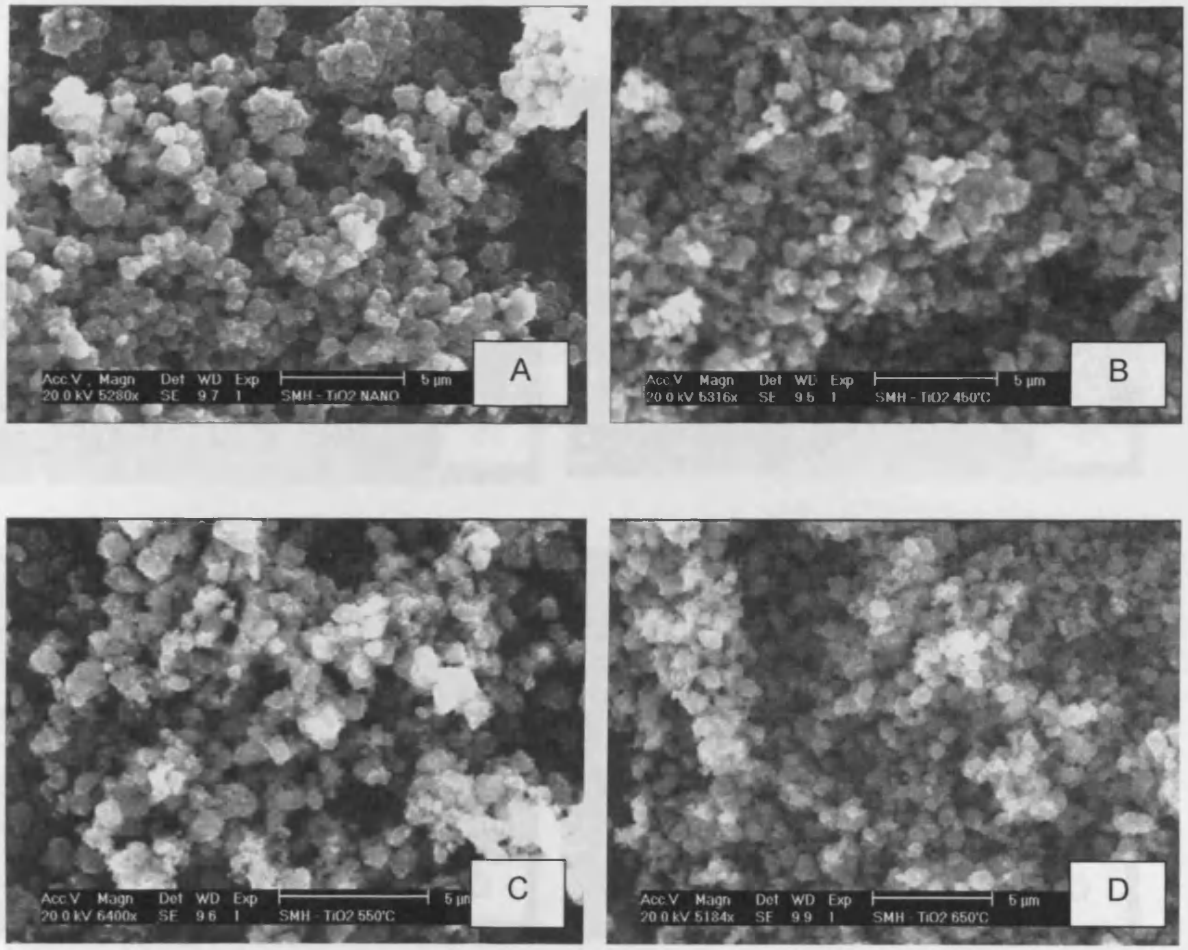

Figure 4.4: SEM images of a) undoped anatase, b) N-A450, c) N-A550 and d) N-A650.

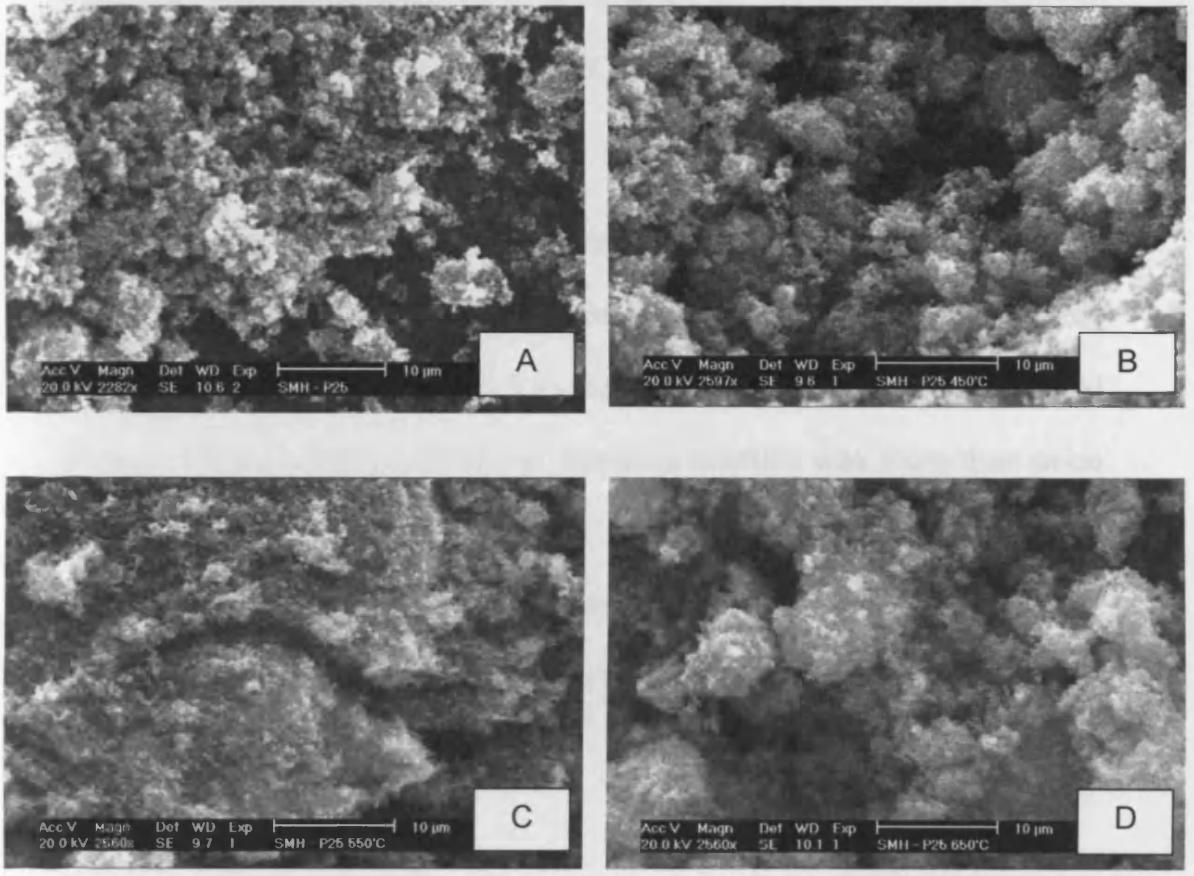

Figure 4.5: SEM images of a) undoped P25, b) N-D450, c) N-D550 and d) N-D650.

4.3.2. The photocatalytic activity of nitrogen doped titania catalysts.

None of the materials described previously showed any photocatalytic activity in UV light as it was found that no hydrogen was produced by illuminating N-doped titania suspended with water alone or with a water/methanol mixture. To enhance their activity, pd was added to the catalysts and investigated in an attempt to inhibit the recombination process, but this does not necessarily mean that all metals had a positive effect on the activity[61].

0.5% palladium was loaded on N-P25 by the same method as mentioned in Chapter 3. The amount of hydrogen produced was compared with the standard run in our work (0.5 % Pd/TiO_2 P25 in liquid phase). Figure 4.6 shows that the standard reaction was more than twice as active as the N-doped P25. After three hours, 0.5% Pd/N-D450 and 0.5%Pd/N-D550 had generated 4ml and 3.5 ml of hydrogen, respectively. However, 0.5% Pd/N-D650 produced only 1.5ml of hydrogen.

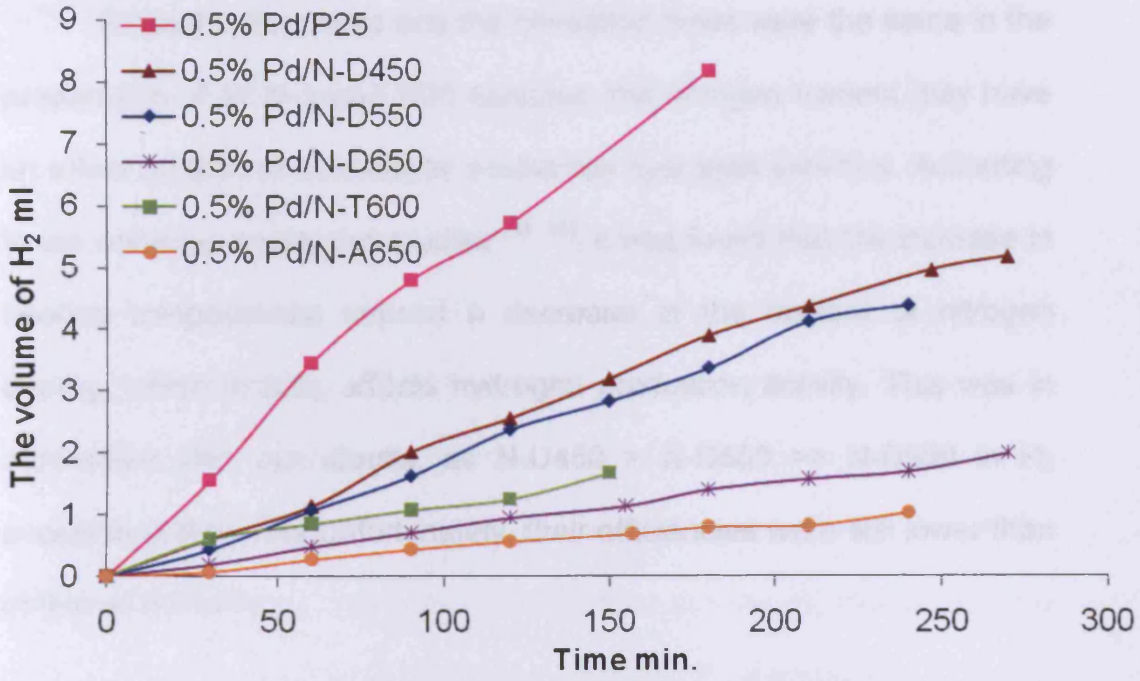

Figure 4.6: Hydrogen production over 0.5% Pd loaded on P25, N-P25, N-anatase or N-TiO_2 (CHFS).

As seen in section 4.3.1.1, nitrogen doping of P25 did not change its phase structure at each temperature. Additionally, BET surface areas of P25 before and after doping were almost the same. Nonetheless, their photocatalytic activities were all different except for Pd/N-D450 and Pd/N-D550, which have a similar level of activity as that for reforming methanol to H_2 and CO_2. The reasons for the decrease in activity after doping may be limited to two factors: the heat treatment and the nitrogen doping, which may change the mechanism of reforming methanol. As mentioned previously, the formation of midgap nitrogen states is accompanied by the creation of oxygen vacancies below CB. These vacancies may act as recombination sites of photogenerated electrons and holes.

Since the flow rates and the nitridation times were the same in the preparation of all N-doped P25 samples, the nitrogen content may have an effect on their photocatalytic production hydrogen activities. According to the previous analogous studies [38, 62], it was found that the increase in heating temperatures caused a decrease in the content of nitrogen doping, which in turn, affects hydrogen production activity. This was in agreement with our results, as N-D450 > N-D550 >> N-D650 in H_2 evolution activity, but unfortunately, their efficiencies were still lower than of that of Pd/TiO_2.

On the other hand, Yuan et al.[38] investigated the effect of the calcination temperature on the activity of N-doped TiO_2 (synthesized anatase) in water splitting in the presence of Na_2SO_4 as a hole scavenger. This effect was interpreted based on the phase transformation from anatase to rutile. On the basis of the positions of the conduction band of these phases, the potential of CB is higher than that of H^+/H_2 in the case of anatase and nearly matches that of the rutile phase. However, the band gap of anatase (3.2) is larger than that of rutile (3.0) making rutile the preferred option in water reduction. Accordingly, the combination of the properties of anatase and rutile represented in Degussa P25 resulted in higher activity. Hence, it was proposed that the transformation of anatase to rutile might partly enhance the activity. This explanation is quite plausible when Pd/N-D650 is compared with Pd/N-A650, producing 1.7ml and 1ml of hydrogen respectively after four hours; even with BET surface area of N-A650 being greater than that of N-D650.

Regarding nitrogen-doped TiO_2 prepared by CHFS, its activity in hydrogen production after Pd loading was lower than that of Pd/N-D450 and Pd/N-D550 though higher than that of Pd/N-D650. This difference may be ascribed to the phase form of TiO_2, as it is noticeable that N-T600 in the anatase phase only. At the same time, its BET surface area being higher than that of N-A650 would be expected to make its reactivity higher despite titania being formed from one phase (anatase). If the catalysts are compared on the basis of reactivity per unit area, N-T600 is the worst performing. However, it is not clear that the N_2 measured area is relevant here since the light cannot reach all of the surface.

Similar to what has been said about Pt/N-TiO_2[59], the general mechanism of hydrogen production over Pd/N-TiO_2 can be explained as follows:

When Pd/N-TiO_2 was irradiated using a Xe lamp, a photogenerated electron and hole were produced. Pd loading of N-TiO_2 enhanced the separation between these charge carriers. Regardless of the source of the photoinduced electrons, that is, whether from VB of TiO_2 or nitrogen midgap levels, these electrons were trapped by Pd and, reacted with the hydrogen ions to produce hydrogen gas, while methanol molecules adsorbed on the surface of TiO_2 as electron scavengers consumed the photogenerated holes located in VB.

4.3.3. Mixing N-P25 with $PdCl_2$ in the solution

The effect of physically mixing N-doped titania with palladium solution was investigated to clarify more the interactions between the palladium and the modified supports.

0.2 g of N-D450, N-D550 or N-D650 were irradiated with 1.5 ml of a solution of $PdCl_2$ (3.7 mM), 100ml of deionised water and 100µl of methanol. Samples were taken from the gas phase every 30 minutes and analysed to detect any H_2 produced. The results are plotted in Figure 4.7. Table 4.3 summarizes the rates of hydrogen production over N-P25 after either loading or mixing with $PdCl_2$ in the solution to make a comparison.

Under the same conditions, N-D450 mixed with $PdCl_2$ still had a higher H_2 production than others did, as seen in Pd/N-D450. For N-D550+$PdCl_2$, the rate of production was less. There was no hydrogen produced at all in the case of N-D650+$PdCl_2$. However, when undoped P25 was mixed with $PdCl_2$, it gave a higher rate than nitrogen doped P25 in the same experiment.

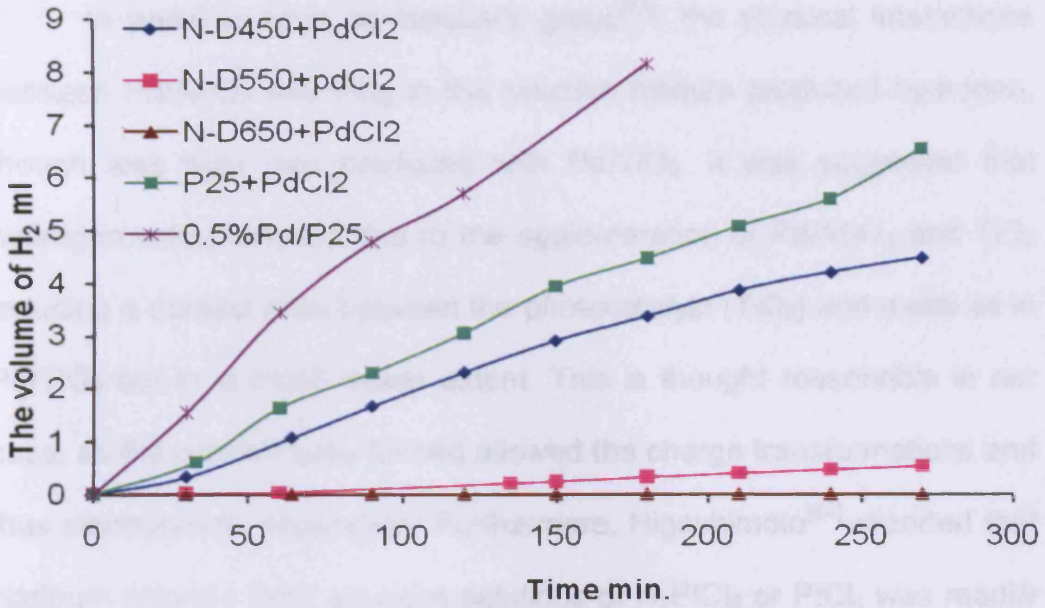

Figure 4.7: Hydrogen produced from mixing N-P25 with $PdCl_2$ in the solution.

Table 4.3: H_2 production rates of the photocatalysts.

Photocatalyst	Rate (the slope) µl/min
0.5% Pd/P25	47.7
0.5% Pd/N-D450	20.3
0.5% Pd/N-D550	18.8
0.5% Pd/N-D650	7.4
0.5% Pd/N-T600	11.3
0.5% Pd/N-A650	4.2
N-D450+$PdCl_2$	17.8
N-D550+$PdCl_2$	1.8
N-D650+$PdCl_2$	0
P25+$PdCl_2$	24.3

In previous work by Bowker's group[63], the physical interactions between Pd/Al_2O_3 and TiO_2 in the reaction mixture produced hydrogen, though less than was produced with Pd/TiO_2. It was suggested that hydrogen was produced due to the agglomeration of Pd/Al_2O_3 and TiO_2 inducing a contact area between the photocatalyst (TiO_2) and metal as in Pd/TiO_2 but to a much lesser extent. This is thought reasonable in our case, as the contact area formed allowed the charge transformations and thus electron-hole separation. Furthermore, Higashimoto[64] reported that platinum chloride from aqueous solutions of H_2PtCl_6 or $PtCl_4$ was readily adsorbed on the surface of TiO_2, which was as Ti—OH, forming Ti—O—$PdCl_x$. Such a strong interaction had a clear effect on the activity of the degradation of acetic acid over $PtCl_x/N\text{-}TiO_2$, which was higher than either $N\text{-}TiO_2$ or Pt/TiO_2. According to this study, palladium chloride might exhibit the same behaviour, making it active in H_2 production, but with a lower activity rate than Pd/TiO_2. Further investigation is required to clarify the interpretation of the difference between these reaction rates.

4.3.4. Hydrogen production over Ag/TiO_2 and Sr/TiO_2.

The activities of Ag/TiO_2 or Sr/TiO_2 in hydrogen production were investigated; 50mg of the catalysts were mounted on a glass slide held above 15ml of deionised water and 100µl of methanol. The amount of hydrogen produced is plotted against the time in Figure 4.8.

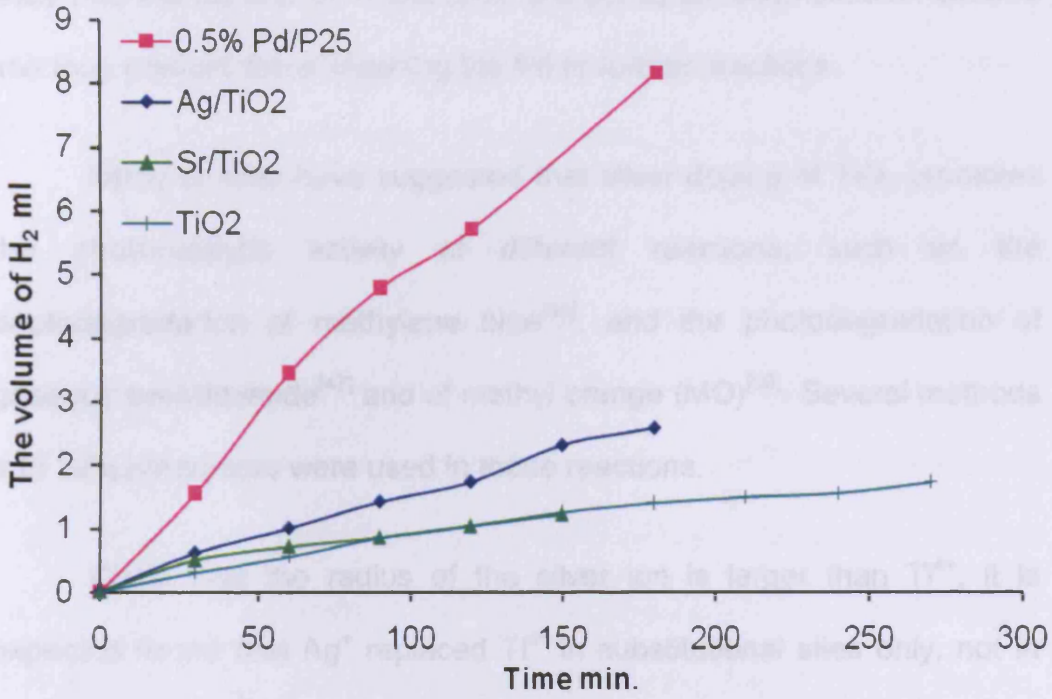

Figure 4.8: Hydrogen production over Pd/P25, Ag/TiO_2, Sr/TiO_2 and TiO_2 alone doped.

This figure shows that the activity of Ag/TiO_2 was more than twice as high as that of Sr/TiO_2 but both were much lower than the standard catalyst in this project (0.5% Pd/TiO_2 P25). In fact, the amount of H_2 produced over TiO_2 (P25) alone in the presence of methanol is similar to that produced by Sr/TiO_2. The requirements of such photocatalysts to be active were provided, such as the high surface areas and small particles size; however, their activity was low. Interestingly, the loading of Pd on these catalysts did not result in any change in their activity rates. It seams

likely that the Ag and Sr in this case are acting as recombination centres and thus prevent the e^- reaching the Pd to further reactions.

Many studies have suggested that silver doping of TiO_2 promotes the photocatalytic activity of different reactions, such as the photodegradation of methylene blue[65], and the photodegradation of gaseous acetaldehyde[47] and of methyl orange (MO)[66]. Several methods and TiO_2 precursors were used in these reactions.

Given that the radius of the silver ion is larger than Ti^{4+}, it is expected found that Ag^+ replaced Ti^{4+} in substitutional sites only, not in interstitial sites [67, 68]. Besides, because the charge value of the silver ion is less than of that of Ti^{4+}, the incorporation of the silver ion into TiO_2 leads to the formation of oxygen vacancies[69], which play a role in the separation of photogenerated electrons and holes by trapping, thus affecting the efficiency of the photoreaction. This factor may be expected to make doped TiO_2 more active than undoped TiO_2.

On the other hand, XPS detected both Ag^o and Ag^+. The presence of these chemical states enhances the process of the charges separation. The following equations illustrate that silver ion doped can be reduced and oxidized during the photoreaction[47]:

$$TiO_2 + hv \longrightarrow e^- + h^+ \qquad (4\text{-}1)$$

$$Ag^+ + e^- \longrightarrow Ag^o \qquad (4\text{-}2)$$

$$Ag^o + h^+ \longrightarrow Ag^+ \qquad (4\text{-}3)$$

In contrast, such metal ions act as trapping sites of charge carriers since these kinds of ions make localised d- levels deep in the band gap of TiO_2, which, in turn, affect the redox reactions over these materials.

The doping of TiO_2 by alkaline earth metals, such as Mg^{2+}, Ba^{2+} and Sr^{2+}, can promote the photocatalytic reactions more than pure TiO_2. XRD and FT-IR studies have proved the effect of the incorporation of Mg^{2+} and Ba^{2+}[70]. According to such ions' radii, Mg^{+2} can be deposited substitutionally or interstitially, as its ionic radius is larger than Ti^{4+} but smaller than O^{2-}. In contrast, Ba^{2+} has an ionic radius that is much larger than a titanium ion, so it was deposited on the surface of TiO_2 as $BaCO_3$. The doping of such metal ions enhances the adsorption of the species being degraded and also leads to a reduction in the particle sizes of TiO_2, thus increasing the efficiency of some photocatalytic reactions. Based on this study, it is expected that Sr^{2+} doping may be similar to Ba^{2+} (1.41 Å) since its ionic radius (1.32 Å) is close to Ba^{2+}.

4.4 Conclusion

In this Chapter, nitrogen doped on different photoactive supports (P25, nanopowder anatase or TiO_2 [anatase] prepared by CHFS) were prepared at different temperatures and characterized by XRD, BET surface area and SEM. The XRD technique did not detect the nitrogen except at the highest temperature as TiN was formed. Similar results were obtained in the case of cationic (Ag and Sr) doping which may be

ascribed to the small particle size of metals or their low contents. For BET surface areas of these catalysts, the temperature has a different effect on the surface areas, depending on the kind of TiO_2. It was shown that BET surface areas of P25 were the same before and after nitrogen doping at the three different temperatures. In the case of nanopowder anatase, their surface areas decreased with increasing the temperature which may be attributed to the agglomeration. N-T600 has a small surface area. In contrast, Ag/TiO_2 and Sr/TiO_2 prepared by CHFS have surface areas larger than all the catalysts mentioned in this work. SEM techniques did not provide any information on any aspect to distinguish between the samples.

The activities of all these catalysts in the presence of methanol were much less than 0.5% Pd/TiO_2, but they do absorb light under the visible region. However, the hydrogen production rate over Pd loaded N-D450 > N-D550 > N-T600 > N-D650 > N-A650. Without Pd loading and/or without methanol, no hydrogen was detected over these catalysts. The hydrogen produced in the presence of Ag/TiO_2 and Sr/TiO_2 was small compared to Pd/TiO_2 as well. The low activity of these catalysts was ascribed to that the non-metal doped may be act as a recombination centers for photogenerated electrons and holes. Even though Pd loading over these catalysts enhanced their activities in term of hydrogen production, their rates were still more less than the standard catalyst (0.5% Pd/TiO_2). The Pd content may be not the optimum loading for these catalysts.

4.5 References

[1] R. Asahi, T. Morikawa, T. Ohwaki, K. Aoki and Y. Taga, *Science* **2001**, *293*, 269-271.

[2] J.-M. Herrmann, J. Disdier and P. Pichat, *Chemical Physics Letters* **1984**, *108*, 618-622.

[3] Z. Luo and Q.-H. Gao, *Journal of Photochemistry and Photobiology A: Chemistry* **1992**, *63*, 367-375.

[4] S. Sato, *Chemical Physics Letters* **1986**, *123*, 126-128.

[5] S. U. M. Khan, M. Al-Shahry and W. B. Ingler, Jr., *Science* **2002**, *297*, 2243-2245.

[6] A. Fujishima, *Science* **(2003)**, 1673a.

[7] K. S. Lackner, *Science* **(2003)**.

[8] K. Noworyta and J. Augustynski, *Electrochemical and Solid-State Letters* **2004**, *7*, E31-E33.

[9] C. S. Enache, J. Schoonman and R. V. Krol, *Journal of Electroceramics* **2004**, *13*, 177-182.

[10] B. Neumann, P. Bogdanoff, H. Tributsch, S. Sakthivel and H. Kisch, *The Journal of Physical Chemistry B* **2005**, *109*, 16579-16586.

[11] J. H. Park, S. Kim and A. J. Bard, *Nano Letters* **2006**, *6*, 24-28.

[12] K. S. Raja, M. Misra, V. K. Mahajan, T. Gandhi, P. Pillai and S. K. Mohapatra, *Journal of Power Sources* **2006**, *161*, 1450-1457.

[13] L. M. Berger, W. Gruner, E. Langholf and S. Stolle, *International Journal of Refractory Metals and Hard Materials* **1999**, *17*, 235-243.

[14] T. Umebayashi, T. Yamaki, H. Itoh and K. Asai, *Applied Physics Letters* **2002**, *81*, 454-456.

[15] T. Umebayashi, T. Yamaki, S. Yamamoto, A. Miyashita, S. Tanaka, T. Sumita and K. Asai, *Journal of Applied Physics* **2003**, *93*, 5156-5160.

[16] T. Ohno, M. Akiyoshi, T. Umebayashi, K. Asai, T. Mitsui and M. Matsumura, *Applied Catalysis A: General* **2004**, *265*, 115-121.

[17] W. Ho, J. C. Yu and S. Lee, *Journal of Solid State Chemistry* **2006**, *179*, 1171-1176.

[18] H. M. Yates, M. G. Nolan, D. W. Sheel and M. E. Pemble, *Journal of Photochemistry and Photobiology A: Chemistry* **2006**, *179*, 213-223.

[19] J. M. Mwabora, T. Lindgren, E. Avendano, T. F. Jaramillo, J. Lu, S.-E. Lindquist and C.-G. Granqvist, *The Journal of Physical Chemistry B* **2004**, *108*, 20193-20198.

[20] Y. Nakano, T. Morikawa, T. Ohwaki and Y. Taga, *Applied Physics Letters* **2005**, *86*, 132104-132103.

[21] O. Diwald, T. L. Thompson, E. G. Goralski, S. D. Walck and J. T. Yates, *The Journal of Physical Chemistry B* **2004**, *108*, 52-57.

[22] B. Liu, L. Wen and X. Zhao, *Solar Energy Materials and Solar Cells* **2008**, *92*, 1-10.

[23] X. Fang, Z. Zhang, Q. Chen, H. Ji and X. Gao, *Journal of Solid State Chemistry* **2007**, *180*, 1325-1332.

[24] M. Miyauchi, A. Ikezawa, H. Tobimatsu, H. Irie and K. Hashimoto, *Physical Chemistry Chemical Physics* **2004**, *6*, 865-870.

[25] I. Takahashi, D. J. Payne, R. G. Palgrave and R. G. Egdell, *Chemical Physics Letters* **2008**, *454*, 314-317.

[26] X. Cui, M. Ma, W. Zhang, Y. Yang and Z. Zhang, *Electrochemistry Communications* **2008**, *10*, 367-371.

[27] R. Nakamura, T. Tanaka and Y. Nakato, *The Journal of Physical Chemistry B* **2004**, *108*, 10617-10620.

[28] S. K. Pradhan and P. J. Reucroft, *Journal of Crystal Growth* **2003**, *250*, 588-594.

[29] Y. Suda, H. Kawasaki, K. Doi, J. Nanba and T. Ohshima, *Materials Characterization* **2002**, *48*, 221-228.

[30] Y. Suda, H. Kawasaki, T. Ueda and T. Ohshima, *Thin Solid Films* **2004**, *453-454*, 162-166.

[31] S. Sakthivel, M. Janczarek and H. Kisch, *The Journal of Physical Chemistry B* **2004**, *108*, 19384-19387.

[32] H. Irie, Y. Watanabe and K. Hashimoto, *The Journal of Physical Chemistry B* **2003**, *107*, 5483-5486.

[33] S. Sato, R. Nakamura and S. Abe, *Applied Catalysis A: General* **2005**, *284*, 131-137.

[34] C. Di Valentin, G. Pacchioni, A. Selloni, S. Livraghi and E. Giamello, *The Journal of Physical Chemistry B* **2005**, *109*, 11414-11419.

[35] A. Fujishima, X. Zhang and D. A. Tryk, *Surface Science Reports* **2008**, *63*, 515-582.

[36] S. Livraghi, M. C. Paganini, E. Giamello, A. Selloni, C. Di Valentin and G. Pacchioni, *Journal of the American Chemical Society* **2006**, *128*, 15666-15671.

[37] E. A. Reyes-Garcia, Y. Sun, K. Reyes-Gil and D. Raftery, *The Journal of Physical Chemistry C* **2007**, *111*, 2738-2748.

[38] J. Yuan, M. Chen, J. Shi and W. Shangguan, *International Journal of Hydrogen Energy* **2006**, *31*, 1326-1331.

[39] N. Luo, Z. Jiang, H. Shi, F. Cao, T. Xiao and P. P. Edwards, *International Journal of Hydrogen Energy* **2009**, *34*, 125-129.

[40] C. Di Valentin, E. Finazzi, G. Pacchioni, A. Selloni, S. Livraghi, M. C. Paganini and E. Giamello, *Chemical Physics* **2007**, *339*, 44-56.

[41] C. Burda, Y. Lou, X. Chen, A. C. S. Samia, J. Stout and J. L. Gole, *Nano Letters* **2003**, *3*, 1049-1051.

[42] Shanmugasundaram Sakthivel and Horst Kisch, *ChemPhysChem* **2003**, *4*, 487-490.

[43] O. Diwald, T. L. Thompson, T. Zubkov, S. D. Walck and J. T. Yates, *The Journal of Physical Chemistry B* **2004**, *108*, 6004-6008.

[44] M. Kitano, K. Funatsu, M. Matsuoka, M. Ueshima and M. Anpo, *The Journal of Physical Chemistry B* **2006**, *110*, 25266-25272.

[45] M. Ni, M. K. H. Leung, D. Y. C. Leung and K. Sumathy, *Renewable and Sustainable Energy Reviews* **2007**, *11*, 401-425.

[46] M. Ksibi, S. Rossignol, J.-M. Tatibouët and C. Trapalis, *Materials Letters* **2008**, *62*, 4204-4206.

[47] D. B. Hamal and K. J. Klabunde, *Journal of Colloid and Interface Science* **2007**, *311*, 514-522.

[48] M. Luo, J. Gao, X. Zhang, J. Yang, G. Hou, D. Ouyang and Z. Jin, *Materials Letters* **2007**, *61*, 186-188.

[49] I.-s. Kim and P. N. Kumta, *Materials Science and Engineering B* **2003**, *98*, 123-134.

[50] Z. Wang, W. Cai, X. Hong, X. Zhao, F. Xu and C. Cai, *Applied Catalysis B: Environmental* **2005**, *57*, 223-231.

[51] R. Aghababazadeh, A. R. Mirhabibi, B. Rand, S. Banijamali, J. Pourasad and M. Ghahari, *Surface Science* **2007**, *601*, 2881-2885.

[52] C. Su, B. Y. Hong and C. M. Tseng, *Catalysis Today* **2004**, *96*, 119-126.

[53] W. W. So, S. B. Park, K. J. Kim and S. J. Moon, *Journal of Colloid and Interface Science* **1997**, *191*, 398-406.

[54] Y-H Tseng, H-Y Lin, C-S Kuo, Y.-Y. Li and C.-P. Huang, *NSTI Nanotechnology Conference and Trade Show 9th* (Boston) **2006**.

[55] B. Kosowska, S. Mozia, A. W. Morawski, B. Grzmil, M. Janus and K. Kalucki, *Solar Energy Materials and Solar Cells* **2005**, *88*, 269-280.

[56] I. Burlacov, J. Jirkovsk, M. Müller and R. B. Heimann, *Surface and Coatings Technology* **2006**, *201*, 255-264.

[57] X. Li and S. Liu, *Acta Physico-Chimica Sinica* **2008**, *24*, 2019-2024.

[58] Zhice Zhang, Josephine B.M. Goodall, David J. Morgan, Sonal Brown, Robin J.H. Clark, Jonathan C. Knowles, Nicola J. Mordan, Julian R.G. Evans, Albert F. Carley, M. Bowkerc and J. A. Darra, *Journal of european Ceramic Society* **2009**, *29*, 2343-2353.

[59] T. Sreethawong, S. Laehsalee and S. Chavadej, *Catalysis Communications* **2009**, *10*, 538-543.

[60] Y. Li, X. Sun, H. Li, S. Wang and Y. Wei, *Powder Technology* **2009**, *194*, 149-152.

[61] T. Morikawa, Y. Irokawa and T. Ohwaki, *Applied Catalysis A: General* **2006**, *314*, 123-127.

[62] T. Sreethawong, S. Laehsalee and S. Chavadej, *International Journal of Hydrogen Energy* **2008**, *33*, 5947-5957.

[63] D. W. James in *'The Photocatalytic Reforming of Methanol', MSc Vol.* The University of Reading, **1998**.

[64] S. Higashimoto, Y. Ushiroda, M. Azuma and H. Ohue, *Catalysis Today* **2008**, *132*, 165-169.

[65] C. He, Y. Yu, X. Hu and A. Larbot, *Applied Surface Science* **2002**, *200*, 239-247.

[66] Y. Liu, C.-y. Liu, Q.-h. Rong and Z. Zhang, *Applied Surface Science* **2003**, *220*, 7-11.

[67] X. S. Li, G. E. Fryxell, C. Wang and M. H. Engelhard, *Microporous and Mesoporous Materials* **2008**, *111*, 639-642.

[68] Y. Zhang, H. Zhang, Y. Xu and Y. Wang, *Journal of Solid State Chemistry* **2004**, *177*, 3490-3498.

[69] A. Ahmad, J.Thiel and S. I. Shah in *Structural effects of niobium and silver doping on titanium dioxide nanoparticles*, *Vol. 61* IOP, **2007**, pp. 11-16.

[70] N. Venkatachalam, M. Palanichamy, B. Arabindoo and V. Murugesan, *Catalysis Communications* **2007**, *8*, 1088-1093.

CHAPTER FIVE

Water splitting and back reaction

5.1 Introduction

The need to generate hydrogen as a fuel for electricity and transportation has increased due to the depletion of fossil fuels and global environmental problems. Most of the hydrogen while is produced is from non-renewable sources from which carbon dioxide is also generated. So, scientists have been trying to explore and develop alternative methods to produce clean hydrogen. The splitting of water as an inexhaustible source to produce hydrogen and oxygen, by the use of sunlight is among the promising methods. Photocatalysis was employed to achieve this goal as mentioned previously in chapter one.

The photocatalytic splitting of pure water into hydrogen and oxygen stoichiometrically is an uphill reaction:

$$H_2O \longrightarrow H_2 + \tfrac{1}{2}O_2 \qquad \Delta G = 273 \text{ kJ/mol}$$

This reaction is of great interest due to the storage of solar energy and its conversion to clean hydrogen fuel. As mentioned in Chapter One, this reaction involves two electrons as each electron corresponds to 1.23 eV/e which is also the standard electromotive force. Moreover, the enthalpy change (ΔH) of this reaction is 2.96 eV and therefore the wavelength of the photon to split the water must be equal to or less than 420 nm. Because water absorbs only in the low UV region (λ<200 nm),

photocatalysis could possibly be used to convert the light energy and employ it for water splitting. Photocatalysis could also help to overcome the kinetic energy barrier which is greater than the thermodynamic value (237.2 kJ/mol). According to Born-Haber cycle for the water dissociation, the initial step in the H_2O splitting process is the breakdown of the H—OH bond which requires 494.8 kJ/mol as shown in figure 5.1.

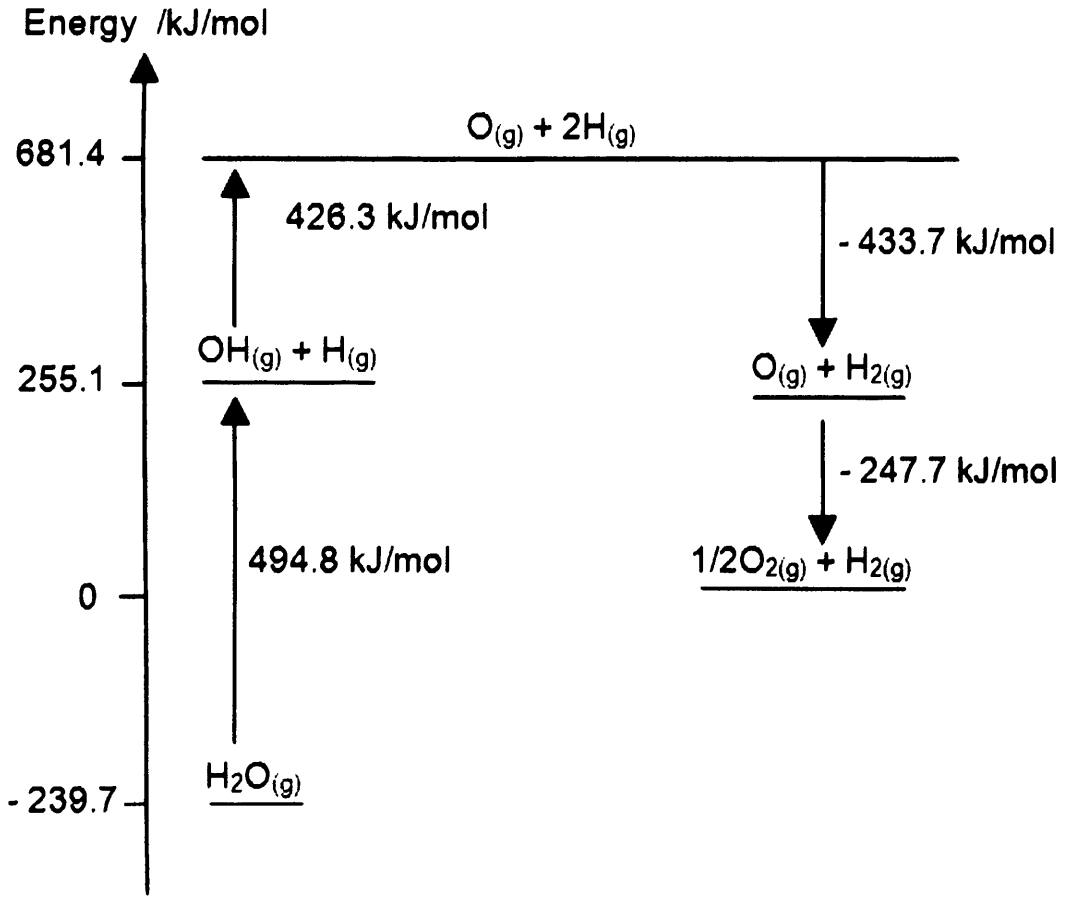

Figure 5.1: Born-Haber cycle for water dissociation into hydrogen and oxygen.

Hence, significant efforts have been made to meet all the requirements necessary to split water into its components

stoichiometrically with high efficiency. The materials used to accomplish this reaction should be able to cause photoabsorption, which is the initial step in the photocatalytic reaction. The next process is the separation of photogenerated charge carriers and migration to the surface where H_2 and O_2 form. This process is affected by the extent of the purity of the photocatalyst because some impurities act as recombination sites. The final step in water photolysis is the employment of photogenerated electrons and holes in H_2 and O_2 generation, respectively.

Without any doubt, photocatalysis succeeds in the field of water and air purification with high efficiency[1, 2]. In such reactions, the position of VB is more important than that of CB, as the conversion of contaminants occurs by holes located in VB. In contrast, the photoproduction of hydrogen depends strongly on the potential value of CB of photocatalysts, which should be more negative than that of hydrogen ion reduction. In fact, the big challenge is splitting pure water by sunlight in the presence of photostable materials prepared by a simple method with a high quantum yield of hydrogen produced. Although there are many photocatalysts that split water[3], most of them do so with low efficiency, or the quantities of hydrogen produced are not economically viable.

The photoelectrochemical cell (PEC) is one of the systems which is capable to split the water into hydrogen and oxygen by converting the light energy to electricity. The Gratzel cell is a photoelectrical solar cell

which was developed in an attempt to produce hydrogen more efficiently using low cost materials and simple design. In the Gratzel cell, a wide band gap semiconductor such as TiO_2 was coated by a monolayer of a charge transfer dye to absorb the light rather than the photocatalyst. The charge carriers (e^-/h^+) separation was accomplished by injecting the electron from the dye in to the semiconductor. The conversion yield of solar energy to electrical energy was ~8 % in simulated solar light[4, 5].

For the type of photocatalytic system of water splitting, heterogeneous catalytic systems are preferred to photoelectrochemical cells (PEC) due to the ease of use and construction. Moreover, powdered photocatalysts are used rather than the single crystals required in some PEC cells, which are difficult to prepare. Yet, the back reaction is one of the big problems in such systems, as the H_2 and O_2 evolved can recombine to form H_2O again in an exothermic process[6], as can be seen in figure 5.1.

Anpo et al[7] designed a photocatalytic cell to investigate the H_2-O_2 separation evolving from water decomposition as shown in figure 5.2. In this H-type glass container, a TiO_2 thin film was mounted on Ti foil on one side and Pt particles on the other side. The foil is placed in the centre of this container which separates it to two parts; one is for hydrogen evolution and the other is for oxygen. In addition to the photocatalyst, the device contains Nafion which connected between the two parts and allows the proton transfer as well. However, in fact, the hydrogen and

oxygen were not produced from pure water splitting, but from NaOH and H_2SO_4 solution, respectively.

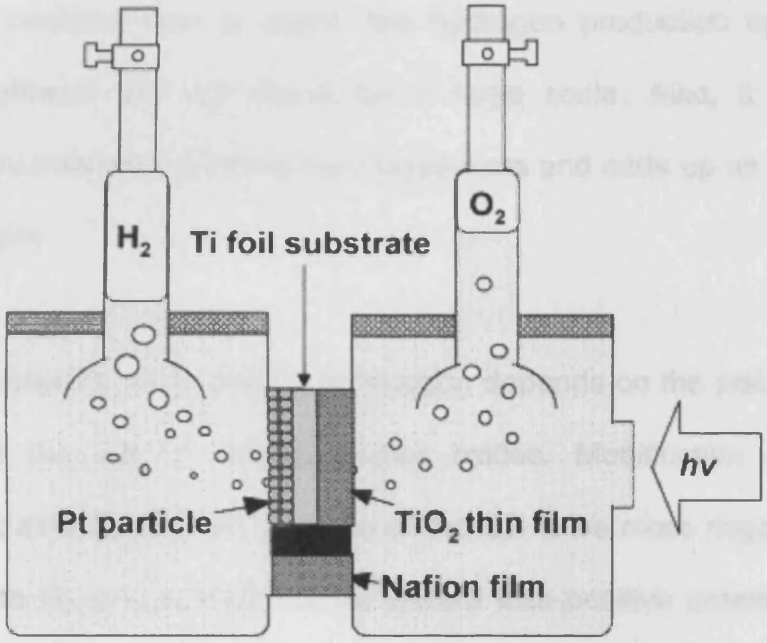

Figure 5.2: H-type glass container for H_2 and O_2 separation.

Since the innovative work of Honda and Fujishima[8], numerous photocatalysts with different levels of activity in water decomposition under UV and visible light have been prepared and tested. Most attempts to promote the efficiency of hydrogen production by water splitting have focused either on chemical additives [9-11] or the modification of the photocatalyst itself [12-15]. As seen in Chapter Three, the addition of hole scavengers, such as methanol, enhances the rate of hydrogen production significantly, while in Chapter Four, the doping of titania by cationic or

anionic dopants gives more hydrogen than does the bare TiO_2. This chapter is focused on the photodecomposition of water alone on different photocatalysts without the addition of methanol. Though methanol is more easily oxidized than is water, the hydrogen production systems including methanol are not viable on a large scale. Also, it is not sustainable as methanol is made from fossil fuels and ends up as CO_2 in the atmosphere.

The efficiency of H_2 and O_2 production depends on the position of the CB and the VB of semiconductor oxides. Modification of the photocatalyst aims to shift the position of the CB to be more negative to reduce H_2O to H_2 and to shift the VB toward less positive potentials to oxidize H_2O to O_2 easily. Many semiconductor oxides have the CB close to the potential value of hydrogen reduction and the VB very far from H_2O oxidation to O_2.

Pure water splitting was investigated over $K_4Nb_6O_{17}$, $Sr_2Nb_2O_7$, $KTaO_3$ $NaTaO_3$, and $NaTaO_3$: La. This extensive study [16] revealed that all these catalysts have activity towards the photodecomposition of water into H_2 and O_2 when Au particles were deposited. The most effective catalyst was $NaTaO_3$:La, as the rates of H_2 and O_2 evolution over unloaded were 404 and 187 μmol/h, respectively. After 1% Au photodeposition, the rates increased by five times to 1950 and 880 μmol/h in the first hours and then decreased gradually. It was found that the reason of this deactivation was the photoreduction of O_2 on Au by

photogenerated electrons, not to the back reaction between H_2 and O_2. This result was proved by introducing oxygen gas before the photocatalytic reaction. As a result of that the activity of Au/ $NaTaO_3$:La in the presence of O_2 is much smaller than of that in the absence of oxygen gas. In another hand, it was found the rates of hydrogen and oxygen consumption over this catalyst was negligible.

NiO-$SrTiO_3$ was among the photocatalysts that succeeded in the photodecomposition of water alone to H_2 and O_2 by 2:1, even though the illumination of NiO and $SrTiO_3$ alone failed to evolve hydrogen or oxygen[17]. The enhancement of water splitting by NiO cocatalysis was proved by another experiment. The rate of water splitting over NiO-$Sr_4Ti_3O_{10}$ was considerably higher than the water splitting before NiO loading [18].

The photodecomposition of water over Pt/Bi_2InNbO_7 was investigated and compared with Pt/TiO_2 (P25) and the rates at which hydrogen was evolved were 1.5 and 0.7 μmol/h, respectively. Oxygen was not observed over either catalyst[19].

Sayama et al.[20] claimed that when Pt–WO_3 was mixed with Pt–$SrTiO_3$ (Cr–Ta-doped) in an NaI aqueous solution, H_2 and O_2 evolved simultaneously. This was the first semiconductor absorbing under visible light that could split water into its components but with low quantum efficiency (QE) (0.1%), while Zou and Arakawa demonstrated that the

decomposition of pure water into its components (molar ratio 2) took place over new photocatalysts (NiO_x or RuO_2-loaded $In_{1-x}Ni_xTaO_4$) absorbing under visible light, but with QE 0.66%[19].

In this chapter, the decomposition of water alone was attempted over Pd/TiO_2, Au/TiO_2 and TiO_2. In addition, nitrogen, Ag and Sr doped TiO_2, absorbing in the visible region, were employed in this reaction.

5.2. Results and discussion

5.2.1. Water splitting over Pd/TiO_2 and Au/TiO_2

Figure 5.3 shows the amounts of hydrogen produced over unloaded Degussa TiO_2 P25 and loaded by gold and palladium in the liquid phase. 0.2 g of TiO_2, 2% Au/TiO_2 and 0.5 % Pd/TiO_2 prepared as mentioned in Chapter Two were suspended in 100 ml deionised water only. The optimum loadings of Au and Pd for methanol photoreforming as proved in Greaves' work[21] and Chapter Three, respectively, were used to compare their activities in terms of decomposition of pure water. This figure shows the different behaviors of these catalysts in hydrogen production. In general, the efficiency of the decomposition of water was very low, compared to that in the presence of methanol. Another point to be noted is that the volume of hydrogen evolved increased continuously with the irradiation time in the case of Au/TiO_2. However, it was shown

that the increase of hydrogen volume over Pd/TiO_2 was only in the initial minutes and it then decreased gradually. TiO_2 produced very small amounts of hydrogen. The final amount of hydrogen produced after three hours showed that Au/TiO_2 was much more active than Pd/TiO_2 in the absence of methanol. In addition, the amount of H_2 evolved over Pd/TiO_2 was double that evolved over TiO_2. However, note that no oxygen was evolved; and so that, whatever reaction is involved, it is probably not water splitting.

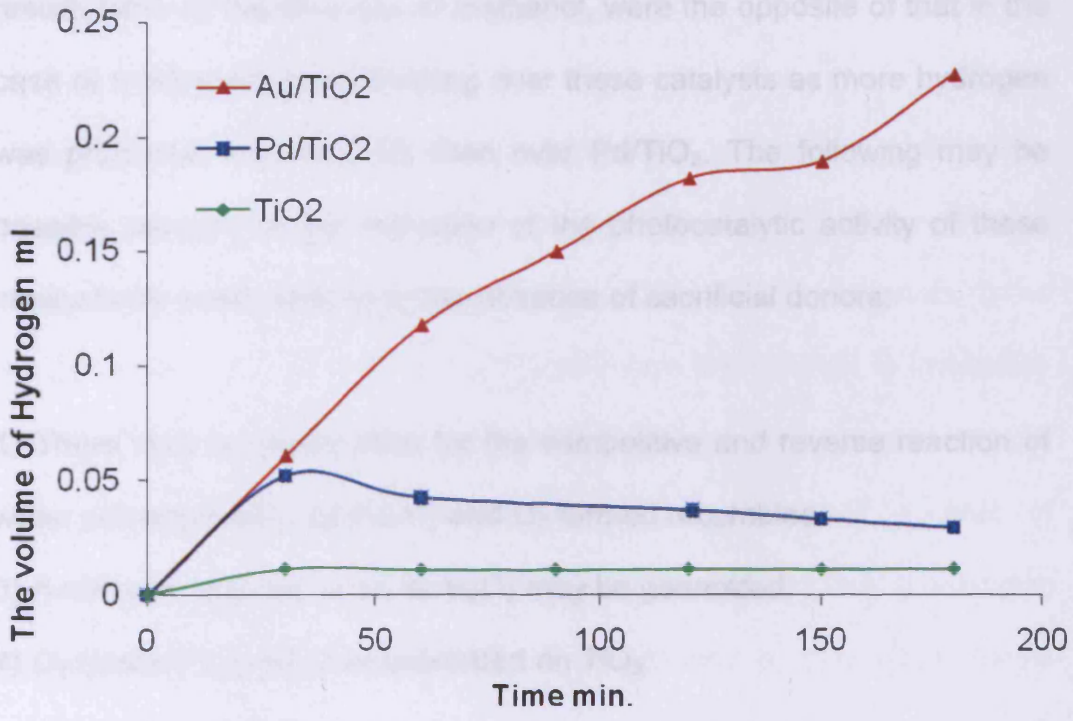

Figure 5.3: The hydrogen production from water splitting over TiO_2, Pd/TiO_2 and Au/TiO_2.

Several studies were conducted over Pt loaded TiO_2. These studies differ in the metal loading method or in the nature of the TiO_2 itself. It was found that no hydrogen was detected over Pt/TiO_2, prepared by single step sol-gel (SSSG), incipient wetness impregnation (IWI) and photochemical deposition (PCD) methods, in water alone[22]

The amount of hydrogen produced over Pd/TiO_2 was much greater than that produced over Au/TiO_2 and unloaded TiO_2 in the presence of methanol, as seen in sections 3.2.9 and 4.3.4, respectively. However, the results here, in the absence of methanol, were the opposite of that in the case of methanol photoreforming over these catalysts as more hydrogen was produced over Au/TiO_2 than over Pd/TiO_2. The following may be possible causes for the reduction of the photocatalytic activity of these catalysts for water splitting in the absence of sacrificial donors:

1) There may be active sites for the competitive and reverse reaction of water decomposition as the H_2 and O_2 formed recombine.
3) A different species, such as H_2O_2 may be generated.
4) O_2 formed may be photoadsorbed on TiO_2.

In the metal-loaded photocatalyst, photogenerated electrons transfer from TiO_2 to the loaded metal, thus enhancing the photogenerated electrons and holes separation. ESR studies proved this idea by comparing the intensity of the Ti^{+3} signal with the irradiation time before and after loading, as Ti^{+3} may be formed because of

photogenerated electrons being trapped by Ti^{+4}[23]. This process increases the photocatalytic activity of TiO_2 [24-27]. Thus metal (Pd and gold) loaded TiO_2 were more active than TiO_2 alone.

There are few studies regarding oxygen evolution from the splitting of water over loaded or unloaded semiconductor oxides[28, 29] but most of the studies, which were conducted on Pt/TiO_2, gave results similar to those over Au/TiO_2 and Pd/TiO_2. None of these catalysts could split water into hydrogen and oxygen stoichiometrically and only hydrogen was observed.

The mechanism of hydrogen production over metal loaded TiO_2 can be proposed on the light of previous studies[3, 30, 31]. Water adsorbs dissociatively as hydroxide and hydrogen. The hydrogen transfers to the metal forming half a mole of hydrogen. When the catalyst is irradiated, the O-H bond breaks by the excited electron forming hydrogen and O^-. The hydrogen migrates to metal releasing another half a mole of hydrogen while electron on O^- may fill the hole in VB and then the oxygen atom migrates to the bulk of TiO_2. If the catalyst is TiO_2 alone, these reactions are very slowly.

The oxygen formed may be chemisorbed as O_2^- on the surface of TiO_2 and can be converted to physisorbed as O_2 by photogenerated holes trapped as OH radicals [19, 32]. In addition, a peroxide species can

be formed from O_2 adsorbed. Most of the O_2^- photogenerated at the TiO_2/water interface preferred to be adsorbed on TiO_2 to free oxygen in the water bulk [33, 34].

Some authors attribute the problem to the reverse reaction, which means that H_2 and O_2 react on the metal surface to form H_2O. Such a reaction occurring on a metal surface is considered among the most frequent problems causing a reduction in the apparent photocatalytic activity. The formation of H_2O from H_2 and O_2 gases over metal is preferred thermodynamically at room temperature under atmospheric pressure as $\Delta G < 0$. In the presence of sacrificial reagents, the back reaction is inhibited because the oxygen is removed by oxidation of the sacrificial agent [30, 35-37].

5.2.2. The back reaction: oxygen hydrogenation

To clarify the difference between Au/TiO_2, Pd/TiO_2 and TiO_2 in terms of the ease with which the back reaction takes place, the rate of hydrogen consumption was measured after introducing of O_2 to a methanol photoreforming reaction mix. 0.2 g of Au/TiO_2 or Pd/TiO_2 were suspended in 100 ml of water and 100 µl methanol. After 60 minutes, the lamp was switched off and 2 ml of O_2 was injected; as shown in Figure 5.4, the reaction of H_2 with O_2 over Pd/TiO_2 took place more easily than the reaction over Au/TiO_2. The hydrogen produced was consumed

completely after 2.5 hours in the case of Pd/TiO_2. In contrast, just 38% of the hydrogen produced was consumed over Au/TiO_2 in the same period.

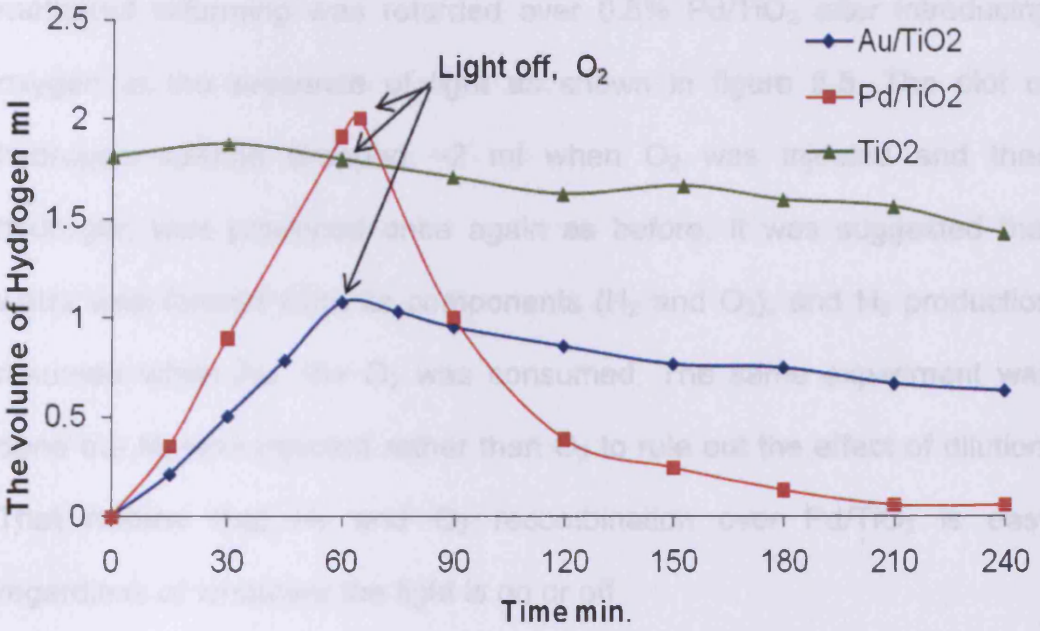

Figure 5.4: The effect of oxygen over Pd/TiO_2, Au/TiO_2 and TiO_2 in the absence of light.

For a similar experiment on TiO_2 alone, hydrogen was loaded into the reactor first, and figure 5.4 shows also the effect of oxygen injection. There is little evidence of any effect of O_2.

Clearly, the catalytic activity of Pd >> Au for the back reaction in the dark. This may be attributed to the strong affinity of Pd for oxygen compared to Au. Hence, the back reaction might be not mainly responsible of the extent of photocatalytic activity of these catalysts since Pd/TiO_2 was more than Au/TiO_2 in terms of hydrogen production. So, the

electron-hole recombination might have an effect more than the back reaction on the photocatalytic hydrogen production over these catalysts.

Millard[38] reported that the hydrogen production rate from methanol reforming was retarded over 0.5% Pd/TiO_2 after introducing oxygen in the presence of light as shown in figure 5.5. The plot of hydrogen volume dropped ~2 ml when O_2 was injected and then hydrogen was produced once again as before. It was suggested that water was formed from its components (H_2 and O_2), and H_2 production resumed when Au, the O_2 was consumed. The same experiment was done but N_2 was injected rather than O_2 to rule out the effect of dilution. That means that H_2 and O_2 recombination over Pd/TiO_2 is easy regardless of whatever the light is on or off.

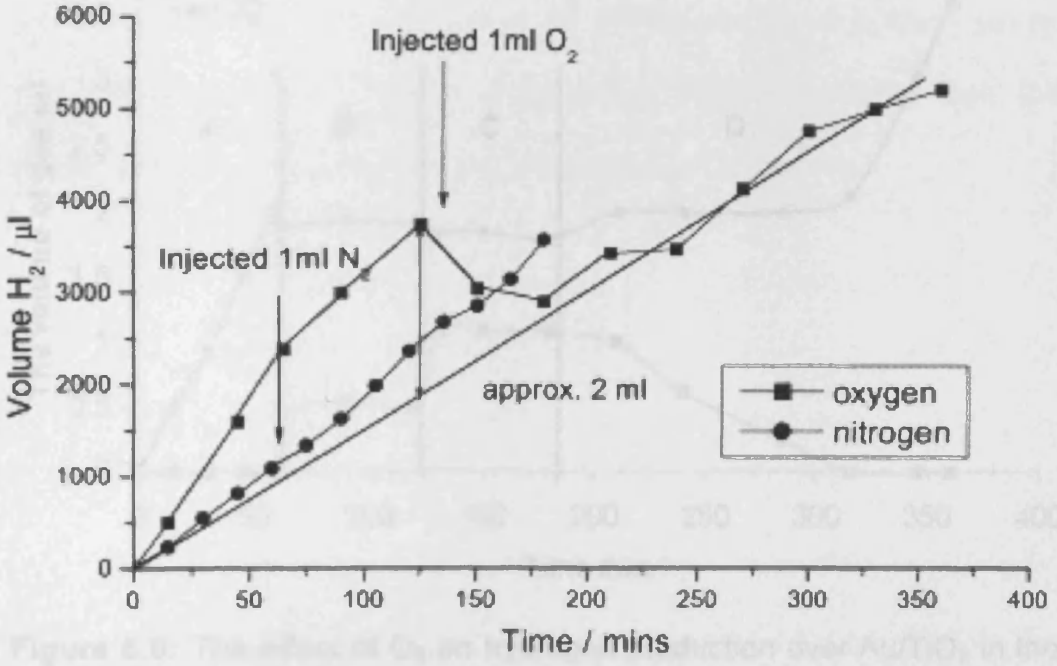

Figure 5.5: The effect of oxygen on H_2 production over Pd/TiO_2 in the presence of light.

The hydrogen oxidation reaction over Au/TiO_2 in the presence of light was investigated in more detail. Figure 5.6 displays the analysis of hydrogen and oxygen by GC. 100 ml of deionized water and 100 µl methanol were stirred with 0.2 g of 2 % Au/TiO_2. The graph was divided into 4 regions as this study was conducted at different conditions. These regions were represented as follows:

(A) Hydrogen production in the presence of light before O_2 injection.

(B) Hydrogen production after switching the lamp off and injecting ~2 ml of O_2.

(C) Injecting ~2 ml more of O_2 at the same condition as above.

(D) Switching the lamp on again.

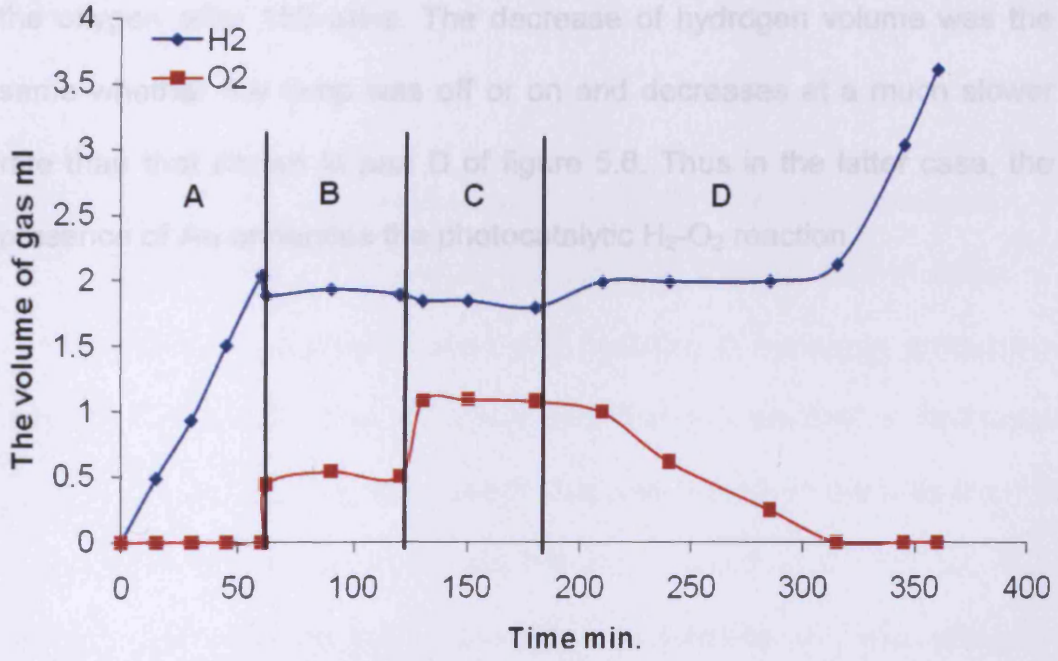

Figure 5.6: The effect of O_2 on hydrogen production over Au/TiO_2 in the presence of light.

Hydrogen increases with irradiation time in peak (A) as usual, when the light is switched off, there is no further H_2 production. When 2 ml of oxygen is injected, the hydrogen level is unchanged. This behavior proves that the reaction between hydrogen and oxygen in the absence of light over Au/TiO_2 is very slow. However, when irradiation is restarted (D), O_2 decreases and the amount of hydrogen remains approximately constant. After all the injected O_2 had been consumed, H_2 increases again. In the early part of D hydrogen is being produced, but is consumed by photoreaction with O_2 at a similar part.

It was found that the behavior of TiO_2 alone in terms of the back reaction was different (figure 5.7). 2 ml of hydrogen was injected and then the oxygen after 150 mins. The decrease of hydrogen volume was the same whether the lamp was off or on and decreases at a much slower rate than that shown in part D of figure 5.6. Thus in the latter case, the presence of Au enhances the photocatalytic H_2-O_2 reaction.

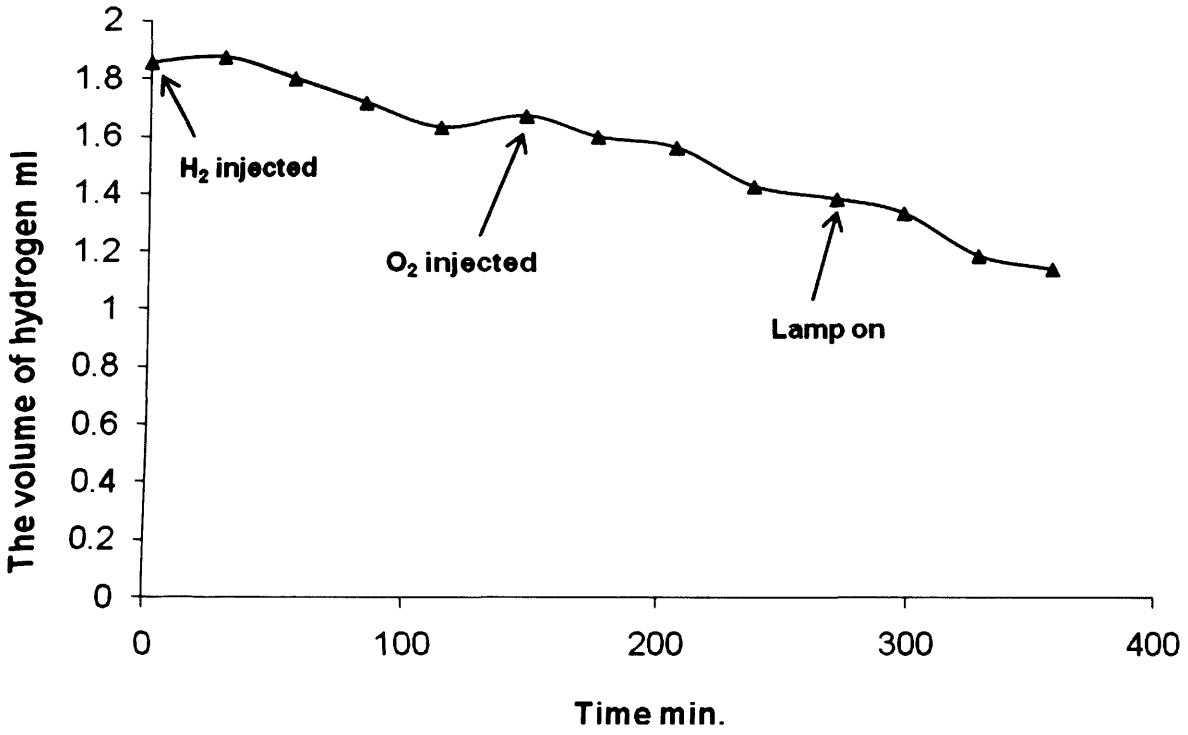

Figure 5.7: The effect of oxygen over bare TiO_2 in the absence and presence of light.

5.2.3. The effect in Ag and Sr and doped TiO_2 in water photolysis

Ag/TiO_2 and Sr/TiO_2 were discussed in Chapter four in terms of their preparation, characterization and activities in hydrogen production from methanol reforming. It was found that the amount of hydrogen production over Ag/TiO_2 was double that over Sr/TiO_2 in the presence of methanol. Nevertheless, they were still less active than 0.5 Pd/TiO_2 P25 (the standard reaction in this project). The activities of these catalysts were investigated in water photolysis without any of the donors that inhibit the back reaction, as discussed earlier. This study was carried out as gas phase reaction because these catalysts were available in small

quantities. 50 mg of Ag/TiO_2 or Sr/TiO_2, supplied by Jawwad Darr at University College London, was mounted on the slide held above 15 ml of deionised water. 0.2 ml of the gaseous products was taken and analysed every 30 min by GC.

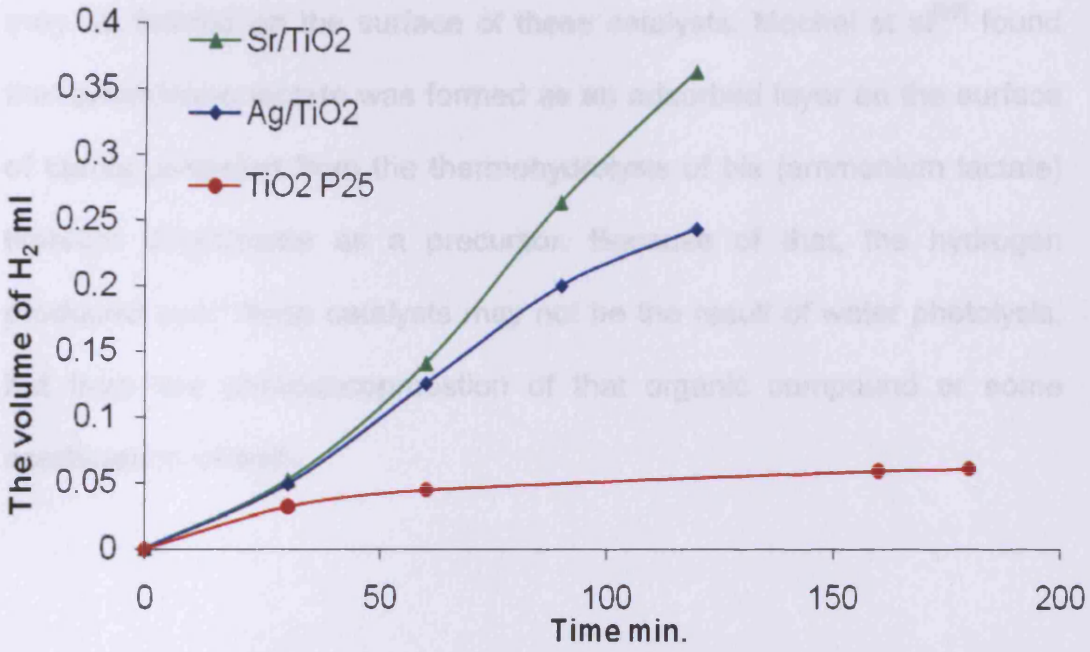

Figure 5.8: Hydrogen production over Ag/TiO_2, Sr/TiO_2 and P25 in gas phase.

Figure 5.8 illustrates the activity of the catalysts and compares it with the activity of TiO_2 P25 in gas phase in terms of the photolysis of water. Here, the rate of hydrogen produced over Sr/TiO_2 was more Ag/TiO_2 in contrast to the reforming of methanol over the same catalysts, even though small quantities of hydrogen are produced in both cases.

Moreover, the activities of Ag/TiO_2 and Sr/TiO_2 were much larger than that of Degussa TiO_2 P25 in water splitting. Again, no oxygen was produced.

During the catalysts preparation, byproduct ammonium lactate may be formed on the surface of these catalysts. Mochel et al[39] found that ammonium lactate was formed as an adsorbed layer on the surface of titania prepared from the thermohydrolysis of bis (ammonium lactate) titanium dihydroxide as a precursor. Because of that, the hydrogen produced over these catalysts may not be the result of water photolysis, but from the photodecopmostion of that organic compound or some combination of both.

5.3. Conclusion

The rate of hydrogen production over Pd/TiO_2, Au/TiO_2 and TiO_2 was very low in terms of water photolysis. Oxygen was not detected over any of the catalysts used.

The evolution of hydrogen may be inhibited by some undesirable reaction such as the back reaction, as hydrogen recombines with oxygen to reform the water. This reverse reaction was studied over Pd/TiO_2, Au/TiO_2 and TiO_2. It was found that H_2/O_2 recombination rate over Pd/TiO_2 was faster than Au/TiO_2 and TiO_2. Additionally, this reaction occurs easily over Pd/TiO_2 whether the light on or off. In the case of

Au/TiO_2, the effect of light was clear on the rate of hydrogen consumption while TiO_2, there was no obvious change in both cases (the presence or absence of light).

The activities of Ag/TiO_2 and Sr/TiO_2 were more than TiO_2 alone in the case of water photolysis. It was thought that the hydrogen was produced from an organic compound remaining through the preparation of these catalysts and not from water splitting.

5.4 References

[1] D. Bahnemann, *Solar Energy* **2004**, *77*, 445-459.

[2] J. Zhao and X. Yang, *Building and Environment* **2003**, *38*, 645-654.

[3] Masao Kaneko and I. Okura, *Photocatalysis: science and technology* Springer, **2002**, p. 244.

[4] B. O'Regan and M. Gratzel, *Nature* **1991**, 353, 737-740.

[5] M. Gratzel, *Journal of Photochemistry and Photobiology A: Chemistry* **2004**, *164*, 3-14.

[6] K. Sayama and H. Arakawa, *J. Chem. Soc., Faraday Trans.* **1997**, *93* 1647.

[7] M. Kitano, M. Takeuchi, M. Matsuoka, J. M. Thomas and M. Anpo, *Catalysis Today* **2007**, *120*, 133-138.

[8] A. Fujishima and K. Honda, *Nature* **1972**, *238*, 37-38.

[9] K. Gurunathan, P. Maruthamuthu and M. V. C. Sastri, *International Journal of Hydrogen Energy* **1997**, *22*, 57-62.

[10] S. G. Lee, S. Lee and H.-I. Lee, *Applied Catalysis A :General* **2001**, *207*, 173-181.

[11] Y. Li, G. Lu and S. Li, *Chemosphere* **2003**, *52*, 843-850.

[12] S. Jin and F. Shiraishi, *Chemical Engineering Journal* **2004**, *97*, 203-211.

[13] J.-C. Xu, Y.-L. Shi, J.-E. Huang, B. Wang and H.-L. Li, *Journal of Molecular Catalysis A: Chemical* **2004**, *219*, 351-355.

[14] M. Okada, Y. Yamada, P. Jin, M. Tazawa and K. Yoshimura, *Thin Solid Films* **2003**, *442*, 217-221.

[15] G. R. Torres, T. Lindgren, J. Lu, C.-G. Granqvist and S.-E. Lindquist, *The Journal of Physical Chemistry B* **2004**,108, 5995-6003.

[16] A. Iwase, H. Kato and A. Kudo, *Catalysis Letters* **2006**, *108*, 7-10.

[17] K. Domen, S. Naito, M. Soma, T. Onishi and K. Tamaru, *J. Chem. Soc. Chem. Commun.* **1980**, 543.

[18] Y. G. Ko and W. Y. Lee, *Catalysis Letters* **2002**, *83*, 157-160.

[19] Z. Zou and H. Arakawa, *Journal of Photochemistry and Photobiology A: Chemistry* **2003**, *158*, 145-162.

[20] K. Sayama, K. Mukasa, R. Abe, Y. Abe and H. Arakawa, *Journal of Photochemistry and Photobiology A: Chemistry* **2002**, *148*, 71-77.

[21] J. Greaves in *Photocatalytic Hydrogen Production using Gold on Titania*, *Vol. PhD* The University of Reading, **2005**.

[22] T. Sreethawong and S. Yoshikawa, *International Journal of Hydrogen Energy* **2006**, *31*, 786-796.

[23] M. Anpo and M. Takeuchi, *Journal of Catalysis* **2003**, *216, 505-516.*

[24] T. Sakata and T. Kawai, *Chemical Physics Letters* **1981**, *80*, 341-344.

[25] A. Patsoura, D. I. Kondarides and X. E. Verykios, *Catalysis Today* **2007**, *124*, 94-102.

[26] S. Teratani, J. Nakamichi, K. Taya and K. Tanaka, *The chemical Society of Japan* **1982**, *55*, 1688-1690.

[27] T. Sakata, *Journal of Photochemistry* **1985**, *29*, 205-215.

[28] S. Sato and J. M. White, *Chemical Physics Letters* **1980**, *72*, 83-86.

[29] T. Kawai and T. Sakata, *Chemical Physics Letters* **1980**, *72*, 87-89.

[30] A. Dickinson, D. James ‹N. Perkins, T. Cassidy and M. Bowker, *Journal of Molecular Catalysis A: Chemical* **1999**, *146*, 211-221.

[31] G. R. Bamwenda, S. Tsubota, T. Nakamura and M. Haruta, *Journal of Photochemistry and Photobiology A: Chemistry* **1995**, *89*, 177-189.

[32] D. Lawless, N .Serpone and D. Meisel, *The Journal of Physical Chemistry* **1991**, *95*, 5166-5170.

[33] K.-i. Ishibashi, A. Fujishima, T. Watanabe and K. Hashimoto, *The Journal of Physical Chemistry B* **2000**, *104*, 4934-4938.

[34] G. Lu, A. Linsebigler and J. J. T. Yates, *The Journal of Chemical Physics* **1995**, *102*, 3005-3008.

[35] A. Galinska and J. Walendziewski, *Energy & Fuels* **2005**, *19*, 1143-1147.

[36] M. Bowker, L. Millard, J. Greaves, D. James and J. Soares, *Gold Bulletin* **2004**, *37*, 170-173.

[37] H. Yi, T. Peng, D. Ke, D. Ke ،L. Zan and C. Yan, *International Journal of Hydrogen Energy* **2008**, *33*, 672-678.

[38] L. Millard and M. Bowker, *Journal of Photochemistry and Photobiology, A: Chemistry* **2002**, *148*, 91-95.

[39] H. Mockel, M. Giersig and F. Willig, *J. Mater. Chem.*, **1999**,9, 3051-3056.

CHAPTER SIX

Conclusions and Future work

6. Conclusions

6.1. Review of the project

Hydrogen production has become one of the most important topics in the field of energy. A great deal of research has been carried out, trying to improve the rate of production to meet economic needs. Water photocatalysis is one method of hydrogen production which was studied in this work.

The objective of this project was divided into three parts; firstly, investigating the hydrogen production photocatalytically from a water/methanol mixture using Pd loaded TiO_2; secondly, using non-metal loaded TiO_2 as a photocatalyst instead of metal-TiO_2 with the same aim (hydrogen production) and finally, studying pure water splitting over different catalysts. In all of these studies, the catalysts were illuminated by a Xe arc lamp and the reactions were achieved within a Pyrex flask under inert atmosphere (argon). The gaseous products were detected and analysed by gas chromatography.

In Chapter Three, reforming of methanol photocatalytically was carried out when Pd/TiO_2 was illuminated by UV light in a water/methanol mixture producing hydrogen and carbon dioxide. Some of the variables which have an affect on the rate of hydrogen production were studied to obtain an optimum rate. The most important factors for determining the rate were: i) the loading of Pd, ii) the of TiO_2 type and iii) the wavelength range of light. In the reaction, one mole of water was split by reacting with one mole of methanol, by ambient temperature, photocatalytic reforming of methanol.

Although most of the work was done as a liquid phase reaction, the rate of H_2 production in the gas phase was much higher than that in the liquid phase. 0.5% wt. Pd loading on TiO_2 P25 gave the optimum rate in the liquid phase reaction where as in the gas phase it was 1% wt Pd. Furthermore, the induction time for the reaction at high loadings were more apparent in the liquid phase than in gas phase due to the sintering of Pd particles in the liquid phase reaction. In both phases, the active region between the support and the metal has a main role in the activity of the catalyst. It was expected that Pd particles may be surrounded by an active area which increases with increasing Pd loading until the optimum area is reached and then decreases when the particles become close to each other.

It was found that the rate of hydrogen production over Pd/TiO_2 increased in the presence of methanol at low concentrations up to 10 µl and then the reaction was of zero order with any increase of methanol concentration. When the metal was entirely covered by methanol molecules, the rate was not affected by any increase. Thus the reaction proceeds in a langmuirian fashion.

If the methanol molecule was replaced by glycerol, which contains three hydroxyl groups, the hydrogen production rate was much higher than methanol reforming over both Pd/TiO_2 or Au/TiO_2. However, the latter was less active than Pd/TiO_2. The mechanism of glycerol reforming was thought to be similar to that of methanol as they produced the same products; hydrogen and carbon dioxide.

Finally, different loadings of palladium on mesoporous TiO_2 as a support instead of P25 were investigated and their results compared with that for methanol. Pd/TiO_2 was still more active than $Pd/MTiO_2$, even though mesoporous TiO_2 has a high surface area. This may be ascribed to the phase structure of titania.

In Chapter Two, nitrogen was doped on different photoactive supports (P25, nanopowder anatase or TiO_2 [anatase] prepared by CHFS) and prepared at different temperatures characterized by XRD, BET surface area and SEM. The XRD technique did not detect the nitrogen except at the highest temperature when TiN was formed. Similar results were obtained in the case of cationic (Ag and Sr) doping which may be ascribed to the small particle size and the low loading. For BET surface areas of these catalysts, the temperature has a different effect on the surface areas, depending on the kind of TiO_2. It was shown that BET surface areas of P25 were the same before and after nitrogen doping at the three different temperatures. In the case of nanopowder anatase, their surface areas decreased with increasing the temperature, which may be attributed to sintering. N-T600 has a small surface area. In contrast, Ag/TiO_2 and Sr/TiO_2 prepared by CHFS have surface areas larger than all the other catalysts used in this work.

The activities of all these catalysts in the presence of methanol were much less than 0.5% Pd/TiO_2, but they absorb under visible region. However, the hydrogen production rate over Pd loaded N-D450 > N-D550 > N-T600 > N-D650 > N-A650. Without Pd loading and/or without methanol, no hydrogen was detected over these catalysts. The hydrogen produced in the presence of Ag/TiO_2 and Sr/TiO_2 was small compared to Pd/TiO_2.

In Chapter Five, the rate of hydrogen production from water alone over Pd/TiO_2, Au/TiO_2 and TiO_2 was examined was very low in the absence of methanol. In addition to that, no oxygen was detected over these catalysts indicating that these catalysts, under these conditions, do not catalyse overall water splitting. This could be due to a very efficient back reaction which was examined. This reverse reaction over Pd/TiO_2 was faster than Au/TiO_2 and TiO_2, and occurred even in the absence of light.

6.2. Future Work

The results obtained from these reactions lead to some questions and suggestions which may be beneficial to understand more about the mechanism of photocatalytic methanol reforming and improve the rate of hydrogen production. The following directions may have a significant role in the field of hydrogen production as a practical alternative energy source:

1) The limitation of using Pd/TiO_2 or Au/TiO_2 economically is due to their absorption under the UV region which represents only 4% of the electromagnetic spectrum. Accordingly, other methods are needed to enhance the activity of the catalysts under the visible region such as a new preparation method.

2) Given glycerol produced hydrogen and carbon dioxide as in the case of methanol but with higher quantities, more studies should be undertaken to understand the mechanism of glycerol reforming and hence improve the rate more.

3) The reaction over Pd loaded mesoporous TiO_2 needs more investigation during and after the irradiation. In addition, varying the Pd loading of this support may give promising results, in terms of higher reaction rates.

4) It was proved that doping of TiO_2 by a non-metal increased absorption in the visible region. However, such catalysts have low activity for hydrogen

production. Various studies have been suggested to try to enhance their activities such as changing the preparation method, type of metal, and the reaction conditions.

5) The reverse reaction (recombination of hydrogen and oxygen) was one of the problems which had an affect on the efficiency of the photoreaction. Designing a photoreactor which makes hydrogen and oxygen generate separately would increase efficiency. In addition to that, further work might be needed to develop a catalyst which is able to inhibit such undesired reactions.